

MATH 704 & 801 - Final Project

The (mathematical) art of souvla ($\sigmaούβλα$) cooking

Marios Andreou

A joint final project for MATH 704 - Methods of Applied Mathematics II and MATH 801 - Topics in Computational Fluid Dynamics at the University of Wisconsin - Madison



WISCONSIN
UNIVERSITY OF WISCONSIN-MADISON

Department of Mathematics
University of Wisconsin - Madison
May 10, 2023

MATH 704 & 801 - Final Project

The (mathematical) art of souvla ($\sigmaούβλα$) cooking

Marios Andreou

Contents

1	What is Souvla ($\Sigmaούβλα$)?	3
2	An all-encompassing model for cooking souvla on a fokou — Conductive and radiative heat transfer and Rayleigh-Bénard Flow	3
2.1	PDE for the "Inside meat" region	4
2.2	PDE for the "Outside meat" region	5
2.3	Initial/Boundary conditions for the "Inside meat" region	6
2.4	Initial/Boundary conditions for the "Outside meat" region	8
2.5	The true model	9
2.6	Non-dimensionalisation of the true model (2.6)	10
3	The simplified model — Heat transfer in Taylor-Couette flow	11
3.1	Non-dimensionalisation of the simplified model (3.4)	14
4	Toy problem; Circular domain with rotating Dirichlet boundary conditions	15
4.1	Existence and uniqueness of solutions to (4.2)	16
4.2	Steady temperature profile/Equilibrium state of (4.2)	16
4.3	Summary of the asymptotic expansion of the solution to (4.2), while $\omega \rightarrow \infty$	17
4.3.1	Sketching the procedure of how to get an approximation to the solution of (4.5) with an asymptotic error of $\mathcal{O}(\varepsilon^{3/2})$	20
4.4	Generalisations to the rotating Dirichlet boundary condition model 4.2	21
5	The next step; Circular domain with rotating Robin boundary conditions	22
6	Optimal cooking time in the rotating Dirichlet and Robin boundary conditions models through first mode approximations	26
6.1	Physical and dimensionless parameters to the non-dimensional simplified model (3.5)	26
6.2	Rotating Dirichlet boundary conditions	29
6.3	Rotating Robin boundary conditions	29
7	Numerical Results	30
7.1	Rotating Dirichlet boundary conditions	30
7.2	Rotating Robin boundary conditions	30
8	Next Steps	34

1 What is Souvla ($\Sigma\sigma\beta\lambda\alpha$)?

Souvla (or $\sigma\sigma\beta\lambda\alpha$ in greek) is widely considered to be the national dish of Cyprus, triumphing among other candidates like koupepia ($\chiou\pi\epsilon\pi\alpha$), and sheftalia ($\sigma\iota\epsilon\phi\tau\alpha\lambda\alpha$). It mainly consists of large chunks of meat, usually lamb, pork, or chicken (stemming from the neck or shoulder for the larger animals), that are pierced with a long metallic skewer, much like a rotisserie, and cooked over a compartment that we call a fokou ($\varphi\sigma\chi\omega\acute{u}$), which is similar to a (usually rectangular shaped) brazier or grill, using charcoal.

While similar in nature to the widely known Greek souvlaki ($\sigma\sigma\beta\lambda\alpha$), it differs in 3 main aspects;

- The meat cuts are much larger in size. Usually souvlaki is cut to be the size of a small meatball, while chunks of souvla tend to be in the size of a medium onion or potato, which usually also includes bones and great contents of fat.
- The cook time is much longer, due to the preferred method of slow cooking these large chunks of meat.
- The perpendicular distance from the heat source (i.e. the distance between the axis of rotation and the charcoal surface), is greater.

Also, in the case of souvlaki, usually the cook manually turns around the meat to uniformly try and cook all its sides, while in the case of souvla, due to how long it takes to cook, it is automatically rotated above the hot charcoal surface using a motor. This makes souvla a closer relative to a whole spit-roasted lamb or pork, known as an ovelias ($\sigma\beta\epsilon\lambda\alpha\varsigma$), than it is to souvlaki. The similarity of the Greek names of these dishes, stems from the fact that in Greek, the -aki (-άκι) suffix, is reserved for the small variant of something; In this case souvlaki is the "mini" or "smaller" version of souvla. Also, since this is not a well known delicacy, we provide some reference to the reader in Figure 1.



Figure 1: Pork souvla being cooked on a fokou (Left: www.checkincyprus.com - Right: www.offsite.com.cy)

As Wikipedia ([34]) summarises really well, the process of souvla cooking usually goes like this:

“The meat is put as far as possible from the charcoal at first. After it is sizzling, it is lowered down closer to the charcoal so that the skin on the meat goes brown. The process takes between 90 minutes to 3 hours, depending on the type of meat, size and heat intensity of fire. Salt, aromatics (such as oregano), oil, and wine are sprinkled or brushed on the meat once the cooking process is well under way. That way the meat stays juicy and does not brown too quickly.”

While all the mentioned details above are important variables in the cooking process, our task in this paper is to develop the theory behind the cooking of souvla using the Heat equation as well as the incompressible Navier-Stokes equations, where at first we pose a nearly all-encompassing model that simulates reality to some decent extend, to which then we will make some warranted assumptions as to simplify it, to then be able to extract some useful and practical results. These results will deal with the cook time of the meat under some assumptions of constant angular velocity and a fixed distance from the charcoal surface, and will inspect their dependency on the said angular velocity.

2 An all-encompassing model for cooking souvla on a fokou — Conductive and radiative heat transfer and Rayleigh-Bénard Flow

(**Note:** In this paper, $\tilde{\cdot}$ denotes that the quantity in question is dimensional, while the omission of the overhead tilde indicates a dimensionless quantity. This is reserved for quantities of significance and only.)

It is known from the theory of heat transfer (*see Chapters 1.5-1.9 of [28], Chapter 1 of [1], and Chapter 1.2 of [19]*), which explains the distribution of thermal energy between bodies in a medium due to a temperature difference (gradient) according to the Second Law of Thermodynamics, that the transfer of thermal energy can be characterised via four fundamental modes:

- (i) **Advection:** By transferring some matter physically, thermal energy is also moved as an intrinsic part of that matter.
- (ii) **Conduction:** Materials that are in physical contact exchange thermal energy between them. It is the property of material to transfer energy diffusely via their molecular structure, or by direct contact for two bodies, and it is explained via Fourier's Heat Law of Conduction.
- (iii) **Convection:** Exchange of thermal energy between an object and its environment takes place due to some underlying fluid motion or movement of flow. It combines the effects of conduction and fluid motion.
- (iv) **Radiation:** The transfer of energy by the emission of electromagnetic radiation, attributed to changes in the electronic configurations of the atoms or molecules.

In our case, the meat that is pierced with the metallic skewer is stationary and rotating rigidly in our environment, *meaning that no heat transfer is happening due to advection, and so it is ignored as a factor of heat transfer*. But, in some form or another, we will consider *all* other forms of heat transfer mentioned above, and include them in our models. In what follows, we will include the units of measurement for each quantity in parentheses, using SI base units.

We begin with the general *convection-diffusion Heat equation, in its dimensional form*, modelling heat distribution in a medium, denoted with \tilde{T} ($^{\circ}\text{C}$), due to conduction and convection, where convection is described by an incompressible background velocity field, $\vec{\tilde{u}}$ (ms^{-1}). It is derived via the Conservation of Energy equation (First Law of Thermodynamics) and Fourier's Heat Law of Conduction (Second Law of Thermodynamics) (*see Chapter 6.7 of [28]*), both in their differential forms, and is given as,

$$\left(\rho C_p \frac{D_{\vec{x}} \tilde{T}}{Dt} \right) = \rho C_p \frac{\partial \tilde{T}}{\partial t} + \rho C_p (\vec{\tilde{u}} \cdot \vec{\nabla}) \tilde{T} = \vec{\nabla}(\kappa \vec{\nabla} \tilde{T}) + f. \quad (2.1)$$

\tilde{t} (s) is the time variable and \vec{x} (m) is the spatial variable. $\frac{\partial \tilde{T}}{\partial \tilde{t}}$ is the temporal change of the scalar temperature field, $(\vec{\tilde{u}} \cdot \vec{\nabla}) \tilde{T}$ is the contribution that comes from the heat transfer via convection by the background velocity field $\vec{\tilde{u}}$, while $\vec{\nabla}(\kappa \vec{\nabla} \tilde{T})$ is the diffusive heat transfer via conduction, which is affected by the thermal conductivity of the material, denoted by $0 < \kappa$ ($\text{W m}^{-1} \text{ } ^{\circ}\text{C}^{-1}$), which in general is anisotropic (it is a rank-2 tensor), non-uniform (depends on the space variable), and could depend implicitly on time via \tilde{T} , and is the controlling transport property for conduction. Finally f (W m^{-3}) is the dissipative balance in the conservation of energy and could function as a heat energy source or sink, based on its sign, or in the case where viscous shear stresses in the fluid are not a negligible factor of heat transfer, it can also function as a viscous dissipation function. This derivation assumes that the background fluid is incompressible, is well approximated by a perfect gas, and that the specific heat capacity, C_p ($\text{J kg}^{-1} \text{ } ^{\circ}\text{C}^{-1}$), and density, ρ (kg m^{-3}), of the medium are uniform and constant. As for the background fluid, it is described by the incompressible Navier-Stokes equations, which we will write down when needed. In the next couple of paragraphs, we will formulate an all-encompassing model for the cooking of souvla on a foukou, which incorporates both conduction, natural convection, and radiation as forms of heat transfer. We will split our model to the "*Inside meat*" and "*Outside meat*" regions, and write down PDEs and initial/boundary conditions for each region respectively.

2.1 PDE for the "Inside meat" region

Starting with the geometry of our setup, our model will assume that the meat chunks are evenly distributed on the metallic skewer both transversely and longitudinally (i.e. the weight is evenly distributed on the rotisserie). We will also assume that the rotisserie, looking face on with the skewer, forms a perfect cylinder. While this is far from the case, due to the uniformity argument we made above, we can just think of this cylinder as being the centroid cylinder in terms of weight, or the arithmetic mean position of all the points in the volume distribution of the meat. Furthermore, we assume that the distribution of charcoal on the foukou is even as well (again both transversely and longitudinally), as to have a uniform heat source parallel to the skewer. We also assume that the hot charcoal surface is held constant in time at a temperature of T_H . Our model will take advantage now of this uniformity assumptions, *and deal with the modelling and calculation of the temperature inside the meat in a two dimensional plane that is perpendicular to the skewer, i.e. in a cross section of our setting, with the skewer being normal to this plane*. This can be seen in Figure 2.

Continuing our uniformity arguments, we also assume that the thermal conductivity of our meat, κ_m , is uniform spatially, isotropic, and doesn't depend on time or temperature, i.e. *it is a scalar constant*. Although this is not always the case, this assumption rarely leads to tremendous inaccuracies. Even in the case where the thermal conduction depends on the temperature (but is still isotropic), we can employ the Kirchhoff transformation (*see [30]*), and can still continue the following analysis to a decent extend, but instead of working with the Kirchhoff variable transformation instead of \tilde{T} , which linearises the problem. Based on this, we can then define the *constant* of thermal diffusivity in the meat as, $D_m = \frac{\kappa_m}{\rho_m(C_p)_m} (m^2 s^{-1})$.

Now, we further assume that the metallic skewer (assumed to have a circular shape in the cross section we are working in), has a zero radius and is not a contributing factor in our model, or that it has a negligible contribution to the dynamics of the problem, specifically in the heat transfer via conduction in the contact with the meat. As such, our cross section meat slab has a circular geometry instead of an annular one. We can compensate for this somewhat by thinking of our meat, for the purposes of our model only (and hopefully not reflecting reality), as a mixture of meat, bones and fat as well as the metallic skewer. This is possible because of the *rule of mixtures*, where it is stated that the thermal conductivity of a composite material is a form of a weighted average of the thermal conductivity of its constituents. This is because the inverse of the thermal conductance of a material, or the thermal resistance, functions exactly as the electrical resistance in circuits, and so we can add thermal resistances in the same manner to that (parallel or in series), and then be able to extract a form of a weighted average for the thermal conductivity, and as such for the thermal diffusivity as well. For radial systems, the theory of determining the effective thermal conductivity of a composite material can be found in *Chapter 3.5.2 of [19]* and *Chapter 3.4 of [28]*.

Also, although it is argued that juices moving inside the meat in the cooking process play a role in the internal temperature and as such the overall cooking time, where their amount being generated is based on the amount of fat content and meat tissue in the meat, we assume that they are negligible. In this case we will assume a uniform distribution for our meat slab consisting of some percentages of meat tissue, fat, and bones (and stainless steel for our model's purposes, awkwardly enough), to which the juices generated play no role or are flat out ignored. For this simplification we can again compensate, by balancing out its omission in our final model by defining our thermal diffusivity parameter in an accommodating way by accounting accordingly for this and the prior simplifications, and modifying its constant value in a systematic and accurate way, similar to our argument in the previous paragraph. So, since we assume such a solid like structure, it can be assumed that there would *not be any convective contribution in the heat distribution inside the meat*. Also, since the heat source in the cooking process comes from the outside (from the fokou), and there are no heat sinks within the meat (we mention here the possibility of incorporating the skewer as a form of heat sink within the meat, e.g. based on the origin as a point sink), *we can also safely assume that the forcing non-homogeneous term, f , is equal to 0 everywhere*. As such the convective term and dissipation terms in (2.1), for the temperature distribution inside the meat, are omitted.

As such, the PDE that will describe the heat distribution inside the meat which we denote with \tilde{T}_m , from (2.1), has taken its usual form of the Heat equation as,

$$\frac{\partial \tilde{T}_m}{\partial \tilde{t}} = D_m \tilde{\nabla}^2 \tilde{T}_m. \quad (2.2)$$

Since our meat slab has a circular shape, we denote the domain of our meat as Ω_m , and its radius with R . As mentioned in our introduction, the meat slab is rotating with some angular velocity $\omega = \omega(\tilde{t})$ via the motor above the hot charcoal surface, which we can assume is in the counter-clockwise direction, without loss of generality, and it is the derivative of the azimuthial displacement function that describes the rotation itself, $\Theta(\tilde{t})$. The center of the slab is situated in the origin of a Cartesian co-plane.

2.2 PDE for the "Outside meat" region

At a distance h from the center of our meat, the hot charcoal surface is situated which rests on the fokou, which we can assume that is of transversal length of $2L$, where $L > R$, for obvious reasons, and of longitudinal length L_f (i.e. the length of the fokou normal to our plane, which we assume to be equal to the length of the metallic skewer or meat distribution). We also assume that $h > R$. This hot charcoal surface transfers thermal energy to the meat via radiation, and because of a non-isothermal flow now being created on the outside of our meat close to the charcoal surface, heat transfer to the meat from the fokou is also happening under natural convection, i.e. we have a buoyancy-driven flow due to the temperature of the fokou affecting the density of the air which is inversely proportional to its temperature (assuming constant pressure), leading to "lighter" hotter air to rise and heat the boundary of our meat. As such, we also have a temperature field outside our meat domain, which

we denote with \tilde{T}_a (a for "air"), and a background incompressible velocity field denoted with $\tilde{\vec{u}}_a$. We denote the domain in which we will analyse this "Outside meat" region with Ω_a , and it is defined by the lines $x = \pm L$, and $y = -h$ and $y = c$ in the Cartesian co-plane we are working in, where $c \gg R$. Making a similar assumption of a constant thermal conductivity for the air outside the meat, we then have a constant thermal diffusivity for the air, D_a (under the assumption of "constant" density; Boussinesq approximation (buoyancy) which we discuss in the next paragraph), and since there are no heat sources or sinks in our domain Ω_a , the PDE that will describe the heat distribution outside the meat which we denote with \tilde{T}_a , from (2.1), becomes,

$$\frac{\partial \tilde{T}_a}{\partial \tilde{t}} + (\tilde{\vec{u}}_a \cdot \tilde{\nabla}) \tilde{T}_a = D_a \tilde{\nabla}^2(\tilde{T}_a) \quad (2.3)$$

The PDE that describes the background flow outside the meat will be the *incompressible Navier-Stokes equations* (conservation of momentum equations) that incorporate the *Boussinesq approximation of natural convection*, which ignores the density differences unless they are multiplied by the gravitational acceleration vector, or that density variations are ignored in the conservation of mass equation (our velocity field is divergence-free or solenoidal), but are important in the buoyancy term due to a temperature gradient in the non-isothermal air. These equations are,

$$\begin{cases} \frac{\partial \tilde{\vec{u}}_a}{\partial \tilde{t}} + (\tilde{\vec{u}}_a \cdot \tilde{\nabla}) \tilde{\vec{u}}_a = -\frac{1}{\rho_0} \tilde{\nabla} \tilde{p} + \nu \tilde{\nabla}^2(\tilde{\vec{u}}_a) + (1 - \alpha(\tilde{T}_a - T_\infty)) \vec{g} \\ \tilde{\nabla} \cdot \tilde{\vec{u}}_a = 0, \end{cases} \quad (2.4)$$

where \tilde{p} ($k\text{gm}^{-1}\text{s}^{-2}$) is the pressure field of the air which functions as a Lagrange multiplier as to enforce incompressibility to $\tilde{\vec{u}}_a$, ν (m^2s^{-1}) is the kinematic viscosity of air (assumed constant in space and time), T_∞ ($^\circ\text{C}$) is the ambient room temperature, ρ_0 (kgm^{-3}) is some reference density or the fixed part of the density variations $\rho = \rho_0 - \alpha \rho_0(\tilde{T}_a - T_\infty)$. α ($^\circ\text{C}^{-1}$) is the coefficient of thermal expansion of air which we assume is constant, and due to our ideal gas assumption we have $\alpha = \frac{1}{T_\infty}$, and lastly $\vec{g} = -g \hat{e}_y$ (ms^{-2}) is the gravitational body force that is perpendicular to the fokou in our cross section plane. The last term in this PDE is the buoyancy term, $(\rho_0 + \Delta\rho)\vec{g} = \rho\vec{g}$.

2.3 Initial/Boundary conditions for the "Inside meat" region

We will now proceed with setting the boundary and initial conditions for (2.2), where we begin by making the change from Cartesian coordinates (\tilde{x}, \tilde{y}) to polar coordinates $(\tilde{\varrho}, \vartheta)$. We start with the dependency of the boundary on the independent dimensional variables.

- For the radial direction, shrinkage of the meat occurs when water evaporates from the surface of the meat and when fat, water, and juices leak from the meat. This shrinkage of the outside boundary can be formulated by a moving boundary condition known as the *Stefan condition*, where by using a parameterisation of a domain boundary $\partial D = \partial D(\tilde{t}), \tilde{s}(\tilde{t})$, the condition is written as $-\beta \hat{n} \cdot \tilde{\nabla} \tilde{T} = \gamma \hat{n} \cdot \tilde{s}'(\tilde{t})$, where $\hat{n} = \hat{n}(\tilde{s}(\tilde{t}))$, is the outward pointing normal to the boundary at \tilde{s} at time \tilde{t} . Since we are working with a circular meat slab, the normal directional derivative is equal to the derivative with respect to the radial variable $\tilde{\varrho}$, meaning the modelling of this moving boundary condition in the radial direction is not difficult, but since this shrinkage will occur in a much slower time scale due to the slow cooking process, compared to the other dynamics of our model, as well as based on our previous assumptions to our model, *we do not assume any shrinkage of the boundary, and as such the boundary is radially constant*.
- For the rotation of our meat slab, instead of the stationary coordinate basis polar vectors $(\hat{e}_{\tilde{\varrho}}, \hat{e}_\vartheta)$, we could use a rotating non-inertial frame of reference with the basis vectors themselves rotating with our system. This a common practice in Classical mechanics (see Chapter 9 of [13]), and by using the classical principle of relativity we can relate the temporal derivatives using the absolute and relative derivatives (known as the transport theorem), by picking up terms like the Coriolis, Euler, and centrifugal forces. But for now we can just simulate the rotation by assuming that the azimuthal coordinate of the boundary conditions depends on time. Using the aforementioned azimuthal displacement function $\Theta(\tilde{t})$ for the rotation, we have $\vartheta(\tilde{t}) = \vartheta - \Theta(\tilde{t})$, where $\Theta'(\tilde{t}) = \omega(\tilde{t})$, is the angular velocity of the meat slab (boundary). This means that after a change of variables to the rotating frame of reference,

$$\begin{aligned} \tilde{t} &\mapsto \tilde{t} := \hat{\tilde{t}} \\ \tilde{\varrho} &\mapsto \tilde{\varrho} := \hat{\tilde{\varrho}} \\ \vartheta &\mapsto \vartheta - \Theta(\hat{\tilde{t}}) := \hat{\vartheta} \\ \tilde{T}(\tilde{t}, \tilde{\varrho}, \vartheta) &\mapsto \tilde{T}(\hat{\tilde{t}}, \hat{\tilde{\varrho}}, \hat{\vartheta} + \Theta(\hat{\tilde{t}})) := \hat{\tilde{T}}(\hat{\tilde{t}}, \hat{\tilde{\varrho}}, \hat{\vartheta}), \end{aligned}$$

we would have $\frac{\partial}{\partial \tilde{t}} = \frac{\partial}{\partial \hat{t}} + \omega(\hat{t}) \frac{\partial}{\partial \hat{\vartheta}}$. More on this in Sections 4 and 5.

With these remarks, we now can define the boundary conditions on $\partial\Omega_m$. We have that due to convection-conduction with the underlying background flow, and radiation from the fokou, the boundary condition will be a *Robin* one, since the heat flux through the surface of the meat, which due to the circular geometry of our meat slab is $-\kappa_m \frac{\partial \tilde{T}_m}{\partial \tilde{\varrho}}$ (and equal to $-\kappa_a \frac{\partial \tilde{T}_a}{\partial \tilde{\varrho}}$ as we note in Section 3), will be *equal to the additive contribution of convection and radiation*. This is based on Newton's law of heating/cooling (*see p. 7 of [20], and p. 8 of [19]*) that models conduction-convection type temperature exchange based on the Second Law of Thermodynamics, and the Stefan–Boltzmann law (*see Sections 13.1-13.3 of [19] and Sections 13.1-13.3 of [28]*).

The convection-conduction contribution is equal to $\tilde{H}_m(\tilde{T}_m - \tilde{T}_a)$, where \tilde{H}_m ($Wm^{-2}^{\circ}C^{-1}$) is the convection heat transfer coefficient of the meat surface, which in general depends on the azimuthial coordinate, since it is affected by the nature of the background outside flow which is non-constant, and so $\tilde{H}_m = \tilde{H}_m(\vartheta - \Theta(\tilde{t}))$, where we take into consideration the aforementioned rotation of the boundary, and we also assume that its dependence on the temperature fields is negligible.

As for the radiative contribution, it is explained via the *radiation exchange equation* and the *Stefan–Boltzmann law*, that describes the radiation exchange between two opaque, diffusive, and gray surfaces. To state the exact radiative contribution for our setup, some assumptions are needed. First, *we assume that our surfaces are approximately black body surfaces that absorb all incident electromagnetic radiation*, i.e. their emissivity constants, $\varepsilon_{meat}, \varepsilon_{charcoal} \approx 1$. This simplification is somewhat warranted since both constants based on the literature, for the temperature interval that we are concerned about, are equal to 0.85 ± 0.05 . Secondly, *that they absorb said incident electromagnetic radiation regardless of frequency or angle of incidence, without reflection* (i.e. they are diffusive surfaces). Lastly, our materials (meat and charcoal surfaces) are opaque by nature, so no simplifications needed here. The radiation exchange equation depends on the surfaces in question and their position in space, via the so called *view factor*. To proceed we assume that our charcoal surface is essentially rectangular, with length of $2L$ and transversal length of L_f , as aforementioned. Then, for a horizontal parallel plate of dimensions $2L$ and L_f emitting heat at distance h from the center of a circular cylinder of the same transversal length (L_f), the view factor, which is the fraction of radiation leaving the charcoal surface (i.e. the horizontal parallel plate) and which is intercepted by the meat slab (i.e. the circular surface), is given by,

$$F_{charcoal \rightarrow meat} = \frac{R \arctan\left(\frac{2L}{h}\right)}{L},$$

(*see p. 19 of [33]*). With these, we find that the radiative contribution to the heat flux of the meat surface is equal to $2\sigma L_f L F_{charcoal \rightarrow meat} (\tilde{T}_m^4 - T_H^4)$, where $\sigma = 5.670 \cdot 10^{-8}$ ($Wm^{-2}^{\circ}C^{-4}$) is the Stefan–Boltzmann constant.

Combining the results above, by superposition, Newton's law of cooling, the radiation exchange equation, the Stefan–Boltzmann law, and lastly the First Law of Thermodynamics (energy balance), we have that the boundary condition on the surface of the meat (for the heat flux of the meat's temperature) is given as,

$$\begin{aligned} -\kappa_m \frac{\partial \tilde{T}_m}{\partial \tilde{\varrho}}(\tilde{t}, R, \vartheta - \Theta(\tilde{t})) &= \tilde{H}_m(\vartheta - \Theta(\tilde{t}))(\tilde{T}_m(\tilde{t}, R, \vartheta - \Theta(\tilde{t})) - \tilde{T}_a(\tilde{t}, R, \vartheta - \Theta(\tilde{t}))) \\ &\quad + (2\sigma L_f R) \arctan\left(\frac{2L}{h}\right) (\tilde{T}_m^4(\tilde{t}, R, \vartheta - \Theta(\tilde{t})) - T_H^4), \quad \tilde{t} > 0, \quad \vartheta \in [0, 2\pi], \end{aligned} \quad (2.5)$$

Usually, we use the linearised radiation rate equation with conduction-convection (*see p. 10 of [19]* and p. 21 of [1]), where we express the boundary condition as,

$$\begin{aligned} -\kappa_m \frac{\partial \tilde{T}}{\partial \tilde{\varrho}}(\tilde{t}, R, \vartheta - \Theta(\tilde{t})) &= \tilde{H}_m(\vartheta - \Theta(\tilde{t}))(\tilde{T}_m(\tilde{t}, R, \vartheta - \Theta(\tilde{t})) - \tilde{T}_a(\tilde{t}, R, \vartheta - \Theta(\tilde{t}))) \\ &\quad + \tilde{H}_r(\vartheta - \Theta(\tilde{t}))(\tilde{T}_m(\tilde{t}, R, \vartheta - \Theta(\tilde{t})) - T_H), \end{aligned}$$

where we now have the *radiation heat transfer coefficient*, \tilde{H}_r , defined as,

$$\tilde{H}_r = (2\sigma L_f R) \arctan\left(\frac{2L}{h}\right) (T_H^2 + \tilde{T}^2(\tilde{t}, R, \vartheta - \Theta(\tilde{t}))) (T_H + \tilde{T}(\tilde{t}, R, \vartheta - \Theta(\tilde{t}))).$$

This can be seen by looking at the first order Taylor expansion of $f(y) = \frac{y^4}{a^3} - a$ around a . This essentially makes the boundary condition a purely convective-conductive one, i.e. fully explained by Newton's law of heating/cooling. But, this now makes \tilde{H}_r strongly dependent on temperature, in contrast to the convective heat transfer coefficient \tilde{H}_m which is very weakly dependent on temperature, especially for our setting as we mentioned above. Also, this linearisation's validity rests on the fact that the temperature difference $\tilde{T}_m - T_H$ is not that large (more so for their non-dimensional counterparts).

As for the azimuthial "boundary condition", we assume that \tilde{T}_m , and all its (mixed) derivatives of any order are periodic in ϑ with period 2π . The same thing is assumed for any quantity that has an azimuthal dependence, like \tilde{H}_m and \tilde{H}_r .

Lastly, for an initial condition, we assume that our meat is at the ambient room temperature of T_∞ .

2.4 Initial/Boundary conditions for the "Outside meat" region

For the "Outside meat" region, which is explained by (2.3), and (2.4), what we essentially have is a *Rayleigh-Bénard natural convection flow driven by buoyancy*, and as such we impose the usual boundary conditions found in such flows, were we incorporate whenever needed the presence of our rotating meat slab in our outside domain, Ω_a .

We start with the boundary conditions in the y -coordinate, at $y = -h$ (hot charcoal surface) and $y = c$ ($c \gg R$). At $y = -h$, \tilde{T}_a is equal to the temperature of the fokou, T_H , and at $y = c \gg R$ it is equal to the ambient room temperature T_∞ , both imposed at all times. This is also how we "define" the constant c ; It is the vertical distance from the center of our meat slab, which is "far enough" from our system as to reach the ambient room temperature again, or where the buoyancy effects wear off. As for the velocity field $\vec{\tilde{u}}_a$, it has no slip boundary conditions at the surface of the fokou, and no penetration boundary conditions at $y = c$. As for the x -coordinate, both the background velocity field, $\vec{\tilde{u}}_a$, and temperature field, \tilde{T}_a , are periodic, as well as their derivatives of any order. At the surface of the meat, $\partial\Omega_m$, the velocity field again has no slip boundary conditions, where because of the rigid body motion of the meat we have $\vec{\tilde{u}}_a = \vec{\omega} \times \vec{x}$ at $\partial\Omega_m$, where $\vec{\omega}$ is the angular velocity pseudo-vector parallel to the metallic skewer (which is normal to our plane) with length ω , and \vec{x} is the position vector or spatial variable that we use for the "Outside meat" part of the problem. As for \tilde{T}_a at $\partial\Omega_m$, we have that it should satisfy *the same Robin boundary condition that we imposed on the "Inside meat" part of the problem*, because continuity of heat flux across the separating surface holds, in this case the surface of our meat, or $-\kappa_a \frac{\partial \tilde{T}_a}{\partial \tilde{\vartheta}} = -\kappa_m \frac{\partial \tilde{T}_m}{\partial \tilde{\vartheta}}$ at $\partial\Omega_m$. We will go more in depth on this in Section 3.4, but for now we assume the veracity of this statement.

As for initial conditions, initially the background velocity field is at rest, while the temperature of air is equal to the ambient one.

2.5 The true model

Combining all these results; (2.2), (2.3), (2.4), (2.5), as well as the observations made in the previous subsections, an all-encompassing initial/boundary-value PDE problem modelling our setup, is given by,

$$\left\{ \begin{array}{l} \text{Inside meat} \\ \tilde{t} \geq 0, \tilde{\varrho} \in [0, R], \vartheta \in [0, 2\pi] \\ \text{Periodicity in } \vartheta \end{array} \right. \left\{ \begin{array}{l} \frac{\partial \tilde{T}_m}{\partial \tilde{t}} = D_m \tilde{\nabla}^2 \tilde{T}_m \\ -\kappa_m \frac{\partial \tilde{T}_m}{\partial \tilde{\varrho}} = \tilde{H}_m(\vartheta - \Theta(\tilde{t}))(\tilde{T}_m(\tilde{t}, R, \vartheta - \Theta(\tilde{t})) - \tilde{T}_a(\tilde{t}, R, \vartheta - \Theta(\tilde{t}))) \\ + (2\sigma L_f R) \arctan\left(\frac{2L}{h}\right) (\tilde{T}_m^4(\tilde{t}, R, \vartheta - \Theta(\tilde{t})) - T_H^4) \\ \tilde{T}_m(0, \tilde{\varrho}, \vartheta) = T_\infty \end{array} \right. \\ \left. \begin{array}{l} \text{Outside meat} \\ \tilde{t} \geq 0, \tilde{x} \in [-L, L] \times [-h, c] \setminus \Omega_m \\ \text{Periodicity in } \tilde{x} \end{array} \right. \left\{ \begin{array}{l} \frac{\partial \tilde{T}_a}{\partial \tilde{t}} + (\tilde{\vec{u}}_a \cdot \tilde{\vec{\nabla}}) \tilde{T}_a = D_a \tilde{\nabla}^2 \tilde{T}_a \\ \frac{\partial \tilde{\vec{u}}_a}{\partial \tilde{t}} + (\tilde{\vec{u}}_a \cdot \tilde{\vec{\nabla}}) \tilde{\vec{u}}_a = -\frac{1}{\rho_0} \tilde{\nabla} \tilde{p} + \nu \tilde{\nabla}^2 \tilde{\vec{u}}_a + (1 - \alpha(\tilde{T}_a - T_\infty)) \vec{g} \\ \tilde{\vec{\nabla}} \cdot \tilde{\vec{u}}_a = 0 \\ \tilde{T}_a = T_H \text{ and } \tilde{\vec{u}}_a = \vec{0}, \text{ at } y = -h \\ \tilde{T}_a = T_\infty \text{ and } \tilde{\vec{u}}_a \cdot \hat{e}_y = 0, \frac{\partial \tilde{\vec{u}}_a}{\partial \tilde{y}} \cdot \hat{e}_x = 0, \text{ at } y = c \\ -\kappa_a \frac{\partial \tilde{T}_a}{\partial \tilde{\varrho}} = -\kappa_m \frac{\partial \tilde{T}_m}{\partial \tilde{\varrho}}, \text{ at } \partial \Omega_m \\ \tilde{\vec{u}}_a = \vec{\omega} \times \tilde{\vec{x}}, \text{ at } \partial \Omega_m \\ \tilde{T}_a(0, \tilde{x}, \tilde{y}) = T_\infty \text{ and } \tilde{\vec{u}}_a(0, \tilde{x}, \tilde{y}) = \vec{0}. \end{array} \right. \quad (2.6)$$

The setting we have is clearly illustrated in Figure 2.

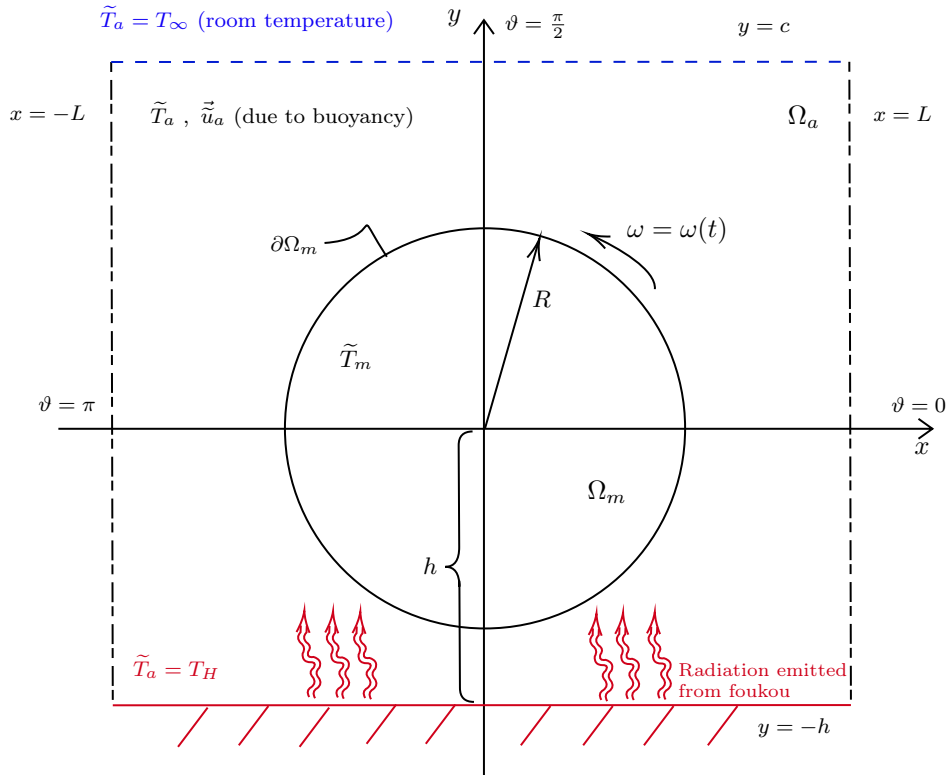


Figure 2: A depiction of the (nearly) all-encompassing model

In the next section we will make some crucial simplifications as to be able to solve this problem. Before that, we proceed with non-dimensionalisation of (2.6) for completion purposes.

2.6 Non-dimensionalisation of the true model (2.6)

We define the following dimensionless coordinate transformations. In the left hand side are the dimensionless counterparts of the quantities in the right hand side. The reciprocal of the scalar appearing in the right hand side is the respective scale of the dimensional quantity with respect to the dimensionless one.

$$\begin{aligned}\varrho &= \frac{1}{R} \tilde{\varrho} \\ \vec{x} &= \frac{1}{R} \tilde{\vec{x}} \\ t &= \frac{D_m}{R^2} \tilde{t} \\ T_m(t, \varrho, \vartheta) &= \frac{\tilde{T}_m(\tilde{t}, \tilde{\varrho}, \vartheta) - T_\infty}{\Delta T}, \text{ where } \Delta T = T_H - T_\infty \\ T_a(t, \varrho, \vartheta) &= \frac{\tilde{T}_a(\tilde{t}, \tilde{\varrho}, \vartheta) - T_\infty}{\Delta T} \\ \vec{u}_a &= \frac{R}{D_m} \tilde{\vec{u}}_a \\ p &= \frac{R^2}{\nu \rho_0 D_m} \tilde{p}\end{aligned}$$

We mention here the rationale behind our choice of time scale. Since we are mainly concerned with the dynamics and evolution of the temperature field inside the meat slab, we choose our time scale to be the characteristic time for heat diffusion for the "Inside meat" part of the problem, $\frac{R^2}{D_m}$, instead of the other one. This time scale is an approximation of the expected time that it takes for the equilibrium state to be reached, and it's the best time scale to use for analysis and observance of the thermal diffusion happening inside our meat slab. We note that in this dimensionless time variable, 1 dimensionless unit of time, corresponds to $\frac{R^2}{D_m}$ seconds in the dimensional system. Usually this value is in the order of $\mathcal{O}(10^6)$, making numerical simulations short, while being able to observe the long-time dynamics of our model efficiently.

With this change of variables, we get the dimensionless form of (2.6),

$$\left\{ \begin{array}{l} \text{Inside meat} \\ t \geq 0, \varrho \in [0, 1], \vartheta \in [0, 2\pi] \\ \text{Periodicity in } \vartheta \\ T_m(0, \varrho, \vartheta) = 0 \end{array} \right. \quad \left\{ \begin{array}{l} \frac{\partial T_m}{\partial t} = \nabla^2 T_m \\ -\frac{\partial T_m}{\partial \varrho} = H_m(\vartheta - \Theta(t))(T_m(t, 1, \vartheta - \Theta(\tilde{t})) - T_a(t, 1, \vartheta - \Theta(t))) \\ + \frac{2\Delta T \sigma L_f R^2}{\kappa_m} \arctan\left(\frac{2L}{h}\right) ((\Delta T \cdot T_m(t, 1, \vartheta - \Theta(t)) + T_\infty)^4 - T_H^4) \\ \frac{DT_a}{Dt} = \frac{D_a}{D_m} \nabla^2 T_a \\ \frac{D_m}{\nu} \frac{D\vec{u}_a}{Dt} = -\nabla p + \nabla^2 \vec{u}_a + \left(\frac{D_m}{\nu F r^2} - Ra T_a \right) \hat{e}_y \\ \vec{\nabla} \cdot \vec{u}_a = 0 \\ T_a = 1 \text{ and } \vec{u}_a = \vec{0}, \text{ at } y = -\frac{h}{R} \\ T_a = 0 \text{ and } \vec{u}_a \cdot \hat{e}_y = 0, \frac{\partial \vec{u}_a}{\partial y} \cdot \hat{e}_x = 0, \text{ at } y = \frac{c}{R} \\ -\kappa_a \frac{\partial T_a}{\partial \varrho} = -\kappa_m \frac{\partial T_m}{\partial \varrho}, \text{ at } \partial \Omega_m \\ \vec{u}_a = 2\pi Ro(\hat{e}_z \times \vec{x}), \text{ at } \partial \Omega_m \\ T_a(0, x, y) = 0 \text{ and } \vec{u}_a(0, x, y) = \vec{0}, \end{array} \right. \quad (2.7)$$

where we have the dimensionless convection heat transfer coefficients $H_m = \frac{R \tilde{H}_m}{\kappa_m}$ and $H_a = \frac{R \tilde{H}_a}{\kappa_a}$, and the following five dimensionless numbers:

- (i) $\frac{D_a}{D_m}$ - Ratio between the thermal diffusivity of air to meat.
- (ii) $\frac{\nu}{D_m}$ - Ratio between the momentum diffusion (kinematic viscosity) of air and heat diffusion of the meat.
Not to be confused with the *Prandtl number* of air, $Pr_a = \frac{\nu}{D_a}$.
- (iii) $Fr^2 = \frac{D_m^2}{gR^3}$ - *Froude number*, which is the ratio of the flow's inertia to the external gravitational field, or $\frac{U^2/L}{g}$, where $U = \frac{D_m}{R}$ is the characteristic velocity and $L = R$ is the characteristic length. The reciprocal of the square of the Froude number is also known as the *Richardson number*, and it describes the effect of buoyancy on flow stability as the ratio of potential over kinetic energy.
- (iv) $Ra = \frac{g\Delta T R^3}{T_\infty \nu D_m}$ - *Rayleigh number*, where its physical interpretation is the ratio between the buoyancy forces and viscous forces, which we can see from,

$$\frac{\text{Buoyancy forces}}{\text{Viscous forces}} = \frac{g\Delta\rho}{\mu D_m / R^3} = \frac{g\rho_0 \alpha \Delta T R^3}{\mu D_m} = \frac{g\Delta T R^3}{T_\infty \nu D_m},$$

where $\mu = \nu \rho_0$ is the dynamic viscosity of the fluid. Notice that the assumption of a perfect gas is made for our setting, i.e. $\alpha = 1/T_\infty$, as well as the fact that $\Delta\rho = \alpha\rho_0\Delta T$ from the Boussinesq approximation.

- (v) $Ro = \frac{fR^2}{D_m}$ ($\vec{\omega} = \omega \hat{e}_z = 2\pi f \hat{e}_z$, where \hat{e}_z is parallel to the skewer, i.e. perpendicular to our plane) - *Roshko number*, which describes the oscillating flow mechanisms due to the flow around the rotating meat slab.

If now the values that we have for our physical parameters lead us to the observation that,

$$H_r = \frac{R\tilde{H}_r}{\kappa_m} = \frac{2\sigma L_f R^2}{\kappa_m} \arctan\left(\frac{2L}{h}\right) (T_H^2 + \tilde{T}^2(\tilde{t}, R, \vartheta - \Theta(\tilde{t}))) (T_H + \tilde{T}(\tilde{t}, R, \vartheta - \Theta(\tilde{t}))) \ll H_m,$$

in order of magnitude, and because of the Strong Maximum Principle for the convection-diffusion PDE (see Section 7.1.4 of [18]), which tells us that $\tilde{T}_a \leq T_H$, or $T_a \leq 1$, then *radiation can be omitted from our model, since it wouldn't be a dominant factor of heat transfer*, simplifying the model even more. We will expand on this in the next section, where we will present a simplified model for extraction of analytical as well as numerical results, via simulations in *Dedalus* (see [27]), where radiation is ignored completely.

3 The simplified model — Heat transfer in Taylor-Couette flow

While the model (2.7) is relatively close to reality, it is too cumbersome to work with, not only analytically but also numerically as well. As such, some further simplifications are warranted as to arrive to a simplified model that we can work with.

For a start, we assume that radiation is indeed a negligible form of heat transfer compared to conduction and natural convection. In addition, instead of having a mix of Cartesian and polar coordinates, we proceed by observing that a somewhat equivalent model is one where the foukou is circular and surrounds the meat slab; We can think of it as a hollow (semi-)cylinder with its axis parallel to the skewer, with no top or bottom, and that the meat slab rotates inside it, thus creating an annular geometry, with the "Outside meat" hollow region's heat transfer being driven by buoyancy and natural convection, while the "Inside meat" region's heat transfer being purely driven by conduction.

To do this in a way that would simulate the reality as truthfully as possible, we would enforce on this circular foukou surface, from $\vartheta \approx 0$ to $\approx \pi$ a heat distribution of $\approx T_\infty$, and in a transition layer of rapid variation of width $\sqrt{\eta}$ at $\vartheta \approx 0$ and $\vartheta \approx \pi$ (where these regions function as the "periodic-walls" we had in the true model, $x = \pm L$), we jump to a temperature of $\approx T_H$ from $\vartheta \approx \pi$ to $\approx 2\pi$, and periodically do so in a *smooth* manner, as to simulate the bottom and top layer in the outside domain of our true model (2.6), which was driven by Rayleigh-Bernard natural convection. This will be the outside boundary condition for \tilde{T}_a in this model. Such a function is given by,

$$\varphi_\eta(\vartheta) = T_\infty + \frac{T_H - T_\infty}{2} - \frac{T_H - T_\infty}{\pi} \arctan\left(\frac{\sin \vartheta}{\eta}\right), \quad (3.1)$$

with $\eta > 0$ (φ_η is called a *smooth square wave*). This function is 2π periodic, with a minimum value of $\approx T_\infty$ from ≈ 0 to $\approx \pi$, and a maximum value of $\approx T_H$ from $\approx \pi$ to $\approx 2\pi$, is infinitely differentiable (smooth), and at the limit of $\eta \rightarrow 0^+$, it converges pointwise to the discontinuous square wave. We can also see that in the inner layers of rapid variation which occur at $\pi\mathbb{Z}$, if we take the derivative of φ_η to find $\varphi'_\eta(\vartheta) = -\frac{(T_H - T_\infty)\eta \cos \vartheta}{\pi(\eta^2 + \sin^2 \vartheta)}$,

and making the change of variables to $x = \frac{\pi - \vartheta}{\delta}$, where $\delta = \delta(\eta)$ and $\delta \rightarrow 0^+$ as $\eta \rightarrow 0^+$ (due to periodicity and symmetry we only need to look at one such point to see the inner layer behaviour, let's say $\vartheta = \pi$), then if $\delta = \mathcal{O}(\sqrt{\eta})$, we have that as $\eta \rightarrow 0^+$, then $\varphi_\eta(x) < \infty$, which gives us a dominant balance. As such, the inner layer of $\varphi_\eta(\vartheta)$ is of width $\mathcal{O}(\sqrt{\eta})$. A plot of φ_η for $\eta = 10^{-3}$ is given below in Figure (3), for $T_\infty = 0$ and $T_H = 1$ - we name this function $\varphi_{\eta,d}$ to indicate that it is the dimensionless counterpart of φ_η . The "jumps" are smooth, making $\varphi_{\eta,d}(\vartheta)$ infinitely differentiable.

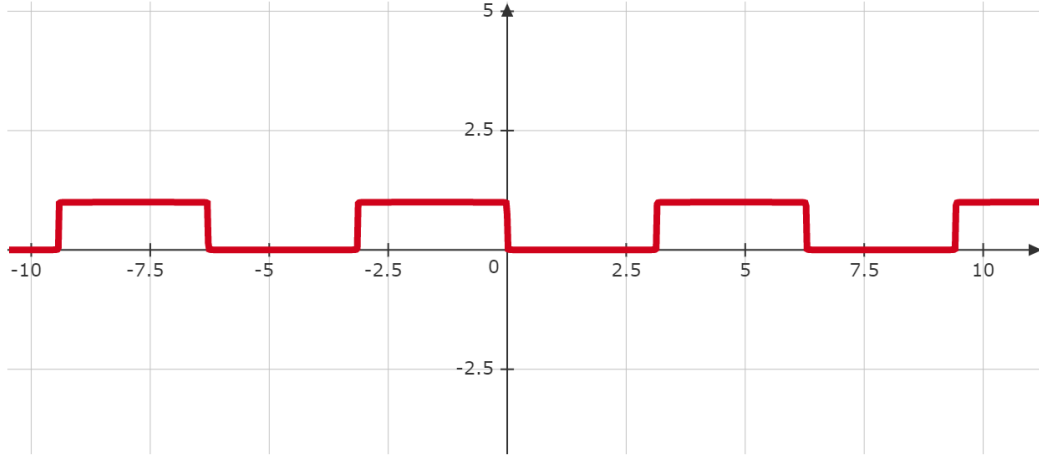


Figure 3: Plot of $\varphi_{\eta,d}(\vartheta) = \frac{1}{2} - \frac{1}{\pi} \arctan \left(\frac{\sin \vartheta}{\eta} \right)$ for $\eta = 0.001$

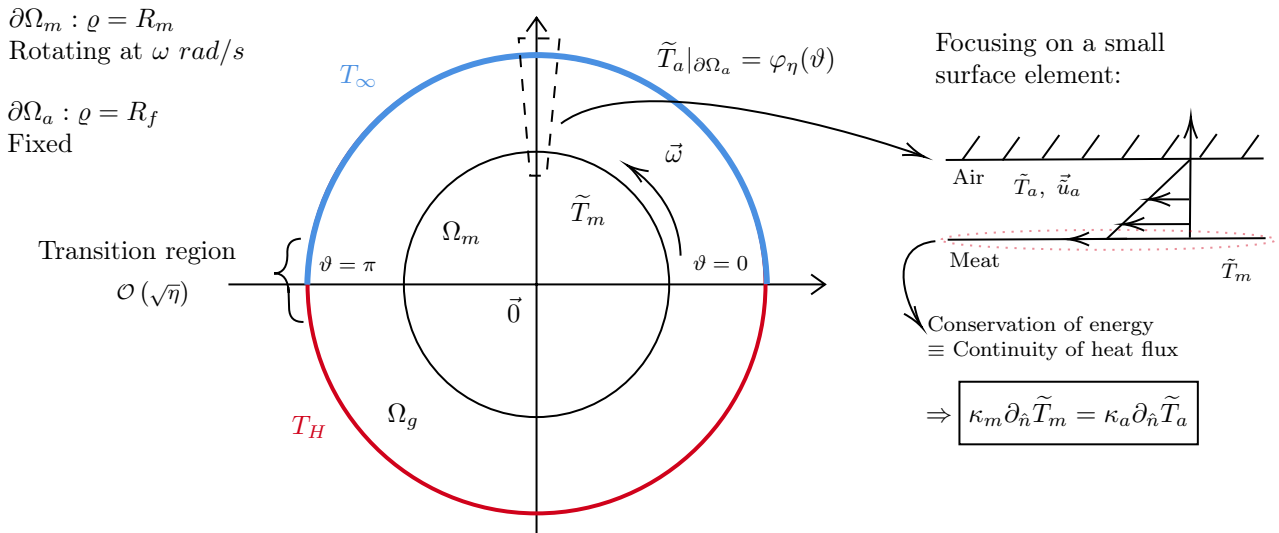


Figure 4: Simplified model of Taylor-Couette flow with a combination of heat transfer in both domains

Before we define the simplified model that will describe our setup, we would first like to reference the continuity of heat flux across a surface, which we mentioned briefly in the previous section; The continuity is given in (3.2), and is also showcased in Figure 4, which depicts our simplified model. A small caveat, is that in the case of our true model, ((2.6) and (2.7)), because of the consideration of radiation being "one-sided" i.e. radiation is significant only from the fokou to the souvla, compared to the radiative heat being lost from the souvla and transferred to the surrounding environment, we have $H_a \neq H_m$, where H_a would be the (dimensionless) convective heat transfer coefficient of air, where in terms of H_a , the Robin boundary condition for T_a would be purely explained by Newton's Law of heating/cooling. This deviates from the ideal case which

is the one we will consider for this simplified model.

First recall the definition of heat flux; The local heat flux at a point P through S , is the rate at which thermal energy flows through the surface S at this point P , per unit surface area, per unit time. It is shown in *Section 1.3, p. 4, of [1]*, that the heat flux across the tangent plane at a point P of a surface element (of a regular surface in the differential geometry sense), varies continuously with the position of the point P , granted that the (oriented) surface's unit-normal vector field (or Gauss map) is continuous. This shows that *the heat flux is continuous over the surface of separation of two media*, let's say of (isotropic, uniform, and constant) heat conductivities κ_i , and temperature fields v_i , $i = 1, 2$. Secondly, recall the differential form of Fourier's Heat Law of Conduction, that states that the local heat flux is equal to the negative local gradient of the product of the rank-2 tensor of heat conduction and temperature, where for isotropic and uniform media reduces down to $\vec{q}_i = -\kappa_i \nabla v_i$, $i = 1, 2$. Combining these two results, if \hat{n} is the outward pointing unit-normal vector field of the separating surface, we have that along the separation surface,

$$\kappa_1 \frac{\partial v_1}{\partial \hat{n}} = \kappa_2 \frac{\partial v_2}{\partial \hat{n}}. \quad (3.2)$$

If we can assume that at the surface of separation the temperatures in the two media are the same, or that the surface of separation is isothermal, then we would have in addition to the above that $v_1 = v_2$ at the surface. But, this assumption is only valid for very intimate contact, such as a soldered joint or in the presence of thermal paste. In all other cases, even for surfaces that look flat to the naked eye and are lightly pressed together (it is well-known that pressure affects positively the coefficient of heat transfer in convection and conduction), the heat transfer between the two media across the surface of separation is described by the rate of heat transfer through the surface and it is proportional to their temperature difference, or,

$$-\kappa_1 \frac{\partial v_1}{\partial \hat{n}} = -\kappa_2 \frac{\partial v_2}{\partial \hat{n}} = H(v_1 - v_2), \quad (3.3)$$

where H is the the convection-conduction heat transfer coefficient of the surface, and could depend on time, point on the surface, and even temperature. This is exactly, Newton's Law of heating/cooling. For small temperature differences it can also incorporate radiation, but we ignore this contribution in this simplified model. We will use this fact for when we will define our boundary conditions, where we note that the outward facing unit-normal is in the increasing radial direction for our setup.

As we did with our true model, we will put in place the equations, boundary conditions, and initial conditions for this simplified model in their dimensional form, and in the next subsection we will proceed with their non-dimensionalisation. Our setup is characterised by a *Taylor-Couette (planar) flow*, which includes heat transfer not only in the hollow region but also inside the bulk solid region, which in our case is our meat slab or souvla cross section. The setup we have is given in Figure 4.

We start with the "Inside meat" domain, Ω_m , which is for $\tilde{\varrho} \in [0, R_m]$, where R_m is the radius of the meat. We have that the temperature field \tilde{T}_m is again described by the usual Heat equation (2.2). At the boundary, which is the surface of the meat, we use (3.2) and (3.3), where we let the convection-conduction heat transfer coefficient, \tilde{H} , to depend only on the azimuthial coordinate, and as such has no temperature dependence. We also assume that it is rotating counterclockwise, with some azimuthial displacement function $\Theta(\tilde{t})$, and so $\vartheta(\tilde{t}) = \vartheta - \Theta(\tilde{t})$, where $\Theta'(\tilde{t}) = \omega$, is the *constant* angular velocity of the meat slab. For an initial condition, we assume the ambient one (room temperature), T_∞ .

As for the "Outside meat" domain, Ω_a , which is for $\tilde{\varrho} \in (R_m, R_f)$, where R_f is the radius of the circular now foukou (making $R_f - R_m = h$ the distance between the meat and the charcoal surface). We assume that the values of our physical parameters, are such that laminar flow is a good approximation of the velocity field in Ω_a (small turbulence), which we see showcased in Figure 4 via the velocity boundary layer. We again assume that the background flow $\tilde{\vec{u}}_a$, is modelled by the incompressible Navier-Stokes equations, that incorporate the Boussinesq approximation of natural convection, and that the temperature field \tilde{T}_a in this region is being driven by this velocity field. As for the boundary conditions, for \tilde{T}_a we again use (3.2) and (3.3) (or the continuity of heat flux) on the surface of the meat, and the temperature field φ_η for the surface of the foukou, and for the velocity field we enforce no slip boundary conditions on both surfaces. For initial conditions, we assume that initially the air temperature is equal to the ambient one, T_∞ , and that the velocity field is at rest.

Combining these remarks, as well as (2.2), (2.3), (2.4), a simplified initial/boundary-value PDE problem

that is "similar" to the all-encompassing one, is given by,

$$\left\{ \begin{array}{l} \text{Inside meat} \\ \tilde{t} \geq 0, \quad \tilde{\varrho} \in [0, R_m], \quad \vartheta \in [0, 2\pi] \\ \text{Periodicity in } \vartheta \\ \\ \frac{\partial \tilde{T}_m}{\partial \tilde{t}} = D_m \tilde{\nabla}^2 \tilde{T}_m \\ -\kappa_m \frac{\partial \tilde{T}_m}{\partial \tilde{\varrho}} = \tilde{H}(\vartheta - \Theta(\tilde{t})) (\tilde{T}_m(\tilde{t}, R_m, \vartheta - \Theta(\tilde{t})) - \tilde{T}_a(\tilde{t}, R_m, \vartheta - \Theta(\tilde{t}))) \\ \tilde{T}_m(0, \tilde{\varrho}, \vartheta) = T_\infty \\ \\ \text{Outside meat} \\ \tilde{t} \geq 0, \quad \tilde{\varrho} \in [R_m, R_f], \quad \vartheta \in [0, 2\pi] \\ \text{Periodicity in } \vartheta \\ \\ \frac{\partial \tilde{T}_a}{\partial \tilde{t}} + (\vec{u}_a \cdot \tilde{\nabla}) \tilde{T}_a = D_a \tilde{\nabla}^2 \tilde{T}_a \\ \frac{\partial \vec{u}_a}{\partial \tilde{t}} + (\vec{u}_a \cdot \tilde{\nabla}) \vec{u}_a = -\frac{1}{\rho_0} \tilde{\nabla} \tilde{p} + \nu \tilde{\nabla}^2 \vec{u}_a + (1 - \alpha(\tilde{T}_a - T_\infty)) \vec{g} \\ \tilde{\nabla} \cdot \vec{u}_a = 0 \\ \tilde{T}_a = \varphi_\eta(\vartheta) \text{ and } \vec{u}_a = \vec{0}, \text{ at } \tilde{\varrho} = R_f \\ -\kappa_a \frac{\partial \tilde{T}_a}{\partial \tilde{\varrho}} = -\kappa_m \frac{\partial \tilde{T}_m}{\partial \tilde{\varrho}}, \text{ at } \tilde{\varrho} = R_m \\ \vec{u}_a = \vec{\omega} \times \tilde{\varrho}, \text{ at } \tilde{\varrho} = R_m \\ \tilde{T}_a(0, \tilde{\varrho}, \tilde{\vartheta}) = T_\infty \text{ and } \vec{u}_a(0, \tilde{\varrho}, \tilde{\vartheta}) = \vec{0}. \end{array} \right. \quad (3.4)$$

3.1 Non-dimensionalisation of the simplified model (3.4)

Let $h = R_f - R_m$ be the width of the gap, and $\lambda = \frac{R_m}{R_f} < 1$ the dimensionless radius ratio. We define the following dimensionless coordinate transformations:

- $\varrho = \frac{1}{h} \tilde{\varrho}$ • $\vec{u}_a = \frac{h}{D_m} \vec{u}_a \bullet t = \frac{D_m \tilde{t}}{h^2} \bullet T_m(t, \varrho, \vartheta) = (\tilde{T}_m(\tilde{t}, \tilde{\varrho}, \vartheta) - T_\infty) / \Delta T$, where $\Delta T = T_H - T_\infty$
- $T_a(t, \varrho, \vartheta) = (\tilde{T}_a(\tilde{t}, \tilde{\varrho}, \vartheta) - T_\infty) / \Delta T$ • $p = \frac{h^2}{\nu \rho_0 D_m} \tilde{p}$.

With this change of variables, we get the dimensionless form of (3.4),

$$\left\{ \begin{array}{l} \text{Inside meat} \\ t \geq 0, \quad \varrho \in \left[0, \frac{\lambda}{1-\lambda}\right], \quad \vartheta \in [0, 2\pi] \\ \text{Periodicity in } \vartheta \\ \\ \frac{\partial T_m}{\partial t} = \nabla^2 T_m \\ -\frac{\partial T_m}{\partial \varrho} = H(\vartheta - \Theta(t)) \left(T_m \left(t, \frac{\lambda}{1-\lambda}, \vartheta - \Theta(t) \right) - T_a \left(t, \frac{\lambda}{1-\lambda}, \vartheta - \Theta(t) \right) \right) \\ T_m(0, \varrho, \vartheta) = 0 \\ \\ \text{Outside meat} \\ t \geq 0, \quad \varrho \in \left[\frac{\lambda}{1-\lambda}, 1\right], \quad \vartheta \in [0, 2\pi] \\ \text{Periodicity in } \vartheta \\ \\ \frac{DT_a}{Dt} = \frac{D_a}{D_m} \nabla^2 T_a \\ \frac{D_m D \vec{u}_a}{Dt} = -\nabla p + \nabla^2 \vec{u}_a + \left(\frac{D_m}{\nu F r^2} - Ra T_a \right) (-\sin \vartheta \hat{e}_\varrho - \cos \vartheta \hat{e}_\vartheta) \\ \tilde{\nabla} \cdot \vec{u}_a = 0 \\ T_a = \varphi_{\eta,d}(\vartheta) \text{ and } \vec{u}_a = \vec{0}, \text{ at } \varrho = \frac{1}{1-\lambda} \\ -\kappa_a \frac{\partial T_a}{\partial \varrho} = -\kappa_m \frac{\partial T_m}{\partial \varrho}, \text{ at } \varrho = \frac{\lambda}{1-\lambda} \\ \vec{u}_a = 2\pi Ro \hat{e}_\vartheta, \text{ at } \varrho = \frac{\lambda}{1-\lambda} \\ \tilde{T}_a(0, \varrho, \vartheta) = 0 \text{ and } \vec{u}_a(0, \varrho, \vartheta) = \vec{0}, \end{array} \right. \quad (3.5)$$

where we have the dimensionless convection heat transfer coefficient $H = \frac{h \tilde{H}}{\kappa_m}$, and the five dimensionless numbers that we also saw in (2.7), and analysed thereafter. Note now that the length scale is h instead of R (R_m) in the expressions of our dimensionless numbers.

With this simplified model in hand, we would like to now analyse the "Inside meat" region problem, which is expressed by the usual Heat equation, with homogeneous initial conditions, but with a *rotating Robin boundary condition*. We start our analysis small at first; with a rotating *Dirichlet* boundary condition as to get a feeling of how the solution behaves, and then proceed with the actual problem that we want to inspect. For both settings we will also provide numerical results in Section 7.

4 Toy problem; Circular domain with rotating Dirichlet boundary conditions

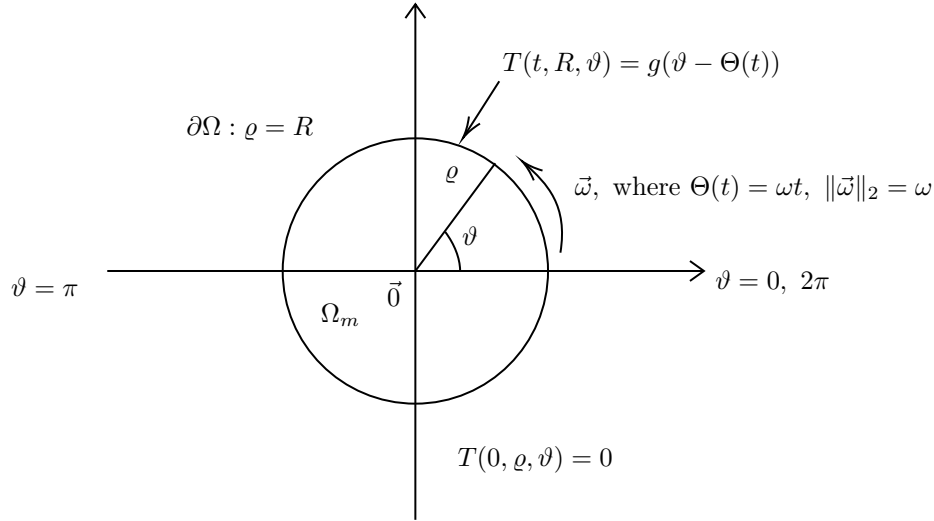


Figure 5: Circular domain with rotating Dirichlet boundary conditions and a fixed initial temperature distribution

We start our analysis in small steps, by first considering the problem of the heat equation in a circular domain, with rotating Dirichlet boundary conditions, and a homogeneous initial condition. The analysis we make can be easily extended to the problem with a general, non-constant, initial temperature profile, $T(0, \rho, \theta) = T_0(\rho, \theta)$, as we will notice in later stages of our analysis. In addition, the simplification we made of a circular domain instead of an annular one (i.e. letting the radius of the skewer to be equal to zero) is not needed as well. A similar analysis to the one we make here can be extended to this generalisations as well. Even if we incorporate the skewer as a force term heat sink in our equation, the analysis can still be extended to include that. For all of these instances of generalised assumptions, we will cite the references needed to make these extensions at the end of this section.

We will be working with the dimensionless equations that we got for the "Inside meat" region part of the problem in (3.5). We let $T_m \rightsquigarrow T$, and $\frac{\lambda}{1-\lambda} \rightsquigarrow R$ for ease of notation. We will analyse the following initial/boundary-value problem in this section,

$$\begin{cases} \frac{\partial T}{\partial t} = \frac{\partial^2 T}{\partial \rho^2} + \frac{1}{\rho} \frac{\partial T}{\partial \rho} + \frac{1}{\rho^2} \frac{\partial^2 T}{\partial \theta^2}, & t > 0, 0 \leq \rho < R, \theta \in [0, 2\pi] \\ T(t, R, \theta) = g(\theta - \Theta(t)), & \theta \in [0, 2\pi], t \geq 0 \\ T(0, \rho, \theta) = 0, & 0 \leq \rho \leq R, \theta \in [0, 2\pi], \end{cases} \quad (4.1)$$

where consistency between the initial and boundary data is assumed, although not required due to the properties of smoothness of the solution to the heat equation, for bounded initial and boundary data (see [18], Chapter 2.3), even in the presence of discontinuities. We also assume the periodicity in θ of T (and all its (mixed) derivatives of any order), due to our geometry, as well as the periodicity of g in its argument, both with a period of 2π . g should not be confused with the gravitational acceleration vector, \vec{g} , and its magnitude.

We now make a change of variables to a rotating frame of reference, where "we move with the boundary condition". This will leave the Laplacian operator unchanged (after all, it is the only second order elliptic operator that is invariant under rotations and translations), but it will change the temporal derivative. Specifically

we make the change of variables,

$$\begin{aligned} t &\mapsto \hat{t} \\ \varrho &\mapsto \hat{\varrho} := \varrho \\ \vartheta &\mapsto \hat{\vartheta} := \vartheta - \Theta(\hat{t}) \\ T(t, \varrho, \vartheta) &\mapsto T(\hat{t}, \hat{\varrho}, \hat{\vartheta}) := \hat{T}(\hat{t}, \hat{\varrho}, \hat{\vartheta}), \end{aligned}$$

where after making this change in (4.1), and dropping the hats for simplified notation, we end up with a model of "stationary" boundary conditions, as we are in the rotational frame of reference, with the interior of the domain now "rotating", leading to a rotating version of the Heat equation (convection-diffusion equation in polar coordinates) as,

$$\begin{cases} \frac{\partial T}{\partial t} = \nabla^2 T - \omega \frac{\partial T}{\partial \vartheta}, & t > 0, 0 \leq \varrho < R, \vartheta \in [0, 2\pi] \\ T(t, R, \vartheta) = g(\vartheta), & \vartheta \in [0, 2\pi], t \geq 0 \\ T(0, \varrho, \vartheta) = 0, & 0 \leq \varrho \leq R, \vartheta \in [0, 2\pi]. \end{cases} \quad (4.2)$$

It is important to remember that this is the "hat" problem; To go back to our original problem we use the inverse of the change of variables we made.

4.1 Existence and uniqueness of solutions to (4.2)

Our rotating initial/boundary-value problem, (4.2), is a homogeneous parabolic equation, of the form $\frac{\partial T}{\partial t} + \mathcal{L}T = \frac{\partial T}{\partial t} - \nabla^2 T + \omega \frac{\partial T}{\partial \vartheta} = 0$, where \mathcal{L} is an elliptic operator *in polar coordinates*, where in non-divergence form it is defined as,

$$\mathcal{L} = -\frac{\partial^2}{\partial \varrho^2} - \frac{1}{\varrho^2} \frac{\partial^2}{\partial \vartheta^2} - \frac{1}{\varrho} \frac{\partial}{\partial \varrho} + \omega \frac{\partial}{\partial \vartheta},$$

accompanied by non-homogeneous boundary conditions. By looking at $u = T - g$, then over the parabolic cylinder with a terminating time of t_f , $U_{t_f} = [0, t_f] \times [0, R] \times [0, 2\pi]$, we can transform this to a non-homogeneous parabolic equation but with homogeneous Dirichlet boundary conditions, of the form (1) of [18], Chapter 7.1, p. 372. This is now a convection-diffusion parabolic equation, with the Laplacian term describing the diffusion and the $\omega \frac{\partial T}{\partial \vartheta}$ term describing the transport or convection. In Chapter 7.1 of [18] the existence and uniqueness of weak solutions over Sobolev spaces to these equations under the Galerkin formulation is studied and proved under mild assumptions on g (after we transition to the u problem) of square integrability over the parabolic cylinder, and in cases of enough regularity in g , we can then achieve repeated energy estimates and regularity results on the weak solutions, similar to Weyl's lemma for elliptic problems, to then construct a unique solution to the u problem which in turn gives a unique solution to our problem, (4.2), in the parabolic cylinder. So while analytically solving the problem with usual means is unfeasible, we can still construct a strong solution to our problem by working over Sobolev energy spaces and constructing a sequence of weak solutions that in some manner recover the solution to (4.2).

Weak and Strong Maximum principle results are also proved in Section 7.1.4 of [18], which also apply to our initial/boundary-value problem, if enough regularity on g is assumed, since our domain is simply-connected with a C^1 boundary.

4.2 Steady temperature profile/Equilibrium state of (4.2)

We proceed with finding the steady state of (4.2), T_S , which will be the long-term behaviour of the solution to (4.2). Using the elliptic operator we defined above, $\mathcal{L} = -\nabla^2 + \omega \frac{\partial}{\partial \vartheta}$, we are looking for the solution to the steady state problem,

$$\begin{cases} \mathcal{L}T_S = 0, & 0 \leq \varrho < R, \vartheta \in [0, 2\pi] \\ T_S(R, \vartheta) = g(\vartheta), & \vartheta \in [0, 2\pi], \end{cases} \quad (4.3)$$

where T_S (and all its (mixed) derivatives of any order) are periodic in ϑ . We define the azimuthial average operator $\langle \cdot \rangle_\vartheta = \frac{1}{2\pi} \int_0^{2\pi} \cdot d\vartheta$. Taking the azimuthial average of both the equation and boundary condition of (4.3), and using the periodicity of T_S in ϑ , gives us,

$$\begin{cases} \nabla^2 \overline{T_S} = 0, & 0 \leq \varrho < R \\ \overline{T_S}(R) = \bar{g}, \end{cases}$$

where $\overline{T_S} = \langle T_S \rangle_\vartheta$, and $\overline{g} = \langle g \rangle_\vartheta$. This Laplace equation boundary-value problem does have a unique solution, due to the constant Dirichlet boundary condition, and it is,

$$\overline{T_S}(\varrho) = \overline{g}, \quad (4.4)$$

which is essentially the solubility condition (*Fredholm's alternative*) to (4.3), which tells us that in this Dirichlet boundary-value problem, *the long term azimuthal average temperature should be equal to the average value of g over $[0, 2\pi]$* , which does agree with our intuition.

4.3 Summary of the asymptotic expansion of the solution to (4.2), while $\omega \rightarrow \infty$

As we mentioned in Subsection 4.1, solving (4.2) via usual means is not feasible, and we instead need to fall back to Galerkin type weak solutions that approximate the strong solution in an energy Sobolev space; Under some mild assumptions such a weak solution can even coincide with the desired solution. What we will do here is try to find an asymptotic expansion of the solution to our problem, T , for when $\omega \rightarrow \infty$.

We define our dimensional (s^{-1} units) asymptotic scale as $\varepsilon = \frac{1}{\omega}$. Now our problem via the small parameter becomes,

$$\begin{cases} \varepsilon \frac{\partial T}{\partial t} = \varepsilon \nabla^2 T - \frac{\partial T}{\partial \vartheta}, & t > 0, 0 \leq \varrho < R, \vartheta \in [0, 2\pi] \\ T(t, R, \vartheta) = g(\vartheta), & \vartheta \in [0, 2\pi], t \geq 0 \\ T(0, \varrho, \vartheta) = 0, & 0 \leq \varrho \leq R, \vartheta \in [0, 2\pi]. \end{cases} \quad (4.5)$$

If we were to assume a regular perturbation expansion of T as a power series in ε , $T(t, \varrho, \vartheta) = \sum_{n=0}^{\infty} \varepsilon^n T_n(t, \varrho, \vartheta)$, then for the zeroth leading order term we would have the following boundary-value problem;

$$\partial_\vartheta T_0 = 0, \quad T_0(t, R, \vartheta) = g(\vartheta),$$

which for general non-constant functions g , it is non-solvable. Notice also the shorthand notation used for partial derivatives for ease of notation, which we will use for the rest of the paper. The non-solvability of the unperturbed problem is attributed to the existence of a boundary layer of some thickness $\mathcal{O}(\delta)$, where $\delta = \delta(\varepsilon)$; $\delta \xrightarrow{\varepsilon \rightarrow 0^+} 0^+$, close to $\varrho = R$. This means the perturbation expansion of T is singular, and its zeroth order term differs from the "solution" of the unperturbed problem, which in this case doesn't even exist.

Due to the geometry, we expect a boundary layer to form close to the boundary $\varrho = R$, of thickness $\mathcal{O}(\delta)$. This splits our domain Ω_m to the regular and boundary layer regions, which for conventional reasons we name the *bulk* and *circumfluent* regions respectively, which we expect to be of the form $\varrho \in [0, R - \mathcal{O}(\delta))$ and $\varrho \in (R - \mathcal{O}(\delta), R]$, correspondingly. Determining the thickness of the boundary layer region is done via the notion of a distinguished limit, which is nothing more than a dominant balance argument. We define now the *circumfluent variable* $X = \frac{R - \varrho}{\delta}$. In the circumfluent region, this is a better variable used to describe the behaviour of T than ϱ , since T would vary much slowly in X than in ϱ . This also gives us $\varrho = R - \delta X$, and $\partial_\varrho = -\frac{1}{\delta} \partial_X$, and so our PDE in (4.5) becomes,

$$\varepsilon \partial_t T = \frac{\varepsilon}{\delta^2} \partial_X^2 T - \frac{\varepsilon}{\delta(R - \delta X)} \partial_X T + \frac{\varepsilon}{(R - \delta X)^2} \partial_\vartheta^2 T - \partial_\vartheta T. \quad (4.6)$$

The dominant term in this case is $\partial_\vartheta T$, and so we would like $\frac{\varepsilon}{\delta^2} \sim 1$, which gives the measure of the thickness to be $\delta = \mathcal{O}(\sqrt{\varepsilon})$, as $\varepsilon \rightarrow 0^+$. The other cases, $\delta \ll \sqrt{\varepsilon}$ and $\delta \gg \sqrt{\varepsilon}$ (or equivalently the other pairs of balance terms), produce the bulk region and an imbalance, respectively. Limits that lead to an imbalance like, $\frac{\varepsilon}{\delta} \sim 1$ or $\frac{\varepsilon}{\delta} \sim \varepsilon$, are fittingly called indistinguished.

And so, in the circumfluent region, we can have a perturbation expansion of the form $T_C = T_{C,0} + \sqrt{\varepsilon} T_{C,1} + \mathcal{O}(\varepsilon)$. We start with the now correct zeroth order term, $T_{C,0}$, which via (4.6) is the solution to the *boundary-value problem*,

$$\mathcal{O}(\varepsilon^0) : \begin{cases} \partial_\vartheta T_{C,0} = \partial_X^2 T_{C,0} \\ T_{C,0}(t, 0, \vartheta) = g(\vartheta), \because X = 0 \equiv \varrho = R, \end{cases}$$

where periodicity in ϑ of $T_{C,0}$ (and its derivatives) is assumed. Although we let $T_{C,0}$ to have a temporal dependency, we wouldn't prescribe it with the initial condition of our problem (in this case a homogeneous

one), for reasons that will be made clear in a bit; Intuitively though, the initial conditions should correspond to the bulk and not the circumfluent region. Proceeding with the method of separation of variables, we assume the separable ansatz $T_{C,0}(t, X, \vartheta) = \mathcal{T}_0(t)\mathcal{X}_0(X)\Psi_0(\vartheta)$, which gives us the spatial and azimuthial separated ODEs,

$$\mathcal{X}_0''(X) = \lambda\mathcal{X}_0(X) \text{ and } \begin{cases} \Psi_0'(\vartheta) = \lambda\Psi_0(\vartheta) \\ \Psi_0(0) = \Psi_0(2\pi), \end{cases}$$

where λ is the separation constant. By the energy method, multiplying the azimuthial equation with $\Psi_0(\vartheta)$, taking the integral from 0 to 2π , and using integration by parts and periodicity, we end up with the solubility condition,

$$\lambda \int_0^{2\pi} \Psi_0^2(\vartheta) d\vartheta = 0.$$

It is then immediate that due to the periodic boundary conditions the separation constant gets quantified over $i\mathbb{Z}$, or $\lambda = im$, $m \in \mathbb{Z}$. This shows that our azimuthial eigenfunctions are $\Psi_0^{(m)}(\vartheta) \propto e^{im\vartheta}$. As for the spatial part, we see that the fundamental solution set of the spatial ODE is $\{e^{\pm(1+i)\sqrt{m}X/\sqrt{2}}\}$ for $m \in \mathbb{N}$ ($\because \sqrt{i} = \pm(1+i)/\sqrt{2}$), $\{e^{\pm(1-i)\sqrt{-m}X/\sqrt{2}}\}$ for $m \in -\mathbb{N}$, and $\{1, X\}$ for $m = 0$. But, here we have an implicit boundary condition on the spatial eigenfunctions, since we would like after we find the zeroth leading order term in the bulk region, to take the intermediate limit in the matching region of $X \rightarrow \infty$, $\varrho \rightarrow R$, $\varepsilon \rightarrow 0^+$, and do an asymptotic match, meaning our solution needs to be bounded. As such, $\mathcal{X}_0^{(m)}(X) \propto e^{-(1+sgn(m)i)\sqrt{|m|}X/\sqrt{2}}$.

Combining our results, we have the following eigenfunction expansion,

$$T_{C,0}(t, X, \vartheta) = \sum_{m \in \mathbb{Z}} \mathcal{T}_0^{(m)}(t) e^{-(1+sgn(m)i)\sqrt{|m|}X/\sqrt{2}} e^{im\vartheta}. \quad (4.7)$$

From the boundary condition we have that $g(\vartheta) = \sum_{m \in \mathbb{Z}} \mathcal{T}_0^{(m)}(t) e^{im\vartheta}$, which shows two things; First, the coefficients $\mathcal{T}_0^{(m)}(t)$ are exactly the Fourier coefficients of g in terms of the orthogonal complex Fourier basis, $\mathcal{T}_0^{(m)}(t) = g_m = \frac{1}{2\pi} \int_0^{2\pi} g(\vartheta) e^{-im\vartheta} d\vartheta$ (which we can also see from Fourier's trick), and that $T_{C,0}$ indeed does not change in time. In addition, for uniform and absolute convergence of this series, we may assume g is regular enough (e.g. Hölder continuous; being L^2 would just give us L^2 -convergence). As such, we end up with,

$$T_{C,0}(X, \vartheta) = \sum_{m \in \mathbb{Z}} g_m e^{-(1+sgn(m)i)\sqrt{|m|}X/\sqrt{2}} e^{im\vartheta}. \quad (4.8)$$

We now proceed with the bulk limit. In that region, we have a regular expansion in terms of a power series in ε , with $T_B = \sum_{n=0}^{\infty} T_{B,n}(t, \varrho, \vartheta) \varepsilon^n$. We begin with the zeroth order term, $T_{B,0}$, which via (4.5) is the solution to the *initial-value* problem,

$$\mathcal{O}(\varepsilon^0) : \begin{cases} \partial_\vartheta T_{B,0} = 0 \\ T_{B,0}(0, \varrho, \vartheta) = 0, \end{cases}$$

where periodicity in ϑ of $T_{B,0}$ (and its derivatives) is assumed. Even in the case of a non-homogeneous initial condition, it would still need to be prescribed here, i.e. enforced on the zeroth order term of the regular expansion of the bulk limit. Here, we can see that $T_{B,0} = T_{B,0}(t, \varrho)$, and that $T_{B,0}(0, \varrho) = 0$. Transitioning now to the intermediate limit or the matching region, where both the bulk and circumfluent solutions are valid, where we can then asymptotically match them, we have,

$$\lim_{X \rightarrow \infty} T_{C,0}(X, \vartheta) = \lim_{\varrho \rightarrow R} T_{B,0}(t, \varrho),$$

where from (4.8) we see that only the zeroth mode survives the limit, and so in $\mathcal{O}(\varepsilon^0)$ we have that $T_{B,0}(t, R) = g_0 \equiv \bar{g} = \langle g \rangle_{\vartheta}$. Notice that this is in accordance so far with (4.4), i.e. the steady state's azimuthial average agrees with the radially symmetric zeroth order bulk limit, at the boundary.

As a general rule of thumb, as mentioned in *Chapter 9, Example 2, p.438-441 of [9]*:

“[...]It is necessary to compute two new terms in the boundary layer expansion for each new term in the outer expansion whenever the thickness of the boundary layer is not $\mathcal{O}(\varepsilon)$, as to be able to do complete asymptotic matching and determine that new term in the outer limit.”

While we could do this here, we will instead take advantage of our geometry, specifically the periodic boundary conditions in the azimuthial coordinate.

Going to the next leading order term in the bulk expansion, we have from (4.5),

$$\mathcal{O}(\varepsilon^1) : \begin{cases} \partial_t T_{B,0} = \nabla^2 T_{B,0} - \partial_\vartheta T_{B,1} \\ T_{B,1}(0, \varrho, \vartheta) = 0, \end{cases}$$

In the same vain as we did with the steady state solution, we take the azimuthial average, $\langle \cdot \rangle_\vartheta$, of the equation, and by using the periodicity of $T_{B,1}$ in ϑ and the fact that $T_{B,0}$ is a function of time and the radial coordinate only, we end up with a Heat equation for $T_{B,0}$, with the initial condition being inherited by our original problem (which in this case is homogeneous), and the boundary condition stemming from the asymptotic match with $T_{C,0}$,

$$\mathcal{O}(\varepsilon^0) : \begin{cases} \partial_t T_{B,0} = \nabla^2 T_{B,0} = \frac{1}{\varrho} \partial_\varrho (\varrho \partial_\varrho T_{B,0}) \\ T_{B,0}(t, R) = \bar{g} \\ T_{B,0}(0, \varrho) = 0. \end{cases}$$

Notice here that due to the radial symmetry of $T_{B,0}$, if we are looking for its steady state we again recover the result of (4.4), but *only* to order $\mathcal{O}(\varepsilon^0)$, which we can see now clearer due to the general "mis-match" of the boundary and initial conditions.

There are several ways to solve this problem now. We could proceed again with separation of variables, or even by taking the Fourier transform in the radial coordinate. As to add to variety, we will solve this via *Laplace transforms*. We will follow the methodology outlined in *Chapter 13.2 of [1]*, by adapting it to our situation.

We start by taking the Laplace transform of the radially symmetric Heat equation that $T_{B,0}$ solves, for $Re(s) > 0$ large enough as for $L\{T_{B,0}\}(s, \varrho) = \int_0^\infty e^{-st} T_{B,0}(t, \varrho) dt$ to converge absolutely. Let this region be $Re(s) \geq \zeta \in \mathbb{R}$, and by using the fact that we have a homogeneous initial condition and properties of the Laplace transform, we have,

$$\partial_\varrho^2 L\{T_{B,0}\} + \frac{1}{\varrho} \partial_\varrho L\{T_{B,0}\} - q^2 L\{T_{B,0}\} = 0 \Leftrightarrow \varrho^2 \partial_\varrho^2 L\{T_{B,0}\} + \varrho \partial_\varrho L\{T_{B,0}\} - \varrho^2 q^2 L\{T_{B,0}\} = 0,$$

where $q^2 = s$. As for the boundary condition, due to the linearity of the Laplace transform and $L\{1\}(s) = \frac{1}{s}$, we have $L\{T_{B,0}\}(s, R) = \frac{\bar{g}}{s}$. The equation above, after the change of variables $y = q\varrho$, becomes *Bessel's modified equation of zeroth order* (in y), which has a fundamental solution set consisting of the zeroth order modified Bessel functions of first and second kind, $\{I_0(q\varrho), K_0(q\varrho)\}$. Since we would like for our temperature field to be bounded in our domain, the modified Bessel function of the second kind of zeroth order has to be excluded since it blows up logarithmically close to the origin. As such, the solution to the above equation with the accompanied boundary condition is given by,

$$L\{T_{B,0}\}(s, \varrho) = \frac{\bar{g} I_0(q\varrho)}{s I_0(qR)}, \quad q = \sqrt{s}.$$

As a sanity check, from the final value theorem of Laplace transforms, we have that,

$$T_{B,0}(\infty, R) = \lim_{s \rightarrow 0^+} s L\{T_{B,0}\}(s, R) = \bar{g},$$

which is consistent. Inverting now as to recover $T_{B,0}$, by using the Bromwich integral formula,

$$T_{B,0}(t, \varrho) = \frac{\bar{g}}{2\pi i} \int_{\gamma-i\infty}^{\gamma+i\infty} e^{st} \frac{I_0(q\varrho)}{s I_0(qR)} ds = \frac{\bar{g}}{2\pi i} \int_{\gamma-i\infty}^{\gamma+i\infty} f(s; t, \varrho) ds,$$

with $\gamma \in \mathbb{R}$ such that the contour path is in $Re(s) \geq \zeta$. The integrand has no branch points, and so if we are to use the residue theorem to calculate the integral above by completing the contour path to a closed curve, there's no need for a contour avoiding branch cuts (since there aren't any), and so we take a semicircle contour in $Re(s) \geq \gamma$ with the contour path in the inversion formula as its diameter, with a counter-clockwise or positive orientation. The isolated singularities of the integrand are in terms of poles, which are exactly the roots of $I_0(\sqrt{s}R) = J_0(i\sqrt{s}R)$, where J_0 is the zeroth order Bessel function of the first kind, and $s = 0$. The roots of $J_0(i\sqrt{s}R)$ are $s = -a_n^2$, where $\pm a_n$, $n \in \mathbb{N}$ ($a_n > 0$) are the roots of $J_0(Ra_n) = 0$, since J_0 is of even order and so it is an even function. As such,

$$T_{B,0}(t, \varrho) = \bar{g} \left[\sum_{n=1}^{\infty} \text{Res}(f, -a_n^2) + \text{Res}(f, 0) \right].$$

The residue of f at 0 is equal to 1 since that's the coefficient of the $\frac{1}{s}$ term in its Laurent series (since $I_0(0) = 1$ and $s = 0$ is a simple pole). As for the first sum, since the poles are simple, we just need to find the coefficient of the first term of the principal part of the Laurent series of f around that pole, which in this case is equal to,

$$\left[e^{st} \frac{I_0(\sqrt{s}\varrho)}{s \frac{d}{ds} I_0(\sqrt{s}R)} \right]_{s=-a_n^2} = \left[e^{st} \frac{I_0(\sqrt{s}\varrho)}{\frac{R}{2} \sqrt{s} I_1(\sqrt{s}R)} \right]_{s=-a_n^2} = -2e^{-a_n^2 t} \frac{J_0(\varrho a_n)}{Ra_n J_1(Ra_n)},$$

where the evenness of J_0 , the oddness of J_1 , the relation between I_ν and J_ν , and the recursive relation between the modified Bessel functions of the first kind was used to prove the above. This is because,

$$\lim_{z \rightarrow z_0} (z - z_0) \frac{f(z)}{h(z)r(z)} = \lim_{z \rightarrow z_0} \frac{f(z)}{h(z) \frac{r(z) - r(z_0)}{z - z_0}} = \frac{f(z_0)}{h(z_0)r'(z_0)},$$

where z_0 is a simple pole (or a simple root of r) and f, h are continuous around z_0 . The above expression recovers the coefficient of the $1/(z - z_0)$ term in the Laurent series of $\frac{f}{rh}$, which has a one-term principal part by assumption of a simple pole.

Notice that we only took the derivative of the I_0 on the denominator. As such, the solution $T_{B,0}$ is given by,

$$T_{B,0}(t, \varrho) = \bar{g} - \frac{2\bar{g}}{R} \sum_{n=1}^{\infty} e^{-a_n^2 t} \frac{J_0(\varrho a_n)}{a_n J_1(Ra_n)}. \quad (4.9)$$

Before we proceed, notice that $\lim_{t \rightarrow \infty} T_{B,0}(t, \varrho) = \bar{g} = \overline{T_S}(\varrho)$, $\forall \varrho \in [0, R]$, i.e. the steady state bulk limit coincides with the steady state of the full solution, up to *all* orders, and in the *whole* domain. This result is rather significant, and is even more explained by the sparsity of the spectrum of the time scales in (4.9), which becomes even more sparse considering our length scale (difference of the radii of our problem, $h = R_f - R_m$) is in the order of 10^{-1} usually. This can also be seen from the following asymptotic expansion,

$$-a_n^2 = -\left(\frac{l}{4R}\right)^2 \left(1 + \frac{2}{l^2} - \frac{62}{3l^4} + \frac{15116}{15l^6} + \mathcal{O}(l^{-8})\right)^2, \quad l = \pi(4n - 1), \quad \forall n \in \mathbb{N}.$$

And so, by adding (4.8) and (4.9), and subtracting the uniform asymptotic match \bar{g} which has been counted twice, we end up with a zeroth order approximation of the solution to (4.2) for $\omega \rightarrow \infty$,

$$T(t, \varrho, \vartheta) = \sum_{m \in \mathbb{Z}} g_m e^{-(1+sgn(m)i)\sqrt{\omega|m|}(R-\varrho)/\sqrt{2}} e^{im\vartheta} - \frac{2\bar{g}}{R} \sum_{n \in \mathbb{N}} e^{-a_n^2 t} \frac{J_0(\varrho a_n)}{a_n J_1(Ra_n)} + \mathcal{O}(\sqrt{\varepsilon}). \quad (4.10)$$

4.3.1 Sketching the procedure of how to get an approximation to the solution of (4.5) with an asymptotic error of $\mathcal{O}(\varepsilon^{3/2})$

What we calculated in (4.10) was $T = T_{C,0} + T_{B,0} + \mathcal{O}(\sqrt{\varepsilon})$, but we can go a bit further, and also calculate $T_{B,1}$, $T_{C,1}$, and $T_{C,2}$. Indeed, from (4.6), we have that $T_{C,1}$ satisfies,

$$\mathcal{O}(\sqrt{\varepsilon}) : \begin{cases} \partial_\vartheta T_{C,1} = \partial_X^2 T_{C,1} - \frac{1}{R} \partial_X T_{C,0} \\ T_{C,1}(t, 0, \vartheta) = 0. \end{cases}$$

This is a non-homogeneous form of the problem that $T_{C,0}$ satisfies but for $T_{C,1}$ (recall that $T_{C,0}$ is known), but with homogeneous boundary conditions. In addition, this shows that $T_{C,1}$ also doesn't have any temporal dependence, much like $T_{C,0}$. We can go ahead now and prove via Fredholm's alternative that this problem does have a unique solution, by proving that if $\Lambda = -\partial_X^2 + \partial_\vartheta$ (given in its non-divergence form), then $-\frac{1}{R} \partial_X T_{C,0}$ is orthogonal to the kernel of its adjoint Λ^* via the inner product $\langle f, g \rangle = \int_0^{2\pi} \int_0^\infty f(X, \vartheta) g(X, \vartheta) dX d\vartheta$. While now there exists a unique solution to this problem, recovering it via Galerkin weak solutions over an energy Sobolev space and Weyl's Lemma (*as outlined in Chapter 6 of [18]*) is unfortunately unfeasible since the quadratic part of Λ is not positive definite, which means Λ is not uniformly elliptic. But, theoretically, such a solution exists, and can be found by using the Green's function for this elliptic operator, see we can also see that even the 1/2-th leading order term in the circumfluent region, does not depend on time, much like the zeroth order term.

As for $T_{B,1}$, that can also be recovered from,

$$\mathcal{O}(\varepsilon^1) : \begin{cases} \partial_t T_{B,0} = \nabla^2 T_{B,0} - \partial_\vartheta T_{B,1} \\ T_{B,1}(0, \varrho, \vartheta) = 0, \end{cases}$$

since $T_{B,0}$ is known. Taking the indefinite integral in ϑ of $\nabla^2 T_{B,0} - \partial_t T_{B,0}$, and by enforcing the initial condition, as well as the asymptotic match condition by matching with the circumfluent limit, and by using the bounded assumption, we can find $T_{B,1}$.

But, as we mentioned above, to asymptotically match the first order bulk limit with the first order circumfluent limit, we would need also $T_{C,2}$ (which also doesn't depend on time, since $T_{C,0}$ and $T_{C,1}$ don't, via (4.6)), which we can find from the $\mathcal{O}(\varepsilon)$ order terms of (4.6) by substituting $T_C = T_{C,0} + \sqrt{\varepsilon}T_{C,1} + \varepsilon T_{C,2} + \mathcal{O}(\sqrt{\varepsilon^3})$. But as we did for the zeroth order terms, we can avoid this by instead taking advantage of periodicity and "doing an asymptotic match by instead using the solvability condition for $T_{B,2}$ ".

Combining these results, theoretically would give us,

$$T(t, \varrho, \vartheta) = (\text{Expression from (4.10)}) + \sqrt{\varepsilon}T_{C,1} + \varepsilon(T_{C,2} + T_{B,1}) - T_{match,1} + \mathcal{O}(\sqrt{\varepsilon^3}),$$

where $T_{match,1}$ is the asymptotic match stemming from taking the intermediate limit ($X \rightarrow \infty$, $\varrho \rightarrow R$, $\varepsilon \rightarrow 0^+$) in the matching region, and asymptotically matching the first order bulk limit and the 1/2-th and first order circumfluent limits in first leading order, $\mathcal{O}(\varepsilon)$. Such a procedure can be seen in *Examples 1-3, Section 9.4, of [9]*.

4.4 Generalisations to the rotating Dirichlet boundary condition model 4.2

As promised, we provide sources for solving this problem with some further generalisations.

- (i) The method employed above, as explored in *Subsection 7.6 and Appendix I of [1]*, can also be extended for initial temperatures that have a canonical expansion in terms of the zeroth order Bessel function of the first kind, and surface temperatures of particular forms (linear in time, sines, cosines), by using Duhamel's principle.
- (ii) For general initial temperatures and surface temperature distributions (possibly at the same time), a solution can be found via the Green's function for the radially symmetric heat equation in polar coordinates in \mathbb{R}^2 . For Dirichlet boundary conditions the exact solution can be found in *Subsection 1.2.1-3 of [26]*, with the derivation outlined in *Subsection 14.8, (I) of [1], with results taken from Subsections 10.2, 10.3, and 14.1*. It is described as the contribution of the influence of the initial condition via the Green's function and the added influence of the boundary condition via its time convolution with the first spatial derivative of the Green's function for this PDE (Maxwell's reciprocity holds, even if the heat operator is not self-adjoint; See *[21] Subsection 11.3.5*). We will explore this method more in the next section.
- (iii) If we have a homogeneous initial condition, but instead the geometry of the meat slab was an annulus or a hollow cylinder, then the Laplace transform method can still be used, even if the boundary condition is of Robin type, granted that all coefficients appearing don't depend on the time variable (in the PDE or BC). The method of extracting a solution to this case can be found in *Subsection 13.4 of [1]*. In the case of a non-homogeneous initial temperature, but where we still have an annular meat slab, we will have to resort to the Fundamental Solution/Green's Function for this problem. The outline of this method can be found in *Subsection 14.8, (IV) of [1]*.
- (iv) If we incorporate the metallic skewer as a heat sink within our meat slab, i.e. as a sink forcing term in our original equation, it would only affect the bulk region terms, where for $T_{B,0}$ for example, we would have the radially symmetric heat equation, with a forcing term, which in this case could be the azimuthal average of the heat sink function we incorporated in our equation. That can again be solved by using Duhamel's principle, as can be seen from *Subsection 1.2.2 of [26]*.

5 The next step; Circular domain with rotating Robin boundary conditions

We will now proceed with solving the actual problem we are concerned about, specifically for the "Inside meat" region, which from (3.5), is the following initial/boundary-value problem,

$$\begin{cases} \partial_t T_m = \nabla^2 T_m \\ -\partial_\varrho T_m = H(\vartheta - \Theta(t)) \left(T_m \left(t, \frac{\lambda}{1-\lambda}, \vartheta - \Theta(t) \right) - T_a \left(t, \frac{\lambda}{1-\lambda}, \vartheta - \Theta(t) \right) \right) \\ T_m(0, \varrho, \vartheta) = 0, \end{cases} \quad (5.1)$$

where we will be assuming in the following analysis that T_a is known from the "Outside meat" part of the problem (due to the Taylor-Couette flow in the annular gap), and is just a "parameter" that we plug-in in the rotating Robin boundary condition.

As we did in the previous section, we start with a change of variables to the rotating frame of reference, where we end up with the following initial/boundary-value problem,

$$\begin{cases} \partial_t T_m = \nabla^2 T_m - \omega \partial_\vartheta T_m \\ -\partial_\varrho T_m = H(\vartheta) \left(T_m \left(t, \frac{\lambda}{1-\lambda}, \vartheta \right) - T_a \left(t, \frac{\lambda}{1-\lambda}, \vartheta \right) \right) \\ T_m(0, \varrho, \vartheta) = 0. \end{cases} \quad (5.2)$$

We note here the possibility of further incorporating some scale transformations to the current setup, by dividing all dimensionless temperatures by the azimuthal average of T_a over the surface of the meat slab, i.e. $\langle T_a \rangle_\vartheta = \bar{T}_a$, and by dividing the dimensionless radial variable with the dimensionless length scale $\lambda/(1-\lambda)$. This would simplify the expressions that we get for the following results.

The existence and uniqueness of the solution to (5.2), since our domain has a smooth enough boundary, rests solely on the regularity assumptions that we impose on H , and in the case of both H being bounded or unbounded, existence and uniqueness results to our problem can be found in *Chapter V, Section 4, of [7]*. For our purposes we assume the existence and uniqueness of (5.2), and we proceed with recovering an asymptotic expansion of the solution to our problem, T_m , for when $\omega \rightarrow \infty$.

As we did in the previous section (4), define our dimensional asymptotic scale $\varepsilon = \frac{1}{\omega}$, and divide our PDE with ω to get,

$$\begin{cases} \varepsilon \partial_t T_m = \varepsilon \left(\partial_\varrho^2 T_m + \frac{1}{\varrho} \partial_\varrho T_m + \frac{1}{\varrho^2} \partial_\vartheta^2 T_m \right) - \partial_\vartheta T_m \\ -\partial_\varrho T_m = H(\vartheta) \left(T_m \left(t, \frac{\lambda}{1-\lambda}, \vartheta \right) - T_a \left(t, \frac{\lambda}{1-\lambda}, \vartheta \right) \right) \\ T_m(0, \varrho, \vartheta) = 0. \end{cases} \quad (5.3)$$

If we start by assuming a regular expansion for T_m as a power series in ε , $T_m = \sum_{n=0}^{\infty} \varepsilon^n T_m^{(n)}$, then for the unperturbed problem we have,

$$\mathcal{O}(\varepsilon^0) : \begin{cases} \partial_\vartheta T_m^{(0)} = 0 \\ -\partial_\varrho T_m^{(0)} = H(\vartheta) \left(T_m^{(0)} \left(t, \frac{\lambda}{1-\lambda}, \vartheta \right) - T_a \left(t, \frac{\lambda}{1-\lambda}, \vartheta \right) \right) \\ T_m^{(0)}(0, \varrho, \vartheta) = 0, \end{cases}$$

which would give $T_m^{(0)} = T_m^{(0)}(t, \varrho)$, but for general non-constant functions H (and even due to the ϑ dependence of T_a), this problem is non-solvable. As such we again have the emergence of a boundary layer, similar to the Dirichlet counterpart of this problem, and the asymptotic expansion of T_m is singular.

In the same vain as in Section 4, by a dominant balance argument, we can see that the thickness of the boundary layer is $\delta = \mathcal{O}(\sqrt{\varepsilon})$, which again divides our meat slab domain Ω_m , to the bulk (regular) region and the circumfluent (boundary layer) region, where $T_m = T_{m,B} + T_{m,C}$.

We start with the boundary layer region, where we define again the circumfluent variable $X = \frac{\lambda/(1-\lambda) - \varrho}{\sqrt{\varepsilon}}$.

This means that $\partial_\varrho = -\frac{1}{\sqrt{\varepsilon}}\partial_X$ and so our PDE in (5.3), in the circumfluent region, becomes,

$$\varepsilon \partial_t T_m = \partial_X^2 T_m - \frac{\varepsilon}{\delta(\lambda/(1-\lambda) - \delta X)} \partial_X T_m + \frac{\varepsilon}{(\lambda/(1-\lambda) - \delta X)^2} \partial_\vartheta^2 T_m - \partial_\vartheta T_m, \quad (5.4)$$

where $\delta = \mathcal{O}(\varepsilon)$, for $\varepsilon \rightarrow 0^+$.

By plugging in $T_{m,C} = T_{m,C}^{(0)} + \sqrt{\varepsilon}T_{m,C}^{(1/2)} + \mathcal{O}(\varepsilon)$ into (5.3) and (5.4), for the zeroth order problem we have that,

$$\mathcal{O}(\varepsilon^0) : \begin{cases} \partial_\vartheta T_{m,C}^{(0)} = \partial_X^2 T_{m,C}^{(0)} \\ \partial_X T_{m,C}^{(0)}(t, 0, \vartheta) = 0, \end{cases}$$

where we notice that now we have a *homogeneous Neumann* boundary condition for the unperturbed problem in the boundary layer region, unlike in Section (4) which has a *non-homogeneous Dirichlet one*, due to the fact that we now have a Robin boundary condition in our original problem. This is in general a rule of thumb; *In the presence of a Neumann or Robin boundary condition, the boundary condition of the original problem cannot be satisfied by the zeroth order term in the boundary layer limit, and is instead satisfied by the next order term in the boundary layer expansion* (in our case $T_{m,C}^{(1/2)}$, or the 1/2-th order term in the circumfluent limit)! As such, we have that the zeroth order term is now a general function of time, $T_{m,C}^{(0)} = T_{m,C}^{(0)}(t)$; To see why this is the case, recall the eigenfunction expansion of $T_{C,0}$, (4.7), and because of the homogeneous Neumann boundary condition, all modes should die out except of the zeroth one in this case. This is another deviation from the Dirichlet counterpart of this problem, where there the zeroth order term in the circumfluent limit had no temporal dependence, as we saw in Section 4. Notice now that our previously defined operator, $\Lambda = -\partial_X^2 + \partial_\vartheta$, has a *non-trivial* kernel under homogeneous Neumann boundary conditions, and as such by Fredholm's alternative this problem *suffers* from non-uniqueness, which we already saw, unless some restrictions are enforced on $T_{m,C}^{(0)}$.

We remain in the boundary layer region, and proceed with the $\mathcal{O}(\sqrt{\varepsilon})$ leading order term, where from (5.3) and (5.4), we have that,

$$\mathcal{O}(\sqrt{\varepsilon}) : \begin{cases} \partial_\vartheta T_{m,C}^{(1/2)} = \partial_X^2 T_{m,C}^{(1/2)} - \frac{1}{\lambda/(1-\lambda)} \partial_X T_{m,C}^{(0)} \equiv \partial_X^2 T_{m,C}^{(1/2)} \\ \partial_X T_{m,C}^{(1/2)}(t, 0, \vartheta) = H(\vartheta) \left(T_{m,C}^{(0)}(t) - T_a \left(t, \frac{\lambda}{1-\lambda}, \vartheta \right) \right). \end{cases}$$

Taking now the azimuthial average, $\langle \cdot \rangle_\vartheta$, of both the equation and boundary condition, using the periodicity of $T_{m,C}^{(1)}$ in ϑ , as well as Leibniz's integral rule, we end up with,

$$\mathcal{O}(\sqrt{\varepsilon}) : \begin{cases} \partial_X^2 \langle T_{m,C}^{(1/2)} \rangle_\vartheta(t, X) = 0 \\ \partial_X \langle T_{m,C}^{(1/2)} \rangle_\vartheta(t, 0) = \left\langle H(\vartheta) \left(T_{m,C}^{(0)}(t) - T_a \left(t, \frac{\lambda}{1-\lambda}, \vartheta \right) \right) \right\rangle_\vartheta, \end{cases}$$

which is a Neumann boundary-value problem for $\langle T_{m,C}^{(1/2)} \rangle_\vartheta$, which provides a solubility condition for the boundary value problem that $T_{m,C}^{(1/2)}$ solves. From these two problems, we can actually recover $T_{m,C}^{(0)}(t)$. Indeed, due to the PDE that $T_{m,C}^{(1/2)}$ solves, from (4.7), we have that its general solution is,

$$T_{m,C}^{(1/2)}(t, X, \vartheta) = \sum_{k \in \mathbb{Z}} \mathcal{T}_{1/2}^{(k)}(t) e^{-(1+sgn(k)i)\sqrt{|k|}X/\sqrt{2}} e^{ik\vartheta}.$$

We see that this solution indeed satisfies the solubility condition $\partial_X^2 \langle T_{m,C}^{(1/2)} \rangle_\vartheta(t, X) = 0$, if we assume uniform convergence of the eigenfunction expansion as to be able to interchange integration and summation. Using now the boundary condition for $\partial_X^2 \langle T_{m,C}^{(1/2)} \rangle_\vartheta$, we see that we can get an explicit equation for $T_{m,C}^{(0)}(t)$, since it doesn't vary with ϑ . Indeed, by taking the derivative of $T_{m,C}^{(1/2)}(t, X, \vartheta)$ with respect to X , plugging in $X = 0$, and then

taking the azimuthial average, by using uniform convergence of the series we see that only the zeroth mode survives but the zeroth mode of $\partial_X \langle T_{m,C}^{(1/2)} \rangle_\vartheta(t, 0)$ is $\left(-\mathcal{T}_{1/2}^{(k)}(t)(1 + \text{sgn}(k)i)\sqrt{|k|}/\sqrt{2} \right) \Big|_{k=0} = 0$, and so,

$$0 = \int_0^{2\pi} H(\vartheta) \left(T_{m,C}^{(0)}(t) - T_a \left(t, \frac{\lambda}{1-\lambda}, \cdot \right) H \right) d\vartheta.$$

Solving for $T_{m,C}^{(0)}$, we end up with,

$$T_{m,C}^{(0)}(t) = \frac{\left\langle T_a \left(t, \frac{\lambda}{1-\lambda}, \cdot \right) H \right\rangle_\vartheta}{\langle H \rangle_\vartheta},$$

where theoretically both H and T_a are known (H is a physical parameter, while T_a is known from the "Outside meat" flow problem). This is a significant result; In the edge case of T_a being constant along the meat slab boundary, $T_{m,C}^{(0)}(0)(t)$ reduces down to a constant. Also, this shows that the effective temperature in the circumfluent region, up to zeroth order accuracy, is the weighted average of the air's temperature on the surface of the meat, by the local Nusselt number or heat transfer coefficient of convection, H . This intuitively makes sense, since we are looking on the case of arbitrarily fast rotations. We note here that in the case that our heat transfer coefficient, H , has a temporal dependence (maybe implicitly via a weak dependence on the temperature fields), then the same expression would still hold.

We now transition to the bulk region of the singular expansion of T_m . There $T_{m,B}$ has a regular expansion in powers of ε , and by plugging in $T_{m,B} = T_{m,B}^{(0)} + \varepsilon T_{m,B}^{(1)} + \mathcal{O}(\varepsilon^1)$ into (5.3), for the zeroth leading order terms we have that,

$$\mathcal{O}(\varepsilon^0) : \begin{cases} \partial_\vartheta T_{m,B}^{(0)} = 0 \\ T_{m,B}^{(0)}(0, \varrho, \vartheta) = 0, \end{cases}$$

which means $T_{m,B}^{(0)} = T_{m,B}^{(0)}(T, \varrho)$, with $T_{m,B}^{(0)}(0, \varrho) = 0$, and by taking the intermediate limit to the matching region ($X \rightarrow \infty$, $\varrho \rightarrow \lambda/(1-\lambda)$, $\varepsilon \rightarrow 0^+$), we have the following asymptotic match,

$$T_{m,B}^{(0)}(t, \lambda/(1-\lambda)) = T_{m,C}^{(0)}(t), \quad \forall t \geq 0,$$

or in other words, *the zeroth leading order uniform approximation of T_m that is valid in all of Ω_m and $\forall t \geq 0$* , is given simply by $T_{m,B}^{(0)}(t, \varrho)$, which means *for as long as we only concern ourselves with zeroth order approximations, T_m has no azimuthal dependence as $\omega \rightarrow \infty$!* In other words, T_m showcases radial symmetry to zeroth order accuracy, making Ω_m a collection of concentric isothermal curves based on the level sets of $T_{m,B}^{(0)}(t, \varrho) = T_m + \mathcal{O}(\sqrt{\varepsilon})$, for $\varrho \in [0, \lambda/(1-\lambda)]$. This is similar to the phenomenon that arises in the homogenisation of passive tracers in potential flow vorticities in planetary gyres (see [2]).

To be able to find $T_{m,B}^{(0)}$, we go to the first leading order term of the bulk expansion, where we have,

$$\mathcal{O}(\varepsilon^1) : \begin{cases} \partial_t T_{m,B}^{(0)}(t, \varrho) + \partial_\vartheta T_{m,B}^{(1)}(t, \varrho, \vartheta) = \nabla^2 T_{m,B}^{(0)}(t, \varrho) \equiv \frac{1}{\varrho} \partial_\varrho (\varrho \partial_\varrho T_{m,B}^{(0)}(t, \varrho)) \\ T_{m,B}^{(1)}(0, \varrho, \vartheta) = 0, \end{cases}$$

where by taking now the azimuthal average, $\langle \cdot \rangle_\vartheta$, of the PDE, and by using the periodicity of $T_{m,B}^{(1)}$ and radial symmetry of $T_{m,B}^{(0)}$, we end up with the following PDE,

$$\partial_t T_{m,B}^{(0)}(t, \varrho) = \frac{1}{\varrho} \partial_\varrho (\varrho \partial_\varrho T_{m,B}^{(0)}(t, \varrho)),$$

which is a radially symmetric Heat equation in Ω_m , for $T_{m,B}^{(0)}(t, \varrho) = T_m + \mathcal{O}(\sqrt{\varepsilon})$. As such, by using our homogeneous initial condition, and boundary condition at $\varrho = \lambda/(1-\lambda)$ due to asymptotic matching, as well as the expression that we have for $T_{m,C}^{(0)}(t)$, we have the following initial/boundary-value problem for $T_{m,B}^{(0)}$,

$$\mathcal{O}(\varepsilon^0) : \begin{cases} \partial_t T_{m,B}^{(0)}(t, \varrho) = \frac{1}{\varrho} \partial_\varrho (\varrho \partial_\varrho T_{m,B}^{(0)}(t, \varrho)) \\ T_{m,B}^{(0)}(t, \lambda/(1-\lambda)) = \frac{\left\langle T_a \left(t, \frac{\lambda}{1-\lambda}, \cdot \right) H \right\rangle_\vartheta}{\langle H \rangle_\vartheta} \\ T_{m,B}^{(0)}(0, \varrho) = 0. \end{cases}$$

We solved the same problem but with constant boundary conditions in Section 4, again for the zeroth order of the bulk limit. There we mentioned that for general non-constant initial temperatures (and even a non-constant/non-zero boundary condition at the same time), that a solution can be found via the Green's Function for the radially symmetric Heat equation. In *Subsections 10.2, 10.3, 14.1, and 14.8 (I) of [1]*, the general methodology of constructing Green's Function for the radially symmetric Heat equation in a circular or annular domain for non-homogeneous initial temperatures, and non-homogeneous boundary conditions of Neumann or Robin type can be found.

From *Subsection 1.2.1-3 of [26], (1) of Subsection 14.1 (note here that in their analysis, the unit-normal is facing inwards) and (5) of Subsection 14.8 of [1] (which is the Green's function to our problem after it is multiplied with the area element in polar coordinates)*, we have that,

$$T_{m,B}^{(0)}(t, \varrho) = \frac{2-2\lambda}{\lambda} \int_0^t T_{m,C}^{(0)}(s) \sum_{n=1}^{\infty} \frac{a_n J_0(\varrho a_n)}{J_1\left(\frac{\lambda a_n}{1-\lambda}\right)} e^{-a_n^2(t-s)} ds,$$

where for this expression to be true, enough regularity on H and T_a is assumed, with details on the exact assumptions found on the aforementioned references. We recall that $\pm a_n$, $n \in \mathbb{N}$ ($a_n > 0$) are the roots of $J_0(\lambda a_n/(1-\lambda)) = 0$, which we can approximate as $a_n = \frac{l(1-\lambda)}{4\lambda} \left(1 + \frac{2}{l^2} - \frac{62}{3l^4} + \frac{15116}{15l^6} + \mathcal{O}(l^{-8})\right)$, $l = \pi(4n-1)$, $\forall n \in \mathbb{N}$.

Combining this together with the observation we made before about the zeroth order uniform approximation of T_m , we have that the zeroth order approximation of the solution to (5.2) for $\omega \rightarrow \infty$ is,

$$T_m(t, \varrho, \vartheta) = \frac{2-2\lambda}{\lambda} \int_0^t \frac{\langle T_a(s, \lambda/(1-\lambda), \cdot) H \rangle_{\vartheta}}{\langle H \rangle_{\vartheta}} \sum_{n=1}^{\infty} \frac{a_n J_0(\varrho a_n)}{J_1\left(\frac{\lambda a_n}{1-\lambda}\right)} e^{-a_n^2(t-s)} ds + \mathcal{O}(\sqrt{\varepsilon}). \quad (5.5)$$

Again, this expression also holds in the case that the local Nusselt number for our problem, H , has a temporal dependence. Now, it is not hard to also find $T_{m,C}^{(1/2)}$, since a "closed" form expression exists for $T_{m,C}^{(0)}$, thus leading to an asymptotic expression for T_m with an error term that is $\mathcal{O}(\varepsilon)$. Specifically, $T_{m,C}^{(1/2)}$, can be found from solving the following boundary-value problem,

$$\mathcal{O}(\sqrt{\varepsilon}) : \begin{cases} \partial_{\vartheta} T_{m,C}^{(1/2)} = \partial_X^2 T_{m,C}^{(1/2)} \\ \partial_X T_{m,C}^{(1/2)}(t, 0, \vartheta) = H(\vartheta) \left(\frac{\left\langle T_a \left(t, \frac{\lambda}{1-\lambda}, \cdot \right) H \right\rangle_{\vartheta}}{\langle H \rangle_{\vartheta}} - T_a \left(t, \frac{\lambda}{1-\lambda}, \vartheta \right) \right), \end{cases}$$

which can be solved either by separation of variables, or more elegantly, by taking the Fourier Transform in the azimuthal coordinate, ϑ . But due to the complexity of solving this boundary-value problem, we omit the details here.

But for higher leading order terms than that, as we saw in Section 4.3.1 for our Dirichlet toy problem, to extend T_m 's perturbation expansion to a higher leading order, we would need to determine not only $T_{m,B}^{(1)}$, but also $T_{m,C}^{(1)}$, as to be able to have a complete asymptotic match and get an asymptotic expansion in the singular perturbation expansion of T_m that is of first leading order, or $\mathcal{O}(\varepsilon)$. While doable (using the *theory and results from Subsections 10.2, 10.3, 14.1, and 14.8 (I) of [1]*), this task would require a great amount of work for comparatively small returns. But the aforementioned references can be used to recover a $\mathcal{O}(\sqrt{\varepsilon})$ leading order approximation, by finding $T_{m,C}^{(1/2)}(t, \varrho, \vartheta)$.

We would like to mention, expanding on the observation made in the previous paragraph, that in the case of *constant in time* air temperature on the meat slab's surface and of the local Nusselt number having no temporal dependence, solving for $T_{m,C}^{(1/2)}$ in the equation provided above is actually much easier. First of all, we can observe that much like in the case of $T_{m,C}^0$, where it is constant under the assumption of constant in time air temperature on the meat's surface, $T_{m,C}^{(1/2)}$ also would not have any temporal dependence! This simplifies solving for $T_{m,C}^{(1/2)}$ tremendously, and no longer requires determining an initial condition for it.

[**NOTE FOR NEXT STEP:** Include here Section 2.2 of the cookrot.pdf (analysis of the case where the air's temperature on the surface is constant), and the details found in Section 2.3 as well, for completeness purposes.]

6 Optimal cooking time in the rotating Dirichlet and Robin boundary conditions models through first mode approximations

In this section, we will try to find explicit expressions for the "cook-through time", or the time that it takes for the souvla to cook under the assumption of a large angular velocity. We will do this for both the case of rotating Dirichlet boundary conditions for our simplified model (Section 4), and rotating Robin boundary condition (Section 5). In both instances, we assume that we have a dimensionless target cooking temperature T_{cook} (since we are working with the dimensionless simplified model (3.5)), and we define the dimensionless cook-through time, $t = t_{\text{cookthrough}}$, to be the time when $T_m(t_{\text{cookthrough}}, 0, 0) = T_{\text{cook}}$, or the time where the center point of our souvla reaches the desired cooking temperature, where this definition of the cook-through time is based on our geometry and the incorporated rotation, as well as our culinary intuition, since we expect the center to be the last point to reach the desired cooking temperature.

Before we proceed with this analysis, we first set the values for the physical and dimensionless parameters that appear on our problem, based on literature findings and previous results. Although we provide an average angular velocity for the motors that are used in the cooking process of souvla, in our analysis we will assume a large enough value such that the results, (4.10) and (5.5) hold, while all other parameters will remain equal to the values provided in Table 1.

6.1 Physical and dimensionless parameters to the non-dimensional simplified model (3.5)

Physical and dimensionless parameters used in the paper are given in Table 1. Details on the dimensionless numbers provided, can be found in Subsection 2.6. We use pork souvla meat which comes from the neck and shoulder of the animal (Boston butt and Picnic shoulder). We utilise the rule of mixtures to calculate the thermal properties of our composite meat slab (as illustrated in *Subsection 3.4 of [28]*), where we assume that our composite meat slab consists of 70% actual meat tissue, 25% fat, where these percentages were taken from pork yield data *from AHDB found in [32]*, 3% bones and 2% AISI 302 stainless steel skewer, where everything is measured at a temperature interval of around 30°C to 100°C , and the transversal length of our meat slab (or metallic skewer, or froukou), L_f , is set to 0.8m to carry out the calculations. The thermal properties of air are measured at surface atmospheric pressure (1atm), and in an average temperature of 100°C .

The (local) dimensionless conductive-convective heat transfer coefficient, H , is exactly the *local Nusselt number of the meat surface*, calculated on a specific azimuthial point on the surface of the meat. In general, the analysis associated with flow past the exterior surface of a solid, especially when rotation is also a variable in the setup, can be quite convoluted, due to the emergence of boundary layers of separation. But, a lot of results exist in the literature for correlations between the *average Nusselt number*, $\bar{H} = \langle H \rangle_\theta$, and various other dimensionless quantities of the flow, where for our setup those usually are the rotational Reynolds number, the Grashof number, and Prandtl number of the background fluid. Due to the assumptions we make for the nature of our flow (natural convection), and the values that we have for the dimensionless parameters affecting the Nusselt number, expressions for the local Nusselt number, as well as correlations for the average Nusselt number, can be found in the literature.

Via dimensional analysis (after making a change of variables to the logarithmic polar coordinates, *in the rotating frame of reference*), from Eqn. (13a) in [10] or Eqn. (14a) in [4], for the local Nusselt number we have,

$$H(\vartheta) = -\partial_\vartheta \left(\frac{T_a - T_\infty}{T_m - T_\infty} \right) \Big|_{\partial\Omega_m}, \quad (6.1)$$

which can then be expressed via the Fourier series of this dimensionless temperature, $\frac{T_a - T_\infty}{T_m - T_\infty}$, in the case that our meat's surface is isothermal, by solving the PDE that this quantity solves (see (3.5)). But since the meat slab itself and its surface, are non isothermal, we need to instead work with the peripheral average Nusselt number at the surface of our meat slab, or \bar{H} , for all azimuthial values. This can be done by either using the

zeroth Fourier mode of the aforementioned dimensionless temperature, which can be seen in *Eqn. (13b) in [10]*, or by using correlations with dimensionless flow numbers, where we choose the latter for its simplicity.

A lot of papers in the literature (see [25], [6], [3], [23]) concern themselves with setups similar to our setting, for various values of Grashof, rotational Reynolds, (blowing) Reynolds, Rayleigh, and Prandtl numbers for the underlying background flow, with a rotating disk (or cylinder with axis perpendicular to the flow) situated in it. All these papers provide correlations for either still or quiescent natural convection mostly driven by buoyancy, but some results are also given for turbulent flow, all under the assumption of steady, non-vortex shedding flow. In all of these references, it is observed that the rate of heat transfer is positively dependent on the Rayleigh Number (product of Grashof and Prandtl numbers) and negatively dependent on the speed of rotation, which we expect to also see in our simulations. Also, the dependence of the average Nusselt number on the Prandtl number is apparent only at low rotational Reynolds numbers, with a significant increase in \bar{H} being apparent when the Prandtl number rises, but for high rotational Reynolds numbers the effect of the Prandtl number on the average Nusselt number is negligible. For our setting, the rotational Reynolds numbers we will inspect are at most in the order of $\mathcal{O}(10^3)$, meaning the average Nusselt number will show great dependence on the Prandtl number, which all the aforementioned references seem to agree on.

Based on our assumptions and values for our problem (see Table 1), we use the correlation result found *in [3] of Sparrow and Kaddle* (for zero-length rods - also validated in [6]). This gives us the following correlation,

$$\bar{H} = \langle H \rangle_\vartheta = 0.535 Re_r^{0.55} Pr_a^{0.37}, \quad (6.2)$$

where Re_r is the rotational Reynolds number, and Pr_a is the Prandtl number of air.

Table 1: Table containing the values of the physical and dimensionless parameters used in this paper

Notation	Value or Expression	Units	Description	Reference in literature
R_m	0.05	m	Radius of meat slab	-
R_f	0.3	m	Radius of circular foukou	-
L_f	0.8	m	Transversal length of meat/foukou	-
$h(= L)$	0.25	m	Gap width ($R_f - R_m$) - distance from foukou (length scale)	-
λ	1/6	d'less	Radius ratio (R_m/R_f)	-
ω	2.1	$rads^{-1}$	Angular velocity of motor	Average from OEMs
ωR_m	0.105	ms^{-1}	Tangential velocity of meat slab	-
T_H	200	$^{\circ}C$	Charcoal surface temperature	-
T_∞	25	$^{\circ}C$	Room/Ambient temperature (initial temp.)	-
ΔT	175	$^{\circ}C$	Temperature difference ($T_H - T_\infty$) (temperature scale)	-
κ_m	0.442	$Wm^{-1}^{\circ}C^{-1}$	Thermal conductivity of souvla (accounting for simplifications)	[28], [5], [19], [14], [24], [11]
$\rho_m(Cp)_m$	$1105.25 \times 3143.44 = 3.474287 \cdot 10^6$	$Jm^{-3}^{\circ}C^{-1}$	Volumetric heat capacity of souvla	[28], [5], [19], [14], [24], [11]
D_m	$1.272 \cdot 10^{-7}$	m^2s^{-1}	Thermal diffusivity of souvla	[28], [5], [19], [14], [24], [11]
h^2/D_m	$4.91274 \cdot 10^5$	s	Characteristic diffusion time (time scale)	-
$D_m/h(= U)$	$5.0888 \cdot 10^{-7}$	ms^{-1}	Characteristic diffusion velocity (velocity scale)	-
κ_a	0.03095	$Wm^{-1}^{\circ}C^{-1}$	Thermal conductivity of air at 1atm and $125^{\circ}C$	[28], [19]
$\rho_a(Cp)_a$	$0.94577 \times 1009 = 954.28193$	$Jm^{-3}^{\circ}C^{-1}$	Volumetric heat capacity of air at 1atm and $125^{\circ}C$	[28], [19]
D_a	$32.4328 \cdot 10^{-6}$	m^2s^{-1}	Thermal diffusivity of air at 1atm and $125^{\circ}C$	[28], [19]
D_a/D_m	254.9337	d'less	Ratio of thermal diffusivities	-
ν	$2.3058 \cdot 10^{-5}$	m^2s^{-1}	Kinematic viscosity of air at 1atm and $125^{\circ}C$	[28], [19]
ρ_0	1.225	kgm^{-3}	Reference density of air	-
α	0.04	$^{\circ}C^{-1}$	Thermal expansion of air	-
η	0.01	d'less	Transition region from/to T_H to/from T_∞ at foukou	-
$\varphi_{\eta,d}(\vartheta)$	Given in (3.1) for $T_H = 1$, $T_\infty = 0$	d'less	Temperature distribution at the surface of the foukou	-
D_a/D_m	254.93378	d'less	Ratio of thermal diffusivities	-
ν/D_m	181.2446	d'less	-	-
$Pr_a = \nu/D_a$	0.71095	d'less	Air's Prandtl number	-
$Fr^2 = U^2/(gL)$	$1.0559 \cdot 10^{-13}$	d'less	Froude Number, squared	-
$Ra = \frac{g\Delta TL^3}{T_\infty \nu D_m}$	$3.65770661737 \cdot 10^{11}$	d'less	Rayleigh number	-
$Ro = (\omega L)/(2\pi U)$	$1.641961 \cdot 10^5$	d'less	Roshko number	-
$Re_a = UL/\nu$	$0.551741 \cdot 10^{-2}$	d'less	Air's (blowing) Reynolds number	-
$Re_r = 2\omega R_m^2/\nu$	455.37341	d'less	Rotational Reynolds number	-
$H(\vartheta)$	See (6.1)	d'less	Local heat transfer coefficient across the surface of the meat slab	[10], [4]
\bar{H}	See (6.2); 13.66583	d'less	Average heat transfer coefficient across the surface of the meat slab	[3], [6]
a_1	12.024	d'less	First root of $J_0(\lambda a/(1-\lambda)) = 0$	-
a_2	27.6005	d'less	Second root of $J_0(\lambda a/(1-\lambda)) = 0$	-
a_3	43.2685	d'less	Third root of $J_0(\lambda a/(1-\lambda)) = 0$	-

6.2 Rotating Dirichlet boundary conditions

Let T_{cook} be a non-dimensional cooking temperature, e.g. $T_{\text{cook}} = 0.228571$, for a cooking temperature of 65°C . Then, for ω large enough, and because there is a significant difference in magnitude in the first two modes of the zeroth order bulk limit, $a_1^2 = 144.577 < 761.788 = a_2^2$, we can decently approximate the cooking temperature $T_{\text{cook}} = T_m(t_{\text{cookthrough}}, 0, 0)$ using a first mode approximation in (4.10), as,

$$T_{\text{cook}} \approx \sum_{m \in \mathbb{Z}} g_m e^{-(1+\text{sgn}(m)i)\sqrt{\omega|m|}\lambda/(\sqrt{2}(1-\lambda))} - \frac{2\bar{g}(1-\lambda)}{\lambda} e^{-a_1^2 t_{\text{cookthrough}}} \frac{1}{a_1 J_1(\lambda a_1/(1-\lambda))} + \mathcal{O}(\sqrt{\varepsilon}).$$

Letting now $\omega \rightarrow \infty$, since only the zeroth mode will survive in the zeroth order circumfluent term, and $g_0 = \bar{g}$, we have that a first mode approximation of the cook-through time, as $\omega \rightarrow \infty$, that is zeroth leading order accurate in the case of rotating Dirichlet boundary conditions, is given as,

$$t_{\text{cookthrough}} \approx \frac{1}{a_1^2} \log \left(\frac{2\bar{g}(1-\lambda)}{\lambda a_1 J_1(\lambda a_1/(1-\lambda))(\bar{g} - T_{\text{cook}})} \right) = 6.91675 \log \left(\frac{10\bar{g}}{6.2423 \cdot (\bar{g} - 0.228571)} \right) \cdot 10^{-3},$$

and so for any boundary condition g , we can extract the dimensionless cook-through time, which by then multiplying by our time scale, $\frac{h^2}{D_m} = 4.91264 \cdot 10^5$, we can find the dimensional cook-through time in seconds.

For concrete results, let's use $g = \varphi_{\eta,d}$ for our rotating Dirichlet boundary condition. A small caveat here is that it can be rightfully argued that with this choice for boundary condition, the "last point" to reach the cooking temperature *will not* be the center point, and instead a point that is close to the boundary (away from the boundary layer) for $\vartheta = \frac{\pi}{2}$, which is also validated in Section 7 in our numerical simulations via Dedalus. But, since this is a toy problem we use as a stepping-stone, we flout this observation as to arrive to concrete results we can use in our analysis.

As such, we have that $\bar{g} = 0.5$ (for almost any value of $0 < \eta < 1$ this is the exact value), which gives as the dimensionless cook-through time, $t_{\text{cookthrough}} \approx 0.00748492$, or in real-time, 3677.07 seconds or about an hour (61.28 mins). In Section 7 we see that this first mode approximation is indeed accurate, even for very small values for ω .

6.3 Rotating Robin boundary conditions

We proceed in the same vain as with the Dirichlet variant of this problem. Let T_{cook} be a non-dimensional cooking temperature; For consistency let $T_{\text{cook}} = 0.228571$. Then, for ω large enough, and because there is a significant difference in magnitude in the first two modes, we can again decently approximate the cooking temperature $T_{\text{cook}} = T_m(t_{\text{cookthrough}}, 0, 0)$ using a first mode approximation at (5.5), as,

$$T_{\text{cook}} \approx \frac{2-2\lambda}{\lambda} \int_0^{t_{\text{cookthrough}}} \frac{\langle T_a(s, \lambda/(1-\lambda), \cdot) H \rangle_{\vartheta}}{\langle H \rangle_{\vartheta}} \frac{a_1}{J_1\left(\frac{\lambda a_1}{1-\lambda}\right)} e^{-a_1^2(t_{\text{cookthrough}}-s)} ds + \mathcal{O}(\sqrt{\varepsilon}).$$

Using now the fact that we will be working with the average Nusselt number or dimensionless heat transfer coefficient, due to the complexity of our setup making it difficult to recover a local expression, i.e. $H \sim \bar{H} = 0.535 Re_r^{0.55} Pr_a^{0.37} = 9.0869\omega^{0.55}$, and after making the rest of the possible substitutions for T_{cook} and the other physical parameters in our model, we recover the following implicit equation for the cook-through time,

$$t_{\text{cookthrough}} \approx \frac{1}{a_1^2} \log \left(1013.29 \int_0^{t_{\text{cookthrough}}} \langle T_a(s, \lambda/(1-\lambda), \cdot) \rangle_{\vartheta} e^{a_1^2 s} ds \right),$$

where in this case this is truly the expected cook-through time, without any caveats (like the ones we had in the Dirichlet variant of the problem). This is again a first mode, zeroth leading order accurate, approximation.

Assuming now the edge case of \bar{T}_a being constant in time along the surface of the souvla, we have that, $\langle T_a(s, \lambda/(1-\lambda), \cdot) \rangle_{\vartheta} := \bar{T}_a(\lambda/(1-\lambda)), \forall t \geq 0$, which means that now after a bit of algebra we have that,

$$t_{\text{cookthrough}} \approx \frac{1}{a_1^2} \left(\log(1013.29) + \log(\bar{T}_a(\lambda/(1-\lambda))) - 2 \log(a_1) + a_1^2 t_{\text{cookthrough}} + \log \left(1 - e^{-a_1^2 t_{\text{cookthrough}}} \right) \right),$$

where by Taylor expanding the last term around 0, and by assuming that the cook-through time will occur at some point in time $t_{\text{cookthrough}}$ far from 0, such that the $\mathcal{O}(e^{-2a_1^2 t_{\text{cookthrough}}})$ terms are negligible in that

expansion (which is what we would expect heuristically), we have now a simpler *explicit* equation for the cook-through time, given as,

$$t_{\text{cookthrough}} \approx \frac{1}{a_1^2} \log \left(\frac{1}{\log(1013.29) + \log(\bar{T}_a(\lambda/(1-\lambda))) - 2 \log(a_1)} \right),$$

which is a first mode, zeroth order accurate, approximation of the cook-through time, in the case of a constant azimuthal average for the air's temperature on the meat slab's surface, when $\omega \rightarrow \infty$.

7 Numerical Results

We proceed with first solving the "toy-problem", (4.2), and then the full simple model, (3.5), using the UNIX-based Python library, Dedalus (/27/). Dedalus is an open-source spectral-based solver, which implements a highly flexible spectral framework, parallelised by MPI, used to solve IVP's, BVP's, and EVP's, in a plethora of domains, for custom-set, user-defined equations. All of the code used to create the following plots, as well as the .mp4 files of the simulations using `ffmpeg`, can be found at my Github page, <https://github.com/marandmath>, under the repository `souvla_cooking`.

7.1 Rotating Dirichlet boundary conditions

We use Dedalus to solve (4.2), using $g(\vartheta) = \varphi_{\eta,d}(\vartheta)$, for $\eta = 10^{-3}$, for $\omega = 2.1$ (which is the true value, corresponding to our setup), $\omega = 75, 200$, and 400 rad/s .

Various snapshots of the numerical (true) solution T (or T_m), as well as of the zeroth order accurate asymptotic expansion of T (denoted with T_ε), and error between them, for the aforementioned angular velocities, are shown in Figures 7, 8, 9, 10, respectively, at various times in the simulation. The arrow shown in the plots is rotating at the specified angular velocity, with the initial position at $\vartheta = 0$. It basically describes the azimuthal displacement, $\Theta(t) = \omega t$.

In Figure 11 we show the azimuthal average of the heat flux of T in $[0, 2\pi]$, as well as the absolute error between $\bar{T}(\varrho)$ and $\bar{\varphi}_{\eta,d}$, both in $[0, \lambda/(1-\lambda)]$, at the beginning, middle, and end of their respective simulations, for all the aforementioned angular velocities.

All of the aforementioned graphs are at the end of the paper, after the references. The .mp4 files of these simulations can also be found in the Github repo `souvla_cooking`.

Lastly, in Figure 6, on the left is the L_∞ grid function norm between the numerical (true) solution and its zeroth order accurate asymptotic approximation against ω in a log-log scale plot, as well as a plot of the simulation's and approximation's (using the zeroth order approximation) cook-through times against ω , calculated as described in Subsection 6.2. In the latter plot, all times are scaled by the problem's time scale, $\frac{h^2}{D_m} = 4.91264 \cdot 10^5$, and measured in minutes.

7.2 Rotating Robin boundary conditions

We use Dedalus to solve our full simplified model, (3.4), in its *dimensional form*. Since our model consists of a coupled double-diffusion system of equations, with conductive-convective Robin-type rotating boundary conditions, and an underlying background fluid on one of these regions leading to complex fluid-solid interactions, as well as multi-phase phenomena, we utilise a mixture of the *Diffuse Domain Method* (DDM) (for the double diffusion part of our equations), as well as the *Volume-Penalty Method* (VPM) (accounting for the immersed meat slab in the background flow in the "Outside meat" region of the problem). Both methods utilise a so called *mask function* (or *phase field function*), to account for the complex geometry, moving boundary, and complicated boundary conditions that arise in a plethora of real-world problems and settings.

As defined in /31/, a function Γ which satisfies,

1. Boundedness: $\Gamma : \mathbb{R} \rightarrow [0, 1]$.
2. $\lim_{x \rightarrow -\infty} \Gamma(x) = 1$ and $\lim_{x \rightarrow \infty} \Gamma(x) = 0$.
3. Monotonicity (Strictly decreasing): $x_2 > x_1 \Rightarrow \Gamma(x_2) < \Gamma(x_1)$.
4. Symmetry: $\Gamma(x) + \Gamma(-x) = 1$,

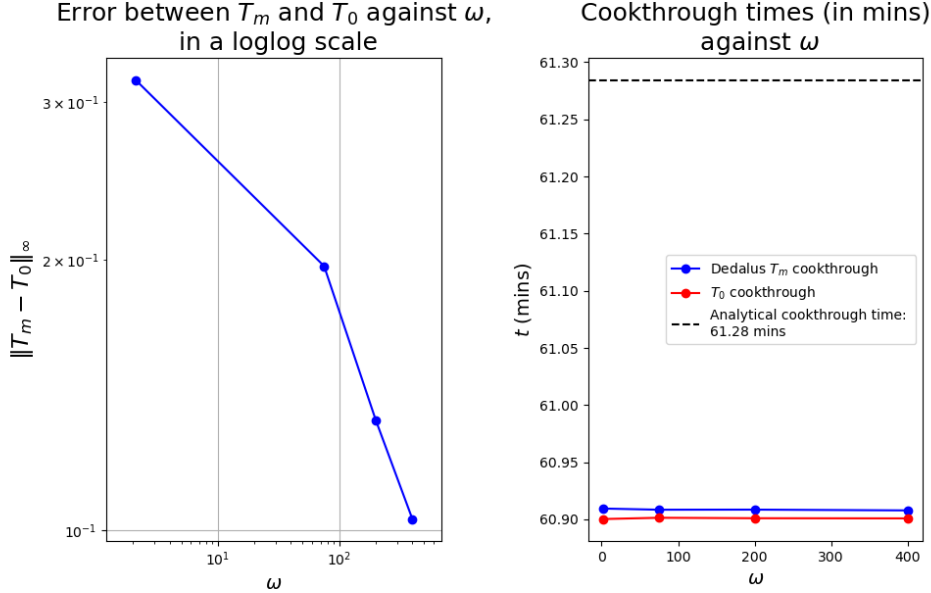


Figure 6: (Left) L_∞ grid function norm between the numerical (true) solution and its zeroth order accurate asymptotic approximation against ω in a log-log scale plot - (Right) Simulation's and zeroth order accurate approximation's cook-through times against ω

is called a *mask function* (notice the deviation from our definition and [31]; We don't assume normalisation, since we use the same mask function for both the DDM and VPM, as to not avoid changing the scalings found in the corrections of [17], Subsections 2.4.1 and 2.5.1). Since no assumptions are made about the regularity of a mask function, this definition includes non-smooth (discontinuous) mask functions. As mentioned in [31], for our means and purposes, such a choice of a mask function is in actuality sub-optimal, and as such we only concern ourselves with smooth mask functions. Examples of such functions are,

$$\Gamma_{\tanh}(x) = \frac{1}{2}(1 - \tanh 2x) \text{ and } \Gamma_{\text{erf}}(x) = \frac{1}{2}(1 - \text{erf}\sqrt{\pi}x).$$

From these, general mask functions can be generated from a normalised mask function Γ through some scaling σ and/or shifting μ ,

$$\Gamma_{\sigma,\mu}(x) = \Gamma\left(\frac{x - \mu}{\sigma}\right).$$

The case of a discontinuous mask is when $\mu = 0, \sigma \rightarrow 0^+$, which to then we inspect the convergence of the masked solution to the true one, when the interface length scale (defined below), η_τ , goes to 0 from above. But, as aforementioned, this is not optimal, as a particular choice of μ and $\sigma = \sigma(\eta_\tau) = \mathcal{O}(\eta_\tau)$, cancels the leading order error in the matched asymptotic expansion between the mask and true solution, leading to a *smaller* overall model error. Smooth mask functions can also be compactified in the interval $[-c, c]$, by the following composition,

$$\widehat{\Gamma}_{[-c,c]}(x) = \Gamma\left(\frac{x}{\sqrt{1 - x^2/c^2}}\right).$$

For our purposes, the smooth normalised function that we will be using is,

$$\Gamma(\varrho) := \frac{1}{2} \left(1 - \tanh \left(3 \frac{\varrho - R_m}{\eta_\tau \sqrt{1 - (\varrho - R_m)^2/\eta_\tau^2}} \right) \right) = \widehat{\Gamma}_{\tanh[-1,1]}\left(\frac{\varrho - R_m}{\eta_\tau}\right),$$

which we then continuously extend to 1 for $\frac{\varrho - R_m}{\eta_\tau} \leq -1$, and 0 for $\frac{\varrho - R_m}{\eta_\tau} \geq 1$. Notice how we needed to take the composition of the compactified tanh function with a signed-distance function that describes the distance of spatial points with the same azimuthial coordinate to the immersed boundary. Points inside the immersed boundary give a negative value to the signed-distance function, while points outside give a positive value.

The Diffuse Domain method (DDM) (see [17], [15], [8], [16]), is used for solving PDEs in complex and moving geometries with Dirichlet, Neumann, or Robin boundary conditions, and utilises an auxiliary mask function, Γ , which replaces the sharp immersed boundary in our domain with a narrow diffusive domain, where now the boundary is represented by a level set of the mask function, specifically the level set $\Gamma = \frac{1}{2}$, and in a transition layer of some small length scale, the mask functions decreases from 1 in the immersed domain of interest, down to 0 outside of it. The benefit of introducing this mask function, is that now we can implicitly incorporate the boundary conditions that we had before in our complex boundary, as lower order terms into our PDE, without changing its order, as to approximate said boundary conditions. Also, it circumvents the need of usual finite element methods to build necessary modifications into the nodal and edge basis functions themselves as to accomodate for the boundary conditions. This diffuse-interface method, unlike the usual *phase-field model*, is able to simulate and encapsulate the behaviour of *two-phase* diffusive passive scalars, explained by advection-diffusion type PDEs. Also, usually the phase-field functions in this method (and for our purposes as well) have no time dependence, and as such no auxiliary phase-field equation is needed to be solved to extract the phase-field function like in the usual phase field model approach (e.g. [29]).

The Volume-penalty method (VPM) (see [31], [22]), similar in premise to the DDM as a fictitious-domain method, it is used to approximate no-slip boundary conditions in complex geometries with moving boundaries, again with the usage of a mask function that introduces rapid linear damping inside the object situated in some background flow. It differs from the usual immersed-boundary method for simulating objects immersed in fluids, which has the main drawback that rigid moving bodies can lead to numerical schemes plagued by stiffness, due to the rigidness of the convolution source term incorporated in the original equation to account for surface tension and bending resistances on the boundary ([12]). Since it again incorporates rapid damping inside the rigid fictitious solid interior, in our case the circular meat slab, it as such avoids the "explicit" tracking of the boundary conditions, instead introducing a lower order source term in our equation to implicitly "track" the boundary conditions, thus making our life easier since dealing with source terms is comparatively easier. While in this paper we won't be analysing such quantities, shear stresses and torque forces on the now "fictitious" can also be easily tracked using boundary integrals via penalised forces and torques introduced by the mask function, e.g. [31], Subsection 3.8.

As mentioned in [31], both methods theory rests on the philosophy that boundary conditions exist to model rapid media changes. In reality, a "solid" wall used as a boundary condition is just an extreme stiffness change in the more elastic properties of a continuum. These methods allow some leeway, where some level of resolved rapid change in the medium properties is permitted.

Both of the aforementioned methods are praised for their simplicity, as they can be easily implemented in a plethora of numerical solvers, like Dedalus, circumventing the need of conforming element grids close to the boundary. Of course, these methods now introduce some equation level error, called the *model error*, which stems from the diffuse interface thickness (DDM) and damping time scale (VPM), needed to force the fluid velocity to tend to the solid velocity within object in the VPM, while in the DDM it forces the passive scalar to tend to the concentration within the enclosed boundary. Using matched asymptotic expansions, a formal justification for the usage of these methods can be provided. For DDM, these results can be found in Li *et al.* ([17]), and for the VPM in Hester *et al.* ([31]). While previous literature used discontinuous penalty mask functions in terms of characteristic/indicator functions, this choice is actually suboptimal, with [17] arriving at diffuse domain approximations in the DDM for Neumann and Robin boundary conditions (like the ones found in (3.4) and (3.5)) that introduce a first order model error ($\mathcal{O}(\eta_\tau)$), with the mention of the possibility of higher-order convergence using Richardson extrapolation (second order in η_τ), where η_τ is the diffusive length scale of the method, while [31] arrived at a model error that improves the previous slow rate of convergence found in the literature, $\mathcal{O}(\sqrt{\eta_a})$ and $\mathcal{O}\left(\sqrt{\frac{\eta_a}{Re}}\right)$ (Re is the fluids Reynolds number), to $\mathcal{O}(\eta_a)$ in all regimes, where η_a is the method's linear damping time scale, which essentially eliminates the displacement length and Reynolds number dependent boundary layer. These results are derived via perturbation theory, using simple smoothing prescriptions for the damping and the mask function, using an orthogonal signed-distance coordinate system that aligns the basis vectors with the boundary (for the boundary layer region), via a signed-distance function of a point in our domain to its nearest point in the boundary interface, which by Approximation Theory when working over the L^2 Hilbert space, should lie in the direction of the unit normal vector of the boundary from the least distance point on the boundary. As aforementioned, negative values are associated with points inside the enclosed domain, while positive values for points outside it. These then add up to a total model error of $\mathcal{O}(\eta_\tau \vee \eta_a)$. In general the model error is controlled by three important factors:

- For both methods; The choice of the non-dimensional penalty damping parameters.
- For both methods; The choice of mask function (in [31], Section 4 the optimal choice for mask function is analysed thoroughly).

- For DDM; The diffuse domain approximation chosen for the respective boundary condition.

η_τ plays the role of a small parameter that sets the width of the diffuse interface layer that bounds the diffusive domain, with the actual length being $2\eta_\tau$, as can be seen after some asymptotic dimensional analysis in (*Li et al., [17]*).

We start from our simplified model in its dimensional form, (3.4). We first make a change of variables to the rotating frame of reference, as outlined in Sections 4 and 5. We then extend all three of our PDEs (for \tilde{T}_m , \tilde{T}_a , and $\vec{\tilde{u}}_a$) from their respective domains to the whole circular region, $\varrho \in [0, R_f]$, and using DDM on our diffusion equations (see [17] and [22]) and VPM in our momentum equation (see [31]), thus incorporating the boundary conditions of those equations on the surface of the meat slab ($\varrho = R_m$) as source terms. We then end up with the following three PDEs and incompressibility/conservation of mass equation,

$$\begin{aligned} \Gamma(\tilde{\varrho})\partial_{\tilde{t}}\tilde{T}_m + \Gamma(\tilde{\varrho})\omega\partial_{\vartheta}\tilde{T}_m - \tilde{\nabla} \cdot (\Gamma(\tilde{\varrho})D_m\tilde{\nabla}\tilde{T}_m) &= -\eta_\tau \frac{\tilde{H}}{\rho_m(Cp)_m}(\tilde{T}_m - \tilde{T}_a)\|\tilde{\nabla}\Gamma\|^2 \\ (1 - \Gamma(\tilde{\varrho}))\partial_{\tilde{t}}\tilde{T}_a + (1 - \Gamma(\tilde{\varrho}))\omega\partial_{\vartheta}\tilde{T}_a + ((1 - \Gamma(\tilde{\varrho}))\vec{\tilde{u}}_a \cdot \tilde{\nabla})\tilde{T}_a - \tilde{\nabla} \cdot ((1 - \Gamma(\tilde{\varrho}))D_a\tilde{\nabla}\tilde{T}_a) &= +\eta_\tau \frac{\kappa_m}{\rho_a(Cp)_a}\partial_{\tilde{\varrho}}\tilde{T}_m\|\tilde{\nabla}(1 - \Gamma)\|^2 \\ \partial_{\tilde{t}}\vec{\tilde{u}}_a + \omega\hat{e}_\vartheta \cdot \nabla\vec{\tilde{u}}_a + (\vec{\tilde{u}}_a \cdot \tilde{\nabla})\vec{\tilde{u}}_a + \frac{1}{\rho_0}\tilde{\nabla}\tilde{p} - \nu\tilde{\nabla}^2\vec{\tilde{u}}_a - (1 - \alpha(\tilde{T}_a - T_\infty))\vec{g} &= -\frac{1}{\eta_a}\Gamma(\tilde{\varrho})(\vec{\tilde{u}}_a - \omega R_m\hat{e}_\vartheta) \\ \tilde{\nabla} \cdot \vec{\tilde{u}}_a &= 0, \end{aligned}$$

with the boundary conditions for \tilde{T}_a , and $\vec{\tilde{u}}_a$ on the surface of the grill ($\varrho = R_f$) remaining unchanged, and likewise for the initial conditions of all state variables. We also need now to enforce a boundary conditions on \tilde{T}_m on the surface of the grill, since we extended its domain from just the "Inside meat" region, to the whole circular region bounded by the grill. Since we will be solving this problem in Dedalus, which is a spectral method PDE solver, we enforce homogeneous Neumann boundary conditions, i.e. $\partial_{\tilde{\varrho}}\tilde{T}_m = 0$ on $\varrho = R_f$, since a Dirichlet BC will have a much greater of a global effect on the spectrum, and as such the natural choice of boundary conditions is the optimal one, also validated by the numerical simulations. Dimensional analysis now indeed validates that that the dimensional temperature damping scale, η_τ , has units of length, while the dimensional fluid scale, η_a , has units of time. As such, by making the following dimensionless coordinate transformations,

$$\begin{aligned} \bullet \varrho &= \frac{1}{\eta_\tau}\tilde{\varrho} \quad \bullet t = \frac{1}{\eta_\alpha}\tilde{t} \quad \bullet \vec{u}_a = \frac{\eta_\alpha\vec{\tilde{u}}_a}{\eta_\tau} \bullet T_m(t, \varrho, \vartheta) = \left(\tilde{T}_m(\tilde{t}, \tilde{\varrho}, \vartheta) - T_\infty\right)/\Delta T, \text{ where } \Delta T = T_H - T_\infty \\ \bullet T_a(t, \varrho, \vartheta) &= \left(\tilde{T}_a(\tilde{t}, \tilde{\varrho}, \vartheta) - T_\infty\right)/\Delta T \quad \bullet p = \frac{\eta_a^2}{\eta_\tau^2\rho_0}\tilde{p}, \end{aligned}$$

leads us to the following dimensionless form of the above equations, accompanied by their dimensionless initial and boundary conditions,

$$\begin{aligned} \Gamma(\eta_\tau\varrho)\partial_t T_m + \eta_a\Gamma\omega\partial_\vartheta T_m - \frac{\eta_a D_m}{\eta_\tau^2}\nabla \cdot (\Gamma\nabla T_m) &= -\frac{\eta_a\tilde{H}}{\eta_\tau\rho_m(Cp)_m}(T_m - T_a)\|\nabla\Gamma\|^2 \\ (1 - \Gamma(\eta_\tau\varrho))\partial_t T_a + (1 - \Gamma)(\vec{u}_a \cdot \nabla)T_a + \eta_\alpha(1 - \Gamma)\omega\partial_\vartheta T_a - \frac{\eta_a D_a}{\eta_\tau^2}\nabla \cdot ((1 - \Gamma)\nabla T_a) &= \frac{\eta_a\kappa_m}{\eta_\tau^2\rho_a(Cp)_a}\partial_\varrho T_m\|\nabla\Gamma\|^2 \\ \partial_t \vec{u}_a + (\vec{u}_a \cdot \tilde{\nabla})\vec{u}_a + \omega\eta_a^2\partial_\vartheta \vec{u}_a + \nabla p - \frac{\nu\eta_a}{\eta_\tau^2}\nabla^2\vec{u}_a + \frac{g\eta_a^2}{\eta_\tau}\left(1 - \frac{\Delta T}{T_\infty}T_a\right)(\sin\vartheta\hat{e}_\varrho + \cos\vartheta\hat{e}_\vartheta) &= -\Gamma\left(\vec{u}_a - \frac{\omega\eta_a R_m}{\eta_\tau}\hat{e}_\vartheta\right) \\ \tilde{\nabla} \cdot \vec{u}_a &= 0 \\ T_a = \varphi_{n,d}(\vartheta) \text{ and } \vec{u}_a = \vec{0}, \text{ at } \varrho = \frac{R_f}{\eta_\tau} & \\ \partial_\varrho T_m = 0, \text{ at } \varrho = \frac{R_f}{\eta_\tau} & \\ T_m(0, \varrho, \vartheta) = T_a(0, \varrho, \vartheta) = 0 \text{ and } \vec{u}_a(0, \varrho, \vartheta) = \vec{0}. & \end{aligned}$$

We will be solving the dimensional variant of this initial/boundary-value problem in Dedalus, to simulate the cooking process of souvla in this simplified model, over the dimensional domain $\Omega = \{(\varrho, \vartheta)^T : \varrho \in [0, R_f], \vartheta \in [0, 2\pi]\}$. Also since our mask functions Γ and $1 - \Gamma$, are 0 outside and inside the meat slab respectively, we ensure that the reformulated mask equations are indeed well posed in the whole domain Ω , by instead working with $\Gamma + \delta_{stability}$ and $1 - \Gamma + \delta_{stability}$, where $\delta_{stability}$ is a small parameter (see [17]). In theory, for the asymptotic analysis, it is sufficient to use any $\delta_{stability} = \mathcal{O}(\eta_\tau)$, but in practice, as to obtain satisfactory numerical

results, a much smaller value is required. In our case we use $\delta_{stability} = 10^{-4}$. **Pretty sure that the better choice would be the dimensionless problem, but need to fiddle around with the multiple scales in our problem since this non-dimensionalisation really slows down time making the simulations inefficient.**

Various snapshots of the numerical (true) solutions \tilde{T}_m , \tilde{T}_a , the radial and azimuthial component of the velocity $\hat{e}_\varrho \cdot \tilde{\vec{u}}_a$ and $\hat{e}_\vartheta \cdot \tilde{\vec{u}}_a$, the component of the vorticity parallel to the metallic skewer, and the pressure, for $\omega = 2.1 \text{rads}^{-1}$ can be found in Figure 12. In Figure 13 the zeroth order accurate asymptotic expansion of \tilde{T}_m , and the error between them, for the aforementioned angular velocity, is shown, at the corresponding time instants in our simulation. For the integration of \tilde{T}_a over the surface of the meat slab we use a composite trapezoidal rule due to its simplicity in implementation. The arrow shown in the plots is rotating at the specified angular velocity, with the initial position at $\vartheta = 0$. It basically describes the azimuthial displacement, $\Theta(\tilde{t}) = \omega \tilde{t}$.

In Figure 14 we show the azimuthal average of the heat fluxes of \tilde{T}_m and \tilde{T}_a in $[0, 2\pi]$, on $[0, R_f]$, at the beginning, middle, and end of the simulation, for $\omega = 2.1$. They seem to match up (taking into consideration the model error) at the boundary of our meat slab, due to the continuation of heat flux across the surface of separation and the incorporation of that boundary condition via the DDM's penalty source term (**not accounting for the blow-up; See Next Steps section**).

All of the aforementioned graphs are at the end of the paper, after the references and the figures from the simulations for the Dirichlet rotating boundary conditions toy-problem. The .mp4 files of these simulations can also be found in the Github repo `souvla_cooking`.

8 Next Steps

- **Fix** the simulations for the full simple model (since they blow up after some time). Find the correct scalings and non-dimensionalisation to be able to study the multi-phase phenomena. This should be the first thing to do. Also make sure that the model being used is indeed warranted. Also the approximation plots seem a bit off, need to fix them (this seems like an easy fix, I think I know what I did wrong).
- Implement a more accurate way to integrate T_a in the simulation to attain the value of the zeroth order accurate asymptotic expression, instead of composite trapezoidal (see (5.5)).
- Validate the Robin cook-through time.
- Clean up the code base a bit, add docstrings, and make it a bit more readable.
- See (5.6) - Include details on the closure of the circumfluent boundary layer limit terms, for when T_a on the meat's surface has no temporal dependence.
- Numerical simulations of the full model, (2.7).
- See how the solution is affected by changing h , both in the true and simple model (this will stem from solving the dimensionless variants of the problem).
- Incorporate radiation back into the model, using [17].
- As illustrated in [31], surface tension, forces, and torque on the meat slab boundary can also be easily incorporated into Dedalus and calculated, for a more thorough description of the problem, if needed.
- Add a conclusion, after all the necessary inclusions are added and "bugs" in the Robin BC version of the simplified model simulation are fixed. The problem is most likely that we need to take a much smaller length scale η_τ in the DDM method (and even time scale η_a in the VPM method, possibly?), and as such need a much higher resolution as to not lead to instabilities. This will require my access to a computer cluster that I can use to quickly run these simulations in an efficient manner (for fine tuning the parameters, etc.).

References

- [1] H.S. Carslaw and J.C. Jaeger. *Conduction of Heat in Solids*. Oxford science publications. Clarendon Press, 1959. ISBN: 9780198533689. URL: <https://books.google.com/books?id=ySRRAAAAMA AJ>.
- [2] Peter B. Rhines and William R. Young. "Homogenization of potential vorticity in planetary gyres". In: *Journal of Fluid Mechanics* 122 (1982), pp. 347–367. DOI: 10.1017/S0022112082002250.

- [3] E. M. Sparrow and D. S. Kadle. "Heat Transfer From Rods or Fins Which Extend Radially Outward From a Rotating Shaft". In: *Journal of Heat Transfer* 106.2 (May 1984), pp. 290–296. DOI: 10.1115/1.3246671. URL: <https://doi.org/10.1115/1.3246671>.
- [4] H.M. Badr and S.C.R. Dennis. "Laminar forced convection from a rotating cylinder". In: *International Journal of Heat and Mass Transfer* 28.1 (Jan. 1985), pp. 253–264. DOI: 10.1016/0017-9310(85)90027-4. URL: [https://doi.org/10.1016/0017-9310\(85\)90027-4](https://doi.org/10.1016/0017-9310(85)90027-4).
- [5] Pedro Sanz, M.D. Alonso, and Rodolfo Mascheroni. "Thermophysical Properties of Meat Products: General Bibliography and Experimental Values". In: *Transactions of the ASAE* 30 (Jan. 1987), pp. 283–289, 296. DOI: 10.13031/2013.30441.
- [6] B. V. S. S. Prasad, A. A. Tawfek, and A. K. Mohanty. "Heat transfer from a circular cylinder rotating about an orthogonal axis in quiescent air". In: *Experiments in Fluids* 10.5 (Feb. 1991), pp. 267–272. DOI: 10.1007/bf00202459. URL: <https://doi.org/10.1007/bf00202459>.
- [7] G M Lieberman. *Second Order Parabolic Differential Equations*. WORLD SCIENTIFIC, Nov. 1996. DOI: 10.1142/3302. URL: <https://doi.org/10.1142/3302>.
- [8] D. M. Anderson, G. B. McFadden, and A. A. Wheeler. "DIFFUSE-INTERFACE METHODS IN FLUID MECHANICS". In: *Annual Review of Fluid Mechanics* 30.1 (1998), pp. 139–165. DOI: 10.1146/annurev.fluid.30.1.139. eprint: <https://doi.org/10.1146/annurev.fluid.30.1.139>. URL: <https://doi.org/10.1146/annurev.fluid.30.1.139>.
- [9] C.M. Bender and S.A. Orszag. *Advanced Mathematical Methods for Scientists and Engineers I: Asymptotic Methods and Perturbation Theory*. Advanced Mathematical Methods for Scientists and Engineers. Springer, 1999. ISBN: 9780387989310. URL: <https://books.google.com/books?id=-yQXwhE6iWMC>.
- [10] F. M. Mahfouz and H. M. Badr. "Heat convection from a cylinder performing steady rotation or rotary oscillation - Part I: Steady rotation". In: *Heat and Mass Transfer* 34.5 (Feb. 1999), pp. 365–373. DOI: 10.1007/s002310050271. URL: <https://doi.org/10.1007/s002310050271>.
- [11] R.L. Stroshine. *Physical Properties of Agricultural Materials and Food Products*. R. Stroshine, 2004. URL: <https://books.google.com/books?id=SmK6HgAACAAJ>.
- [12] Rajat Mittal and Gianluca Iaccarino. "IMMERSED BOUNDARY METHODS". In: *Annual Review of Fluid Mechanics* 37.1 (2005), pp. 239–261. DOI: 10.1146/annurev.fluid.37.061903.175743. eprint: <https://doi.org/10.1146/annurev.fluid.37.061903.175743>. URL: <https://doi.org/10.1146/annurev.fluid.37.061903.175743>.
- [13] John R. Taylor. *Classical Mechanics*. en. University Science Books, 2005. ISBN: 978-1-891389-22-1.
- [14] Refrigerating American Society of Heating and Air-Conditioning Engineers. *2006 ASHRAE Handbook: Refrigeration*. ASHRAE, 2006. ISBN: 9781601197948. URL: <https://books.google.com/books?id=N3rCjwEACAAJ>.
- [15] Andreas Rätz and Axel Voigt. "PDE's on surfaces—a diffuse interface approach". In: *Communications in Mathematical Sciences* 4.3 (2006), pp. 575–590.
- [16] Isabelle Ramière, Philippe Angot, and Michel Belliard. "A fictitious domain approach with spread interface for elliptic problems with general boundary conditions". In: *Computer Methods in Applied Mechanics and Engineering* 196.4-6 (Jan. 2007), pp. 766–781. DOI: 10.1016/j.cma.2006.05.012. URL: <https://doi.org/10.1016/j.cma.2006.05.012>.
- [17] X. Li et al. "Solving pdes in complex geometries". In: *Communications in Mathematical Sciences* 7.1 (2009), pp. 81–107. DOI: 10.4310/cms.2009.v7.n1.a4. URL: <https://doi.org/10.4310/cms.2009.v7.n1.a4>.
- [18] L.C. Evans. *Partial Differential Equations*. Graduate studies in mathematics. American Mathematical Society, 2010. ISBN: 9780821849743. URL: https://books.google.com/books?id=Xnu0o%5C_EJrCQC.
- [19] T.L. Bergman et al. *Fundamentals of Heat and Mass Transfer*. Wiley, 2011. ISBN: 978-0-470-50197-9. URL: <https://books.google.com/books?id=vvyIoXEywMoC>.
- [20] M.A. Pinsky. *Partial Differential Equations and Boundary-Value Problems with Applications: Third Edition*. Pure and applied undergraduate texts. American Mathematical Society, 2011. ISBN: 978-1-4704-1128-2. URL: <https://books.google.com/books?id=yj75twEACAAJ>.
- [21] R. Haberman. *Applied Partial Differential Equations with Fourier Series and Boundary Value Problems, Books a la Carte*. Pearson Education, 2012. ISBN: 9780321797063. URL: <https://books.google.com/books?id=lxJGLwEACAAJ>.
- [22] Benjamin Kadoch et al. "A volume penalization method for incompressible flows and scalar advection-diffusion with moving obstacles". In: *Journal of Computational Physics* 231.12 (June 2012), pp. 4365–4383. DOI: 10.1016/j.jcp.2012.01.036. URL: <https://doi.org/10.1016/j.jcp.2012.01.036>.
- [23] Varun Sharma and Kumar Dhiman. "Heat transfer from a rotating circular cylinder in the steady regime: Effects of Prandtl number". In: *Thermal Science* 16.1 (2012), pp. 79–91. DOI: 10.2298/tsci100914057s. URL: <https://doi.org/10.2298/tsci100914057s>.
- [24] Greg Blonder. *Temperature near bones*. 2013. URL: <https://genuineideas.com/ArticlesIndex/tothebone.html>.

- [25] Reda I. Elghnam. "Experimental and numerical investigation of heat transfer from a heated horizontal cylinder rotating in still air around its axis". In: *Ain Shams Engineering Journal* 5.1 (Mar. 2014), pp. 177–185. DOI: 10.1016/j.asej.2013.09.008. URL: <https://doi.org/10.1016/j.asej.2013.09.008>.
- [26] A.D. Polyanin and V.E. Nazaikinskii. *Handbook of Linear Partial Differential Equations for Engineers and Scientists*. CRC Press, 2015. ISBN: 9781466581494. URL: <https://books.google.com/books?id=zgdCCwAAQBAJ>.
- [27] Keaton J. Burns et al. "Dedalus: A flexible framework for numerical simulations with spectral methods". In: *Phys. Rev. Res.* 2 (2 Apr. 2020), p. 023068. DOI: 10.1103/PhysRevResearch.2.023068. URL: <https://link.aps.org/doi/10.1103/PhysRevResearch.2.023068>.
- [28] Y.A. Çengel and A.J. Ghajar. *Heat and Mass Transfer: Fundamentals & Applications*. McGraw-Hill Education, 2020. ISBN: 9789813158962. URL: <https://books.google.com/books?id=6KmezQEACAAJ>.
- [29] Eric W. Hester et al. "Improved phase-field models of melting and dissolution in multi-component flows". In: *Proceedings of the Royal Society A: Mathematical, Physical and Engineering Sciences* 476.2242 (Oct. 2020). DOI: 10.1098/rspa.2020.0508. URL: <https://doi.org/10.1098/rspa.2020.0508>.
- [30] R. M. S. Gama and R. Pazetto S. Gama. "The Kirchhoff Transformation and the Fick's Second Law with Concentration-dependent Diffusion Coefficient". In: *WSEAS TRANSACTIONS ON HEAT AND MASS TRANSFER* 16 (July 2021), pp. 59–67. DOI: 10.37394/232012.2021.16.9. URL: <https://doi.org/10.37394/232012.2021.16.9>.
- [31] Eric W. Hester, Geoffrey M. Vasil, and Keaton J. Burns. "Improving accuracy of volume penalised fluid-solid interactions". In: *Journal of Computational Physics* 430 (Apr. 2021), p. 110043. DOI: 10.1016/j.jcp.2020.110043. URL: <https://doi.org/10.1016/j.jcp.2020.110043>.
- [32] Agriculture and Horticulture Development Board. *Pork yield guide*. Accessed: 22/04/2023, Link.
- [33] Isidoro Martínez. *RADIATIVE VIEW FACTORS*. Accessed: 21/04/2023, Link.
- [34] Wikipedia. *Souvla - Wikipedia*. URL: <https://en.wikipedia.org/wiki/Souvla>.

Figure 7: Snapshots of T_m , $T_\varepsilon = T_0$ (zeroth order asymptotic approximation of T_m), and the error of this approximation over the dimensionless domain $\varrho \in [0, \lambda/(1 - \lambda)]$, for $\omega = 2.1 \text{ rads}^{-1}$

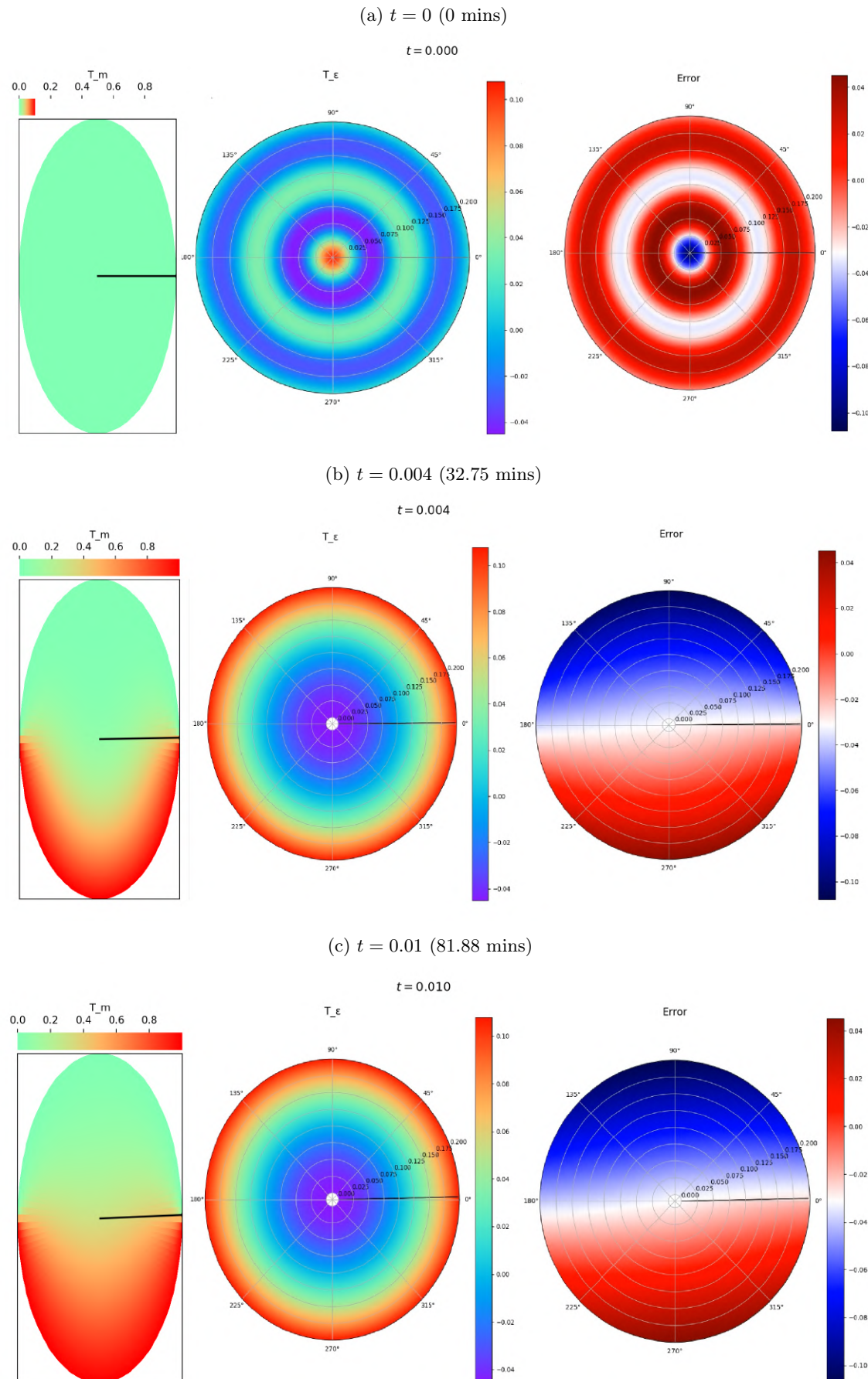


Figure 7: Snapshots of T_m , $T_\varepsilon = T_0$ (zeroth order asymptotic approximation of T_m), and the error of this approximation over the dimensionless domain $\varrho \in [0, \lambda/(1 - \lambda)]$, for $\omega = 2.1 \text{rads}^{-1}$ (Cont.)

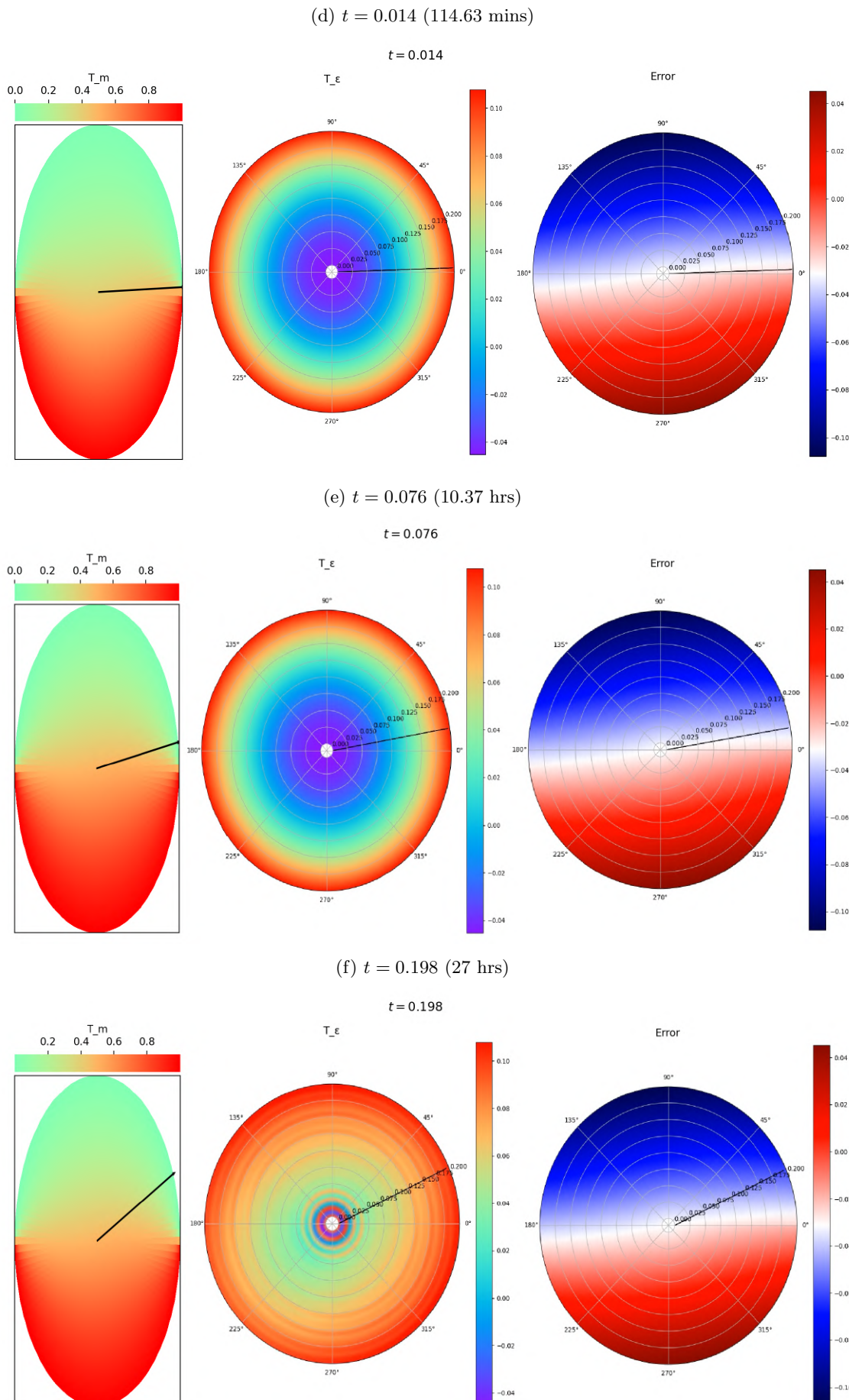


Figure 8: Snapshots of T_m , $T_\varepsilon = T_0$ (zeroth order asymptotic approximation of T_m), and the error of this approximation over the dimensionless domain $\varrho \in [0, \lambda/(1 - \lambda)]$, for $\omega = 75\text{rads}^{-1}$

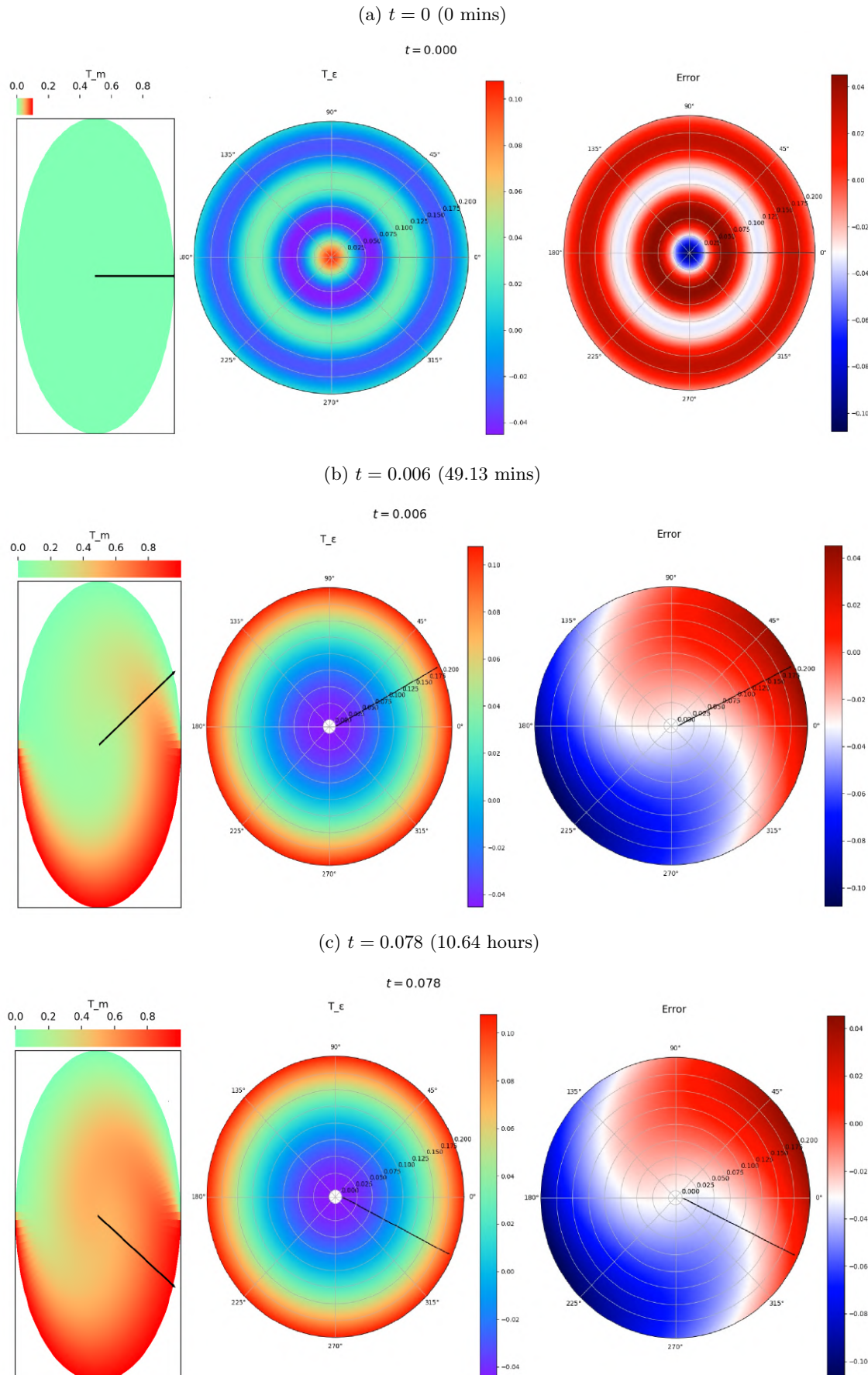


Figure 9: Snapshots of T_m , $T_\varepsilon = T_0$ (zeroth order asymptotic approximation of T_m), and the error of this approximation over the dimensionless domain $\varrho \in [0, \lambda/(1 - \lambda)]$, for $\omega = 200\text{rads}^{-1}$

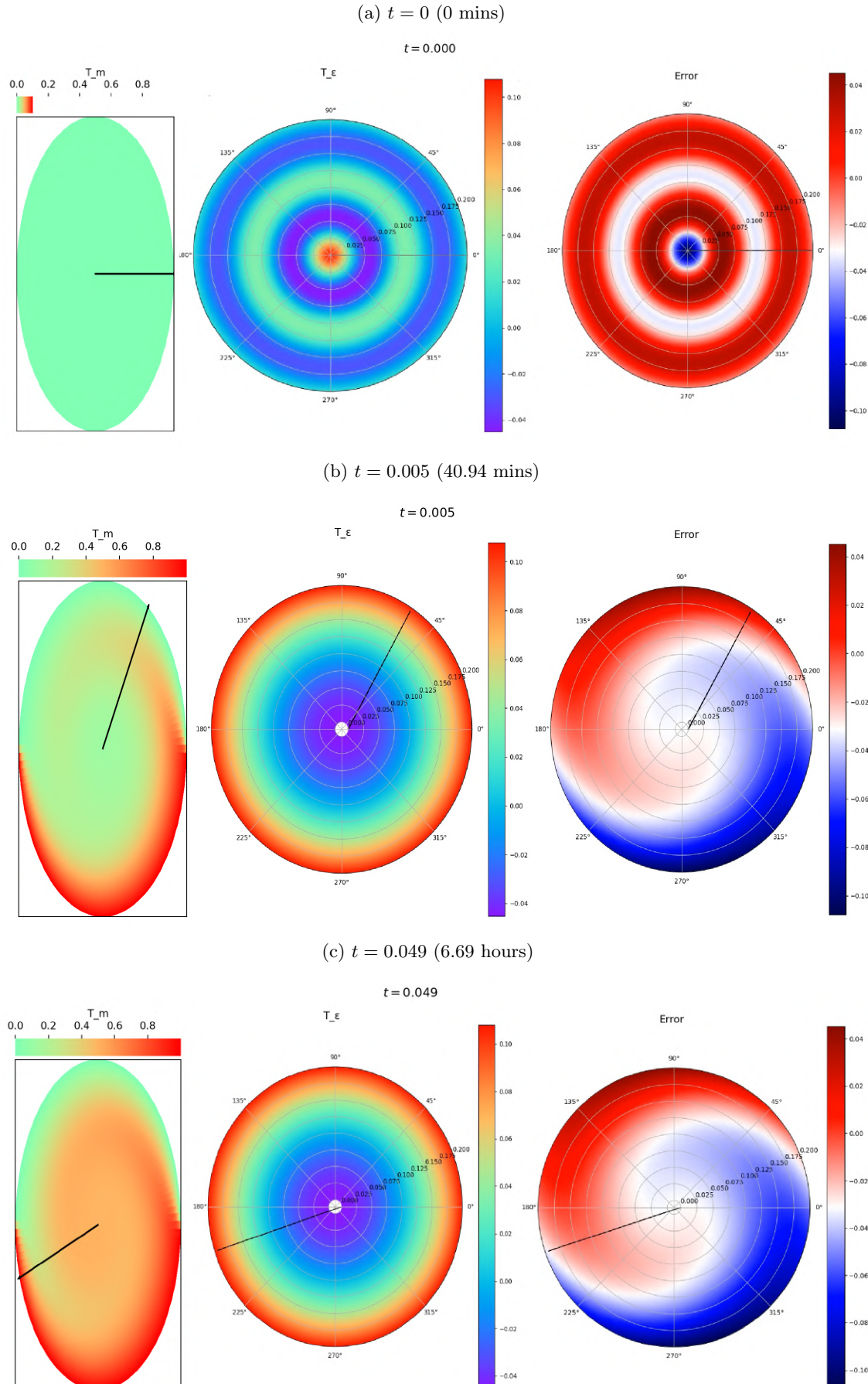


Figure 10: Snapshots of T_m , $T_\varepsilon = T_0$ (zeroth order asymptotic approximation of T_m), and the error of this approximation over the dimensionless domain $\varrho \in [0, \lambda/(1-\lambda)]$, for $\omega = 400 \text{ rads}^{-1}$

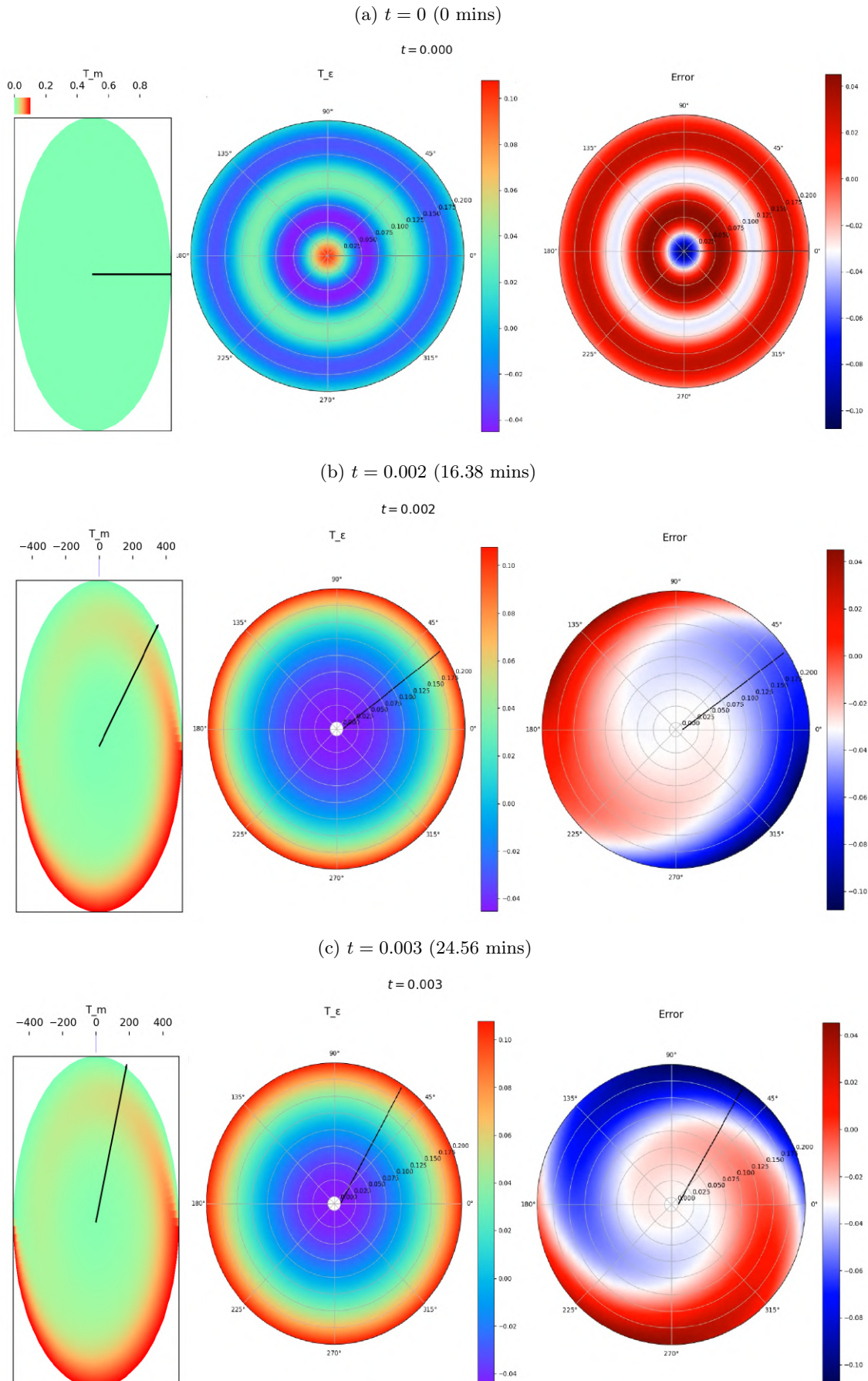


Figure 10: Snapshots of T_m , $T_\varepsilon = T_0$ (zeroth order asymptotic approximation of T_m), and the error of this approximation over the dimensionless domain $\varrho \in [0, \lambda/(1 - \lambda)]$, for $\omega = 400\text{rads}^{-1}$ (Cont.)

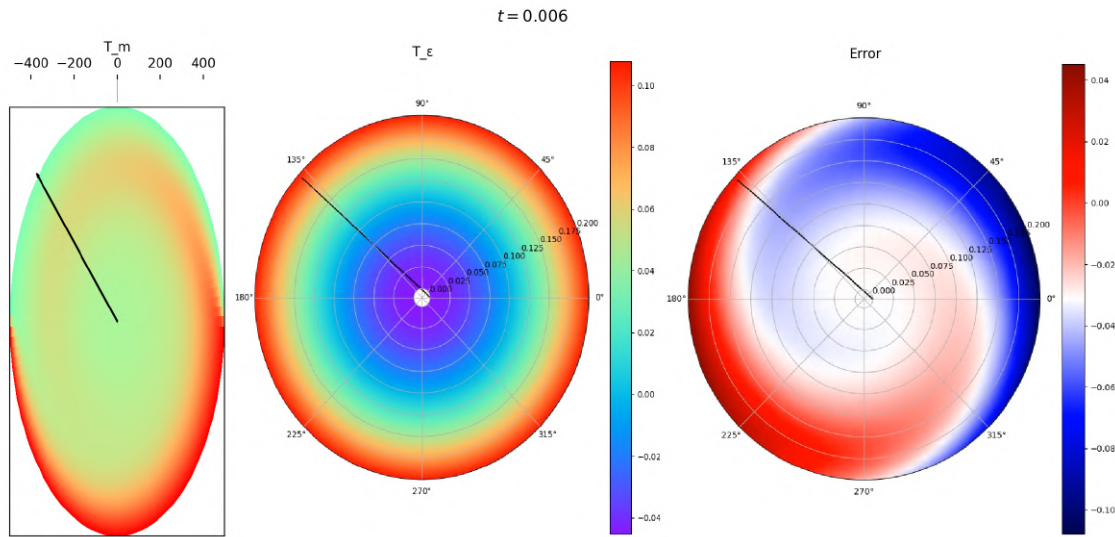
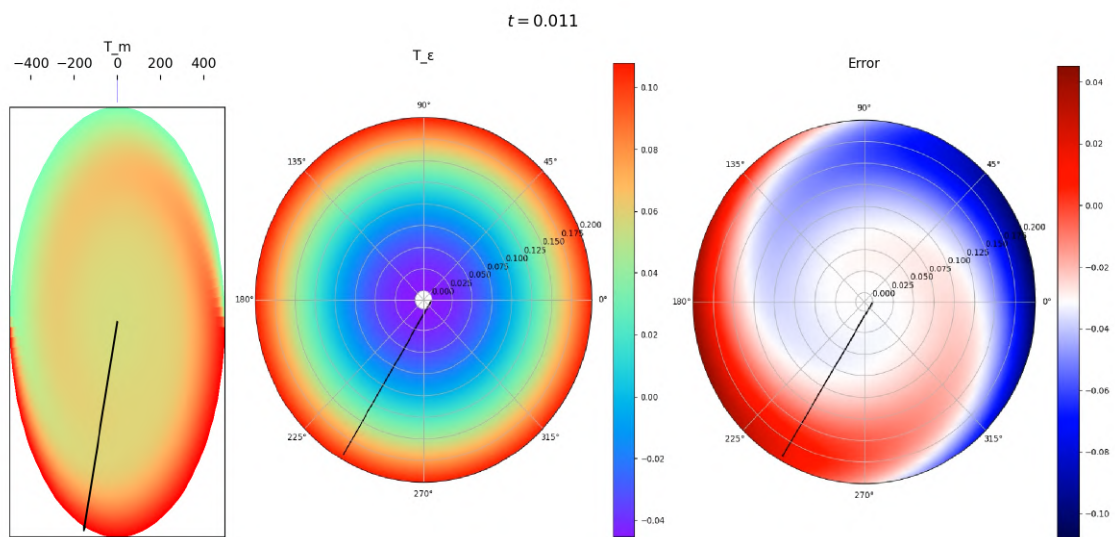
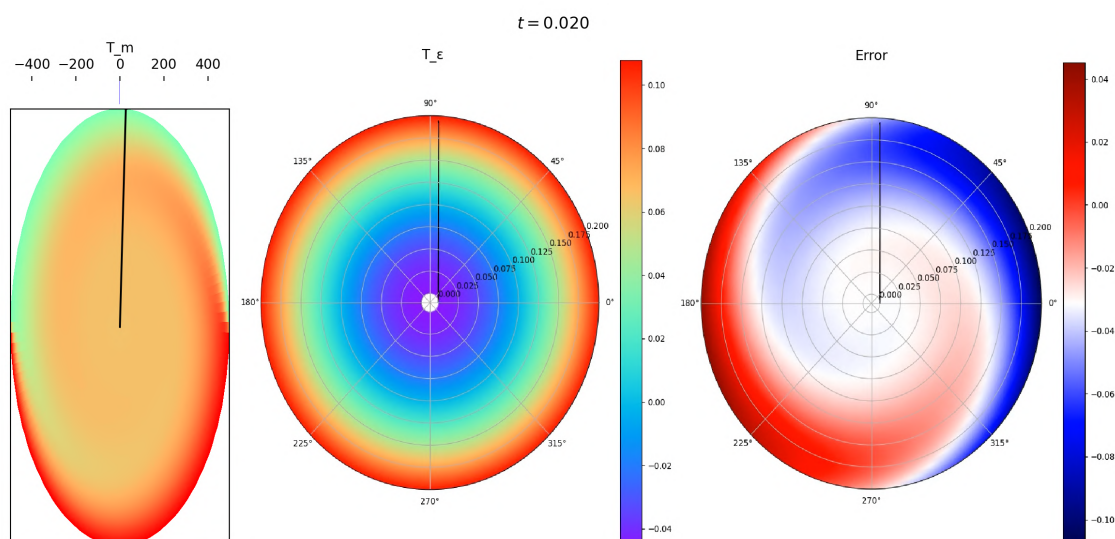
(d) $t = 0.006$ (49.13 mins)(e) $t = 0.011$ (90.07 mins)(f) $t = 0.02$ (2.73 hrs)

Figure 11: (Left) Azimuthial average of the heat flux of T_m in $[0, 2\pi]$, and (Right) the absolute error between $T_m(\varrho)$ and $\overline{\varphi_{\eta,d}}$, both in $[0, \lambda/(1-\lambda)]$, at the beginning, middle, and end of their respective simulations

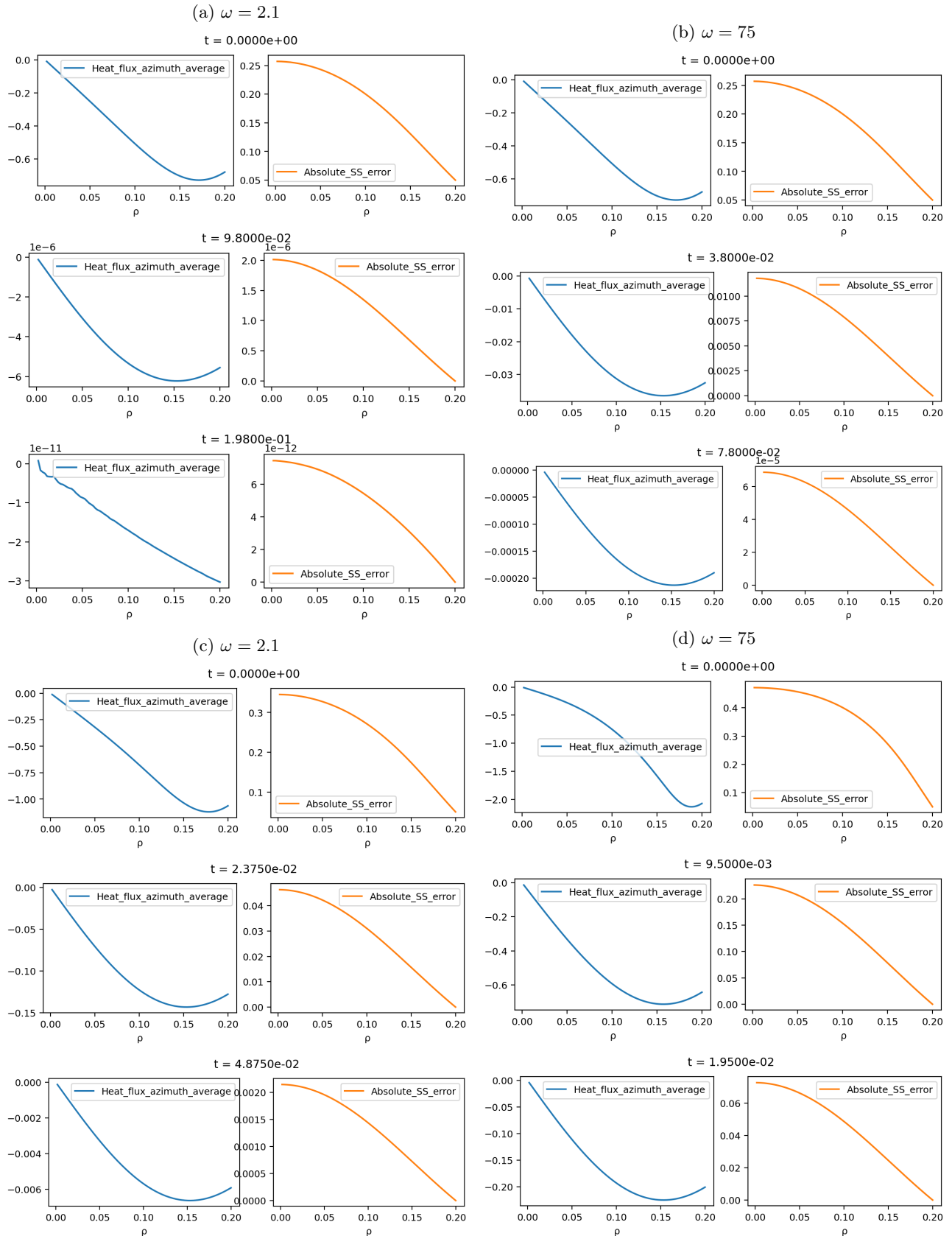


Figure 12: Snapshots of the numerical (true) solutions \tilde{T}_m , \tilde{T}_a , the azimuthial and radial component of the velocity $\hat{e}_\theta \cdot \vec{u}_a$ and $\hat{e}_{\bar{\theta}} \cdot \vec{u}_a$, the component of the vorticity parallel to the metallic skewer, and the pressure, for $\omega = 2.1 \text{ rads}^{-1}$ (In that order, row-wise, starting from the first row)

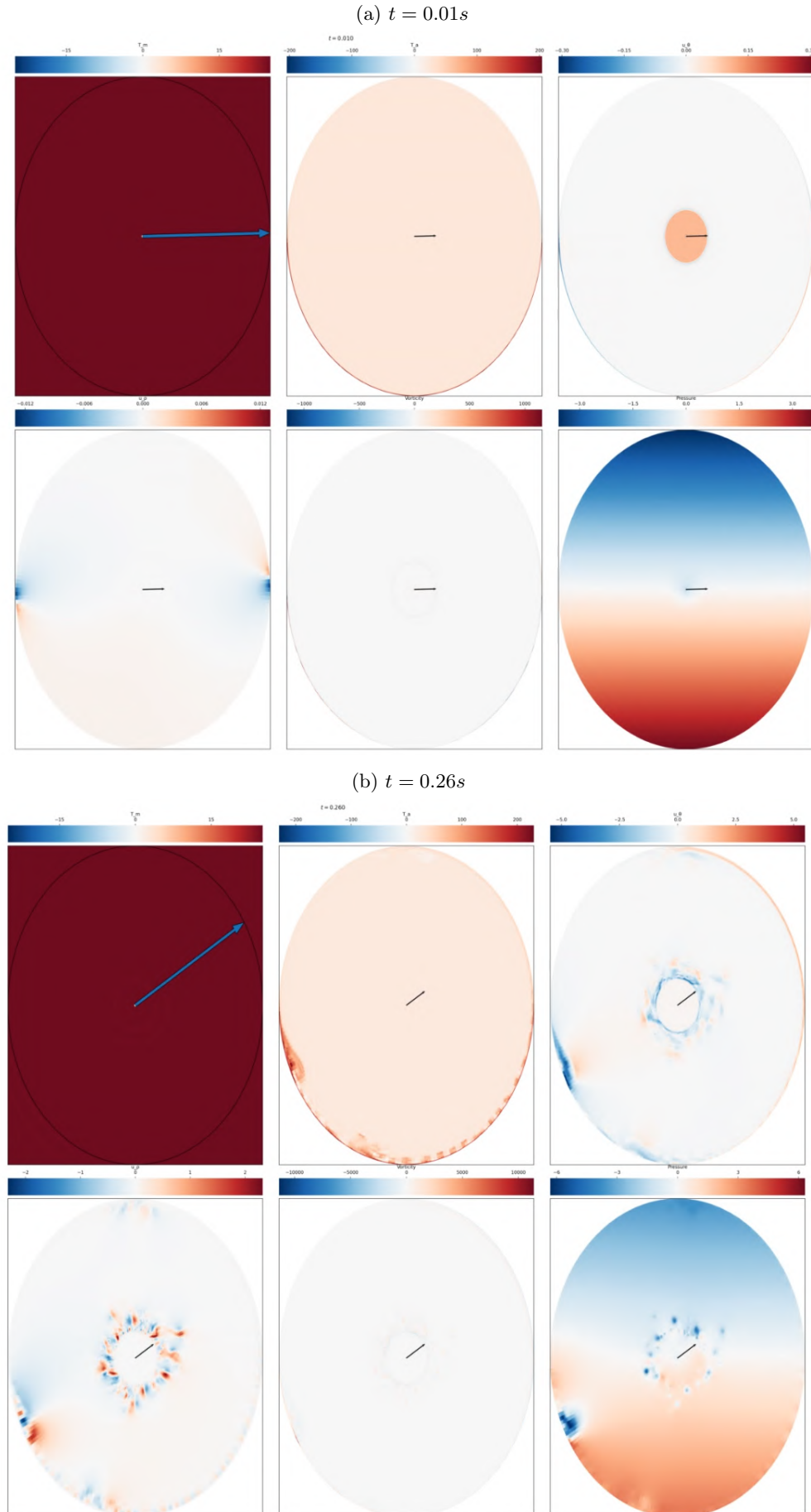


Figure 12: Snapshots of the numerical (true) solutions \tilde{T}_m , \tilde{T}_a , the azimuthial and radial component of the velocity $\hat{e}_\theta \cdot \vec{\tilde{u}}_a$ and $\hat{e}_{\bar{\theta}} \cdot \vec{\tilde{u}}_a$, the component of the vorticity parallel to the metallic skewer, and the pressure, for $\omega = 2.1 \text{ rads}^{-1}$ (In that order, row-wise, starting from the first row) (Cont.)

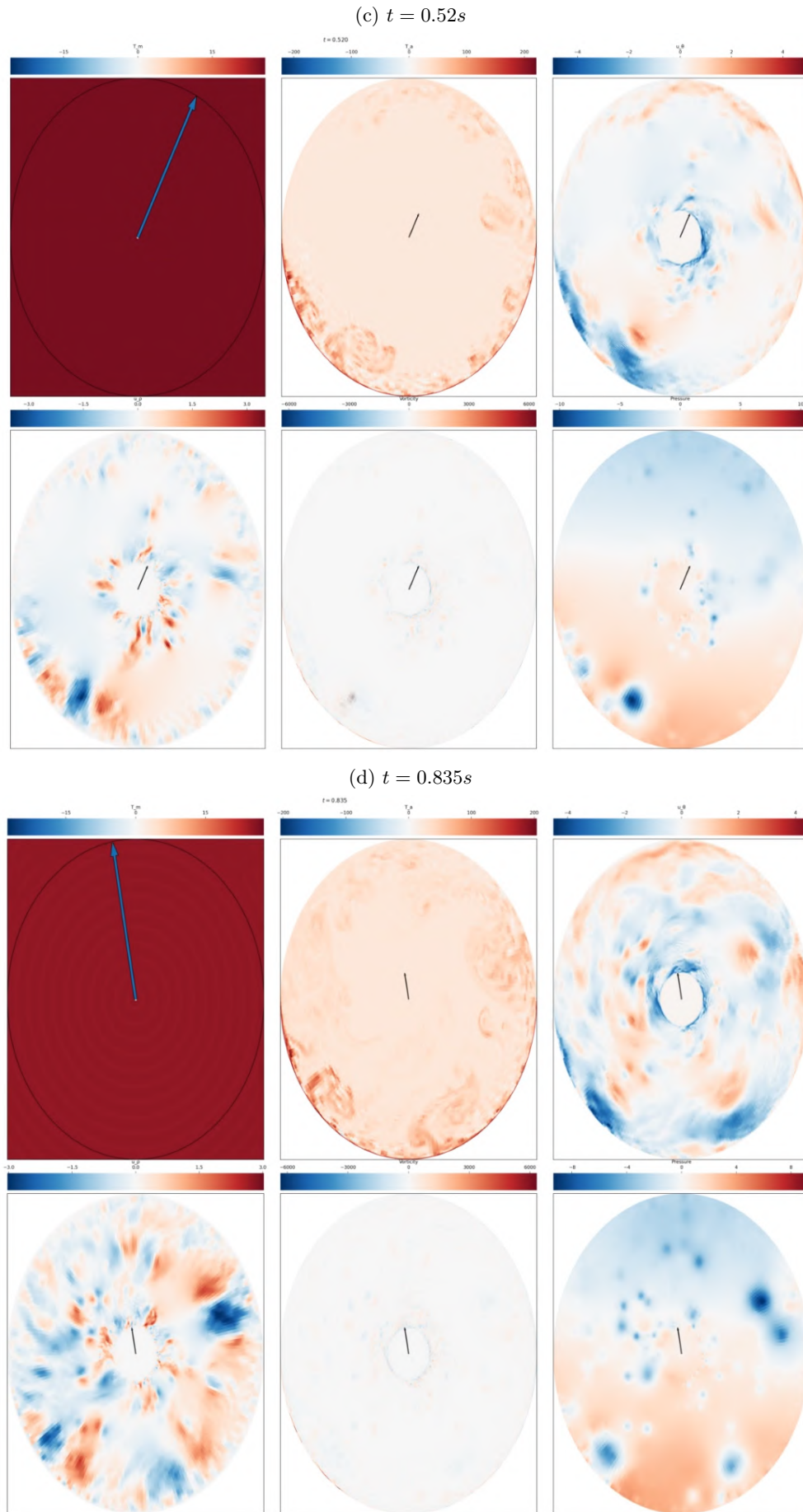


Figure 12: Snapshots of the numerical (true) solutions \tilde{T}_m , \tilde{T}_a , the azimuthial and radial component of the velocity $\hat{e}_\theta \cdot \vec{\tilde{u}}_a$ and $\hat{e}_{\bar{\theta}} \cdot \vec{\tilde{u}}_a$, the component of the vorticity parallel to the metallic skewer, and the pressure, for $\omega = 2.1 \text{ rads}^{-1}$ (In that order, row-wise, starting from the first row) (Cont.)

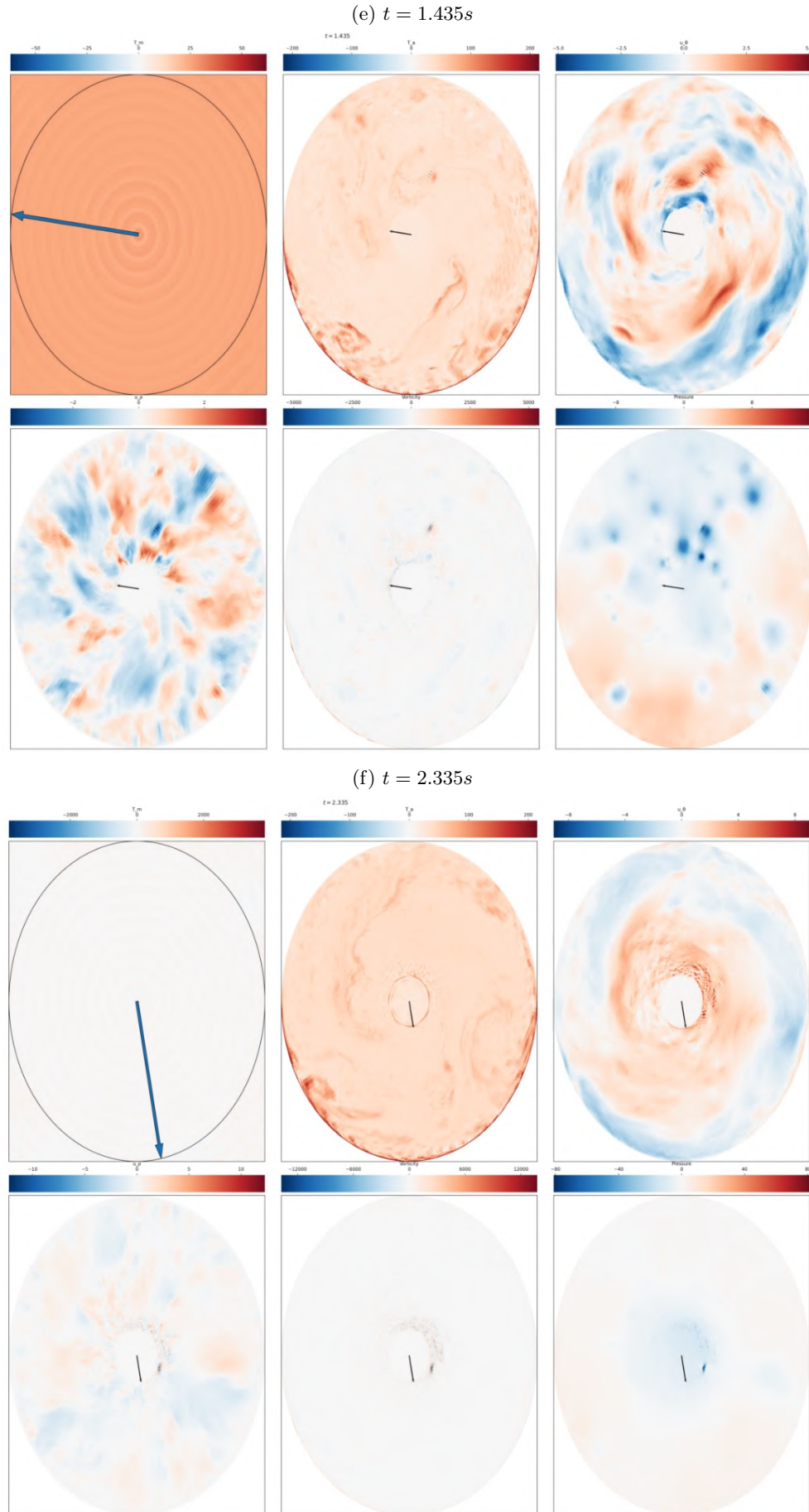


Figure 13: (Left) The zeroth order accurate asymptotic expansion of \tilde{T}_m , and (Right) the error between it and \tilde{T}_m , for $\omega = 2.1 \text{ rads}^{-1}$, at the corresponding time instants in our simulation. For the integration of \tilde{T}_a over the surface of the meat slab we use a composite trapezoidal rule in time

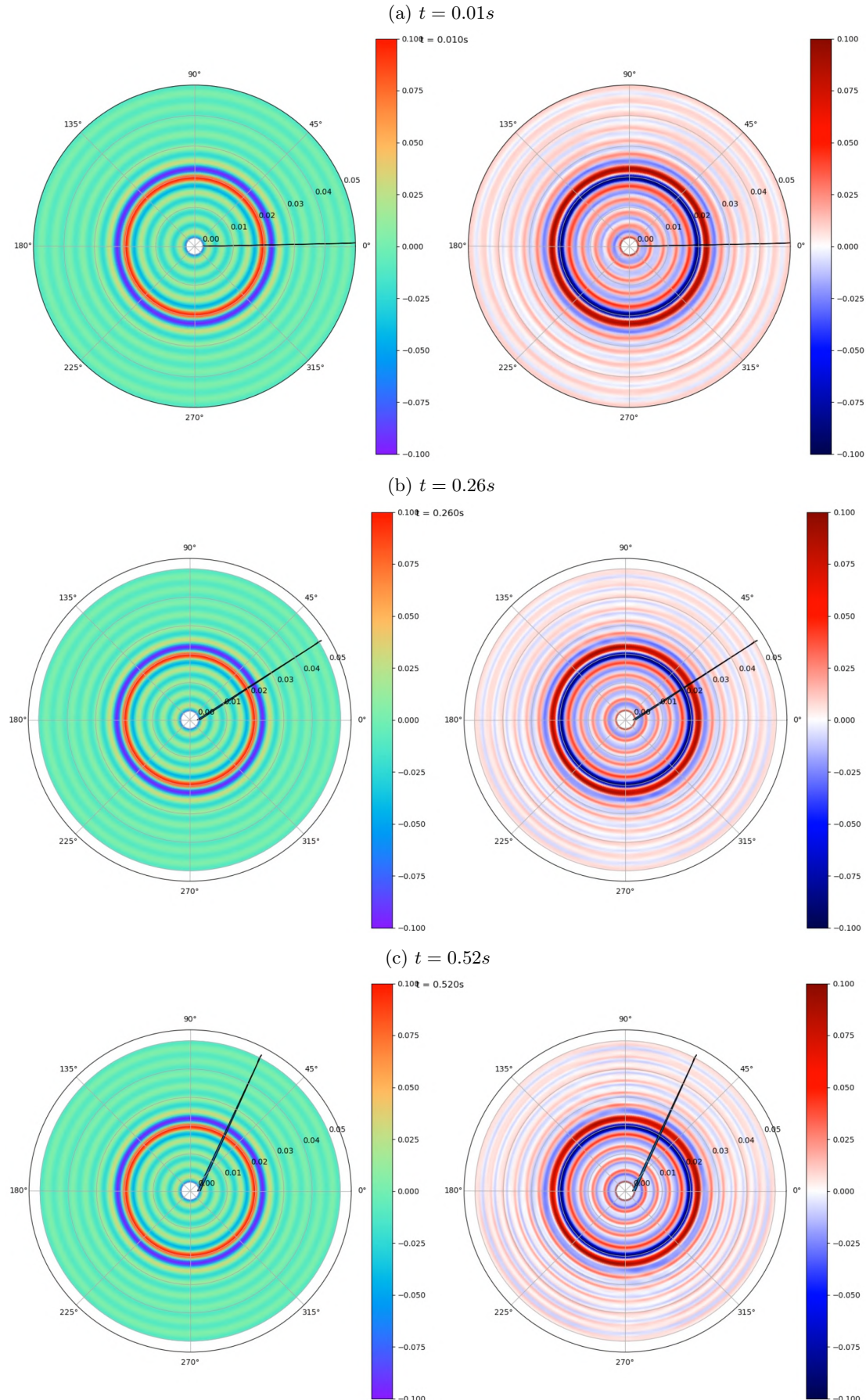


Figure 13: (Left) The zeroth order accurate asymptotic expansion of \tilde{T}_m , and (Right) the error between it and \tilde{T}_m , for $\omega = 2.1 \text{ rads}^{-1}$, at the corresponding time instants in our simulation. For the integration of \tilde{T}_a over the surface of the meat slab we use a composite trapezoidal rule in time (Cont.)

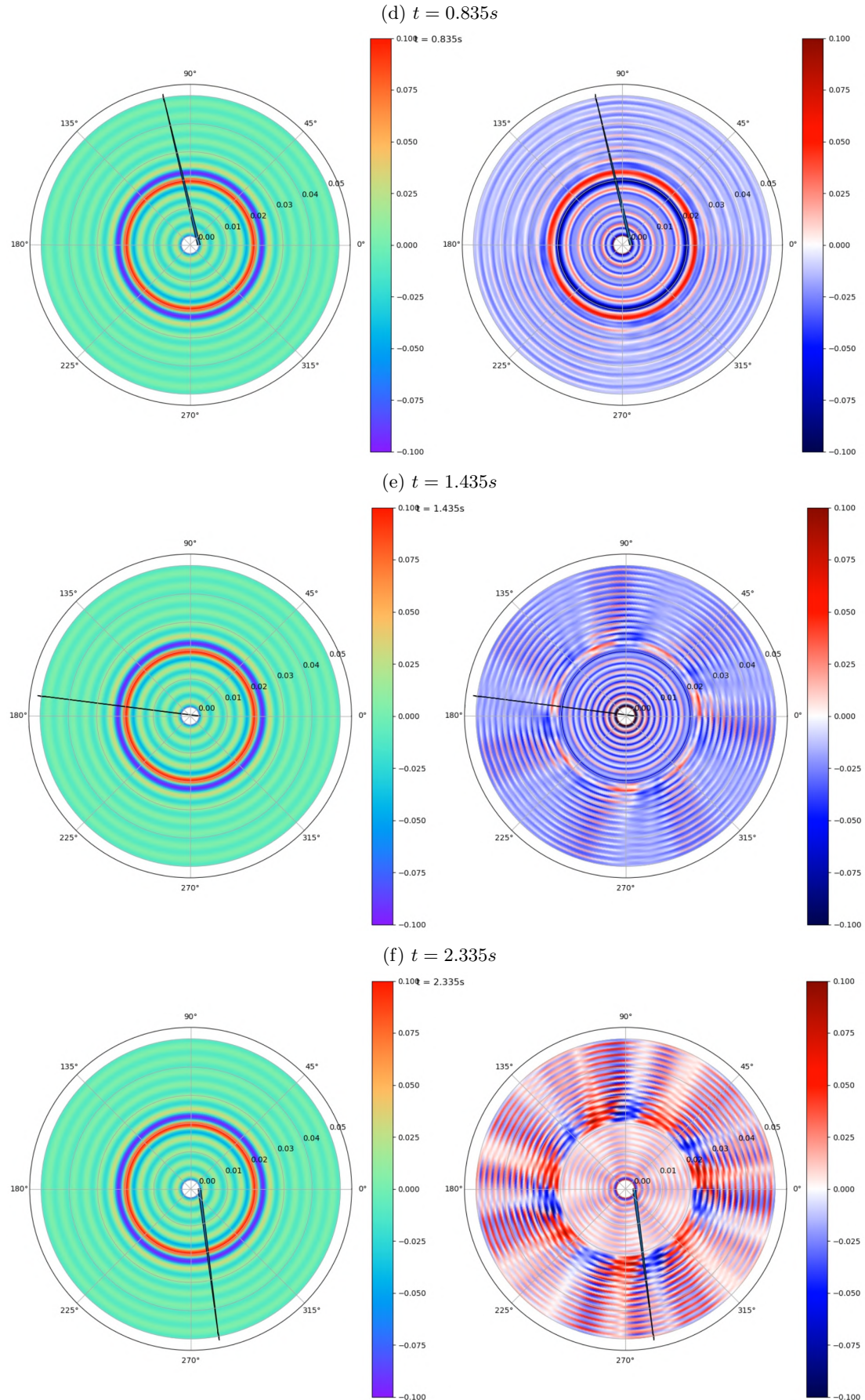


Figure 14: The azimuthal average of the heat fluxes of \tilde{T}_m and \tilde{T}_a in $[0, 2\pi]$, on $[0, R_f]$, $\langle \partial_{\varrho} \tilde{T}_m \rangle_{\vartheta}$ and $\langle \partial_{\varrho} \tilde{T}_a \rangle_{\vartheta}$, at the beginning, middle, and end of the simulation, for $\omega = 2.1$

